4
Functionalization of P3HT-Based Hybrid Materials for Photovoltaic Applications

Michèle Chevrier[1,2], Riccardo Di Ciuccio[2], Olivier Coulembier[2], Philippe Dubois[2], Sébastien Richeter[1], Ahmad Mehdi[1], and Sébastien Clément[1]

[1] *Institut Charles Gerhardt – UMR 5253, Université de Montpellier CNRS, ENSCM – CC1701, Montpellier, France*

[2] *Laboratory of Polymeric and Composite Materials, Center of Innovation and Research in Materials and Polymers, University of Mons – UMONS, Mons, Belgium*

4.1 Introduction

Fossil fuel resources exhaustion, increasing energy demands, and environmental problems have triggered an intensification of research for sustainable sources of energies such as photovoltaic (PV) sources, fuel cells, wind generation, and geothermal and tidal energy. Among these, PV conversion of solar energy is considered to be one of the most significant ways of addressing the growing global energy crisis. Compared with all the other sources (hydropower, wind power, geothermal energy, etc.), sunlight is the only one able to provide enough energy per year to cover the worldwide energy consumption rate [1, 2]. Although the current solar cell market is dominated by PV cells based on silicon and inorganic semiconductors with power conversion efficiencies (PCEs) around 20% [3], emerging technologies such as organic photovoltaics (OPVs) [4], dye-sensitized solar cells (DSSCs) [5], and organic–inorganic hybrid (OIH) solar cells [6] involving organic semiconductors have also attracted huge interest.

Compared with their inorganic counterparts, PV cells based on organic semiconductors (small molecules or conjugated polymers) constitute a cost-effective approach for converting solar energy into electricity since the solution processability of organic materials allows low-cost manufacturing process, for example, inkjet printing and roll-to-roll deposition [7]. Furthermore, due to high absorption coefficients of organic semiconductors, thin films (typically some hundreds of nanometers) are usually required, paving the way to flexible and lightweight applications [8]. Nevertheless, whereas free charges are produced upon photon absorption in inorganic materials, the photogenerated species in most conjugated polymers are neutrally bound electron–hole pairs (excitons). Producing free carriers that are transported through the device to the electrodes without recombining with oppositely charged carriers or traps, and collected by two opposite electrodes, is a basic requirement for a PV material. Thus, a driving force is needed to split excitons into free charge carriers in the conjugated polymers. This driving force is given by offering an energetically favorable pathway for electrons from the polymer (donor) to an electron-accepting material (acceptor) [9]. Since the diffusion length of excitons in a semiconducting polymer is usually shorter than 20 nm [10], excitons must be generated in close proximity to the donor–acceptor (D–A) interface to be dissociated. To fulfill such requirements, the electron acceptor must be intimately mixed with polymer to form an interpenetrated network in the photoactive layer that results in an increase of the contact area and, hence, a more efficient charge separation [4a, 11]. This device structure is called bulk heterojunction (BHJ) and has been extensively studied since its introduction in 1995 [9b]. The most commonly studied systems are BHJ polymer–fullerene combinations, with the polymer acting as the electron donor and the fullerene derivative as the electron acceptor, leading to PCE over 10% [4, 12].

An alternative type of acceptor in polymer solar cells is based on inorganic semiconductor nanocrystals (NCs) [13]. These {conjugated polymers}/{inorganic semiconductor} hybrid materials can take benefit from the properties of both types of materials: easy solution processing of the CPs on one hand and higher thermal and ambient stabilities and higher electron mobility of the inorganic semiconductors on the other. In addition, the morphology of inorganic NCs can be tuned as they can be fabricated in various sizes and shapes, including nanoparticles (NPs) [14], nanorods (NRs) [15], and tetrapods [16]. As such, the possibility to tailor the dimensionality and morphology of inorganic NCs offers the opportunity to optimize the charge transport in polymer–inorganic hybrid solar cells. So far, various hybrid polymer solar cells including inorganic semiconductors such as TiO_2 [17], ZnO [18], CdSe [19], and PbS [20] have been reported. In this chapter, we will focus only on the use of conjugated polymer–inorganic hybrid solar cells based on metal oxide NCs, in particular on TiO_2 and ZnO.

Among the π-conjugated polymers used in polymer solar cells, poly(3-hexylthiophene) (P3HT) is probably the most studied due to its outstanding properties such as its high environmental/thermal stability, its electrical conductivity, and its solution processability [21]. In addition, the availability of synthetic strategy, for example, Kumada Catalyst Transfer Condensative Polymerization (KCTCP) [22], not only enabled to prepare relatively straightforward side-chain and end-functionalized P3HT with multiple topographies (homopolymers, random/block copolymers) and a high degree of control over the final structure and molecular weight but also facilitated the tuning of the optical, self-assembling, and PV properties of the P3HT-based hybrid materials. The scope of this contribution covers recent developments on the synthetic strategies to P3HT, in particular, for end-group and side-chain functionalization. The impact of this functionalization on the resulting P3HT–fullerene and P3HT–metal oxide (ZnO, TiO_2) hybrid nanocomposite materials will also be discussed.

4.2 Design and Synthesis of Regioregular Poly(3-Hexylthiophene)

At the initial stage in the history of P3HT, its synthesis was inspired by the preparation of unsubstituted 2,5-polythiophenes (PTs). The first chemical syntheses of 2,5-coupled PT were described independently by the groups of Yamamoto [23] and the one of Lin and Dudek [24]. In their report, mono-Grignard of 2,5-dibromothiophene was polymerized through metal-catalyzed polycondensation (Scheme 4.1).
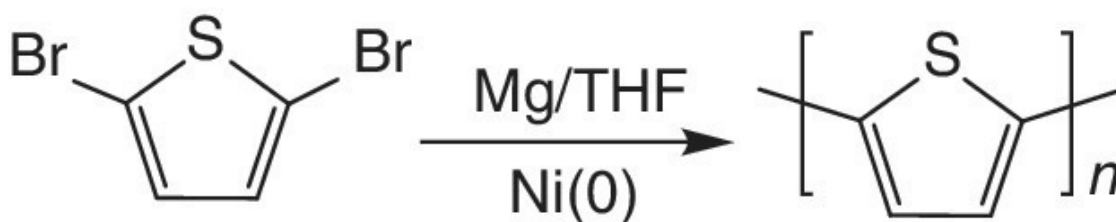
Scheme 4.1 Preparation of PT.

Since then, several synthetic methods were developed such as the metal-catalyzed polycondensation of 2,5-diiodothiophene [25] the Wurtz coupling of 2,5-dilithiothiophene [26], or the electrochemical polymerization [27]. These two latter polymerizations rely on a coupling radical mechanism that leads to a large number of 2,4-couplings and thus decreases the conductivity of the obtained polymer. In general, PTs exhibit excellent thermal stability (weight loss edging up to 42% at 900°C) and conductivity (3.4×10^{-4} to 10^{-1} S.cm^{-1} when polymer is doped with iodine). However, PTs were found to be insoluble in a wide batch of solvents due to the strong π–π interactions between the aromatic rings, as it is the case for a

large number of unsubstituted π-conjugated polymers.

As it was already known that the attachment of flexible side chains onto the backbone of insoluble polymers can dramatically improve their solubility [28], poly(3-alkylthiophenes) (P3ATs) became the subject of intense research. The first environmentally stable and soluble P3ATs were synthesized by Elsenbaumer *et al.* in 1986 using a metal-catalyzed coupling method similar to the one used to prepare 2,5-PT [29]. Unfortunately, this metal-catalyzed polycondensation led to low molecular weight P3ATs. Indeed, in the case of poly(3-butylthiophene), a weight-averaged molecular weight (M_w) of 5000 g.mol^{-1} with a molecular weight distribution ($Đ$) of 2 was obtained. In the same time, high molecular weight P3ATs (M_n = 30 000–300 000 g.mol^{-1}, $Đ$ = 1.3–1.5) were prepared by oxidative polymerization using FeCl$_3$ [30]. Other methods were also developed for synthesizing P3ATs such as the dehalogenation coupling reaction of 2,5-dibromo-3-alkylthiophene by nickel(0) [31] or also the demercuration reaction of 2,5-bis(chloromercurio)-3-alkylthiophene using copper and a catalytic amount of Pd(II) in pyridine (Scheme 4.2) [32]. Although all these methods produce processable P3ATs, it is important to note that the coupling of 3-alkylthiophenes occurs with no regiochemical control and thus produces structurally irregular polymers, termed regioirregular poly(3-alkylthiophenes) (irP3ATs) [22c].
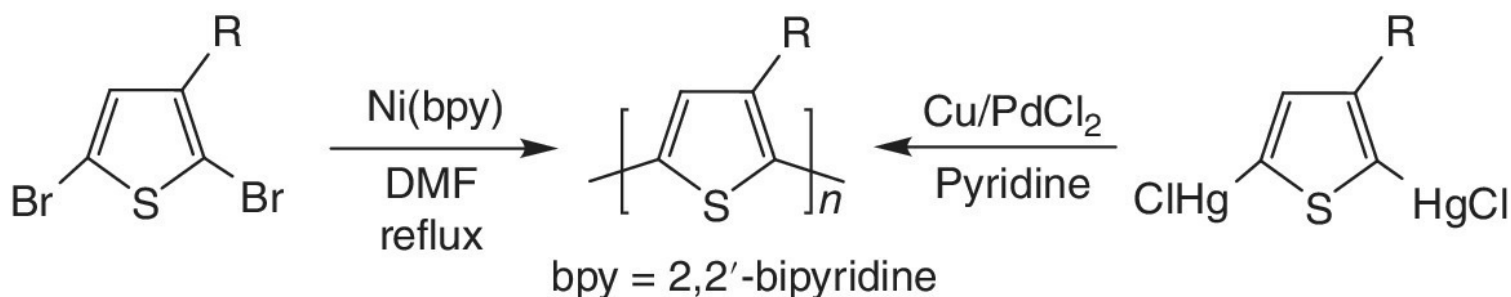
Scheme 4.2 Synthesis of P3ATs by dehalogenation and demercuration reactions.

Indeed, due to the asymmetry of the 3-alkylthiophene molecule, three relative orientations are possible when two 3-alkylthiophene rings are coupled between the 2- and 5-positions (Figure 4.1). The first orientation is 2,5′ or head-to-tail (HT) coupling, the second is 2,2′ or head-to-head (HH) coupling, and the third is 5,5′ or tail-to-tail (TT) coupling. In the case of the coupling of three 3-alkylthiophene rings, the situation becomes even more complicated, leading to four chemically distinct regioisomer triads [33]. irP3ATs prepared by chemical and electrochemical methods described earlier contain mixtures of these isomers, leading to 50–80% HT couplings. The presence of the TT and in particular the HH couplings causes a sterically twisted structure in the polymer backbone, giving rise to a loss of conjugation and thus to a limited conductivity. For example, electrical conductivities of 0.1–20 S.cm^{-1} with an average of 1 S.cm^{-1} when doped with iodine are found for irP3ATs [34]. In addition to electronic properties, it also greatly affects structural and optical properties of this polymer [7b, 11, 21, 22]. Thus, controlling P3HT regiochemistry is of crucial importance. The optimization of such properties requires a high degree of regioregularity and, most particularly, the structurally regioregular HT arrangement.
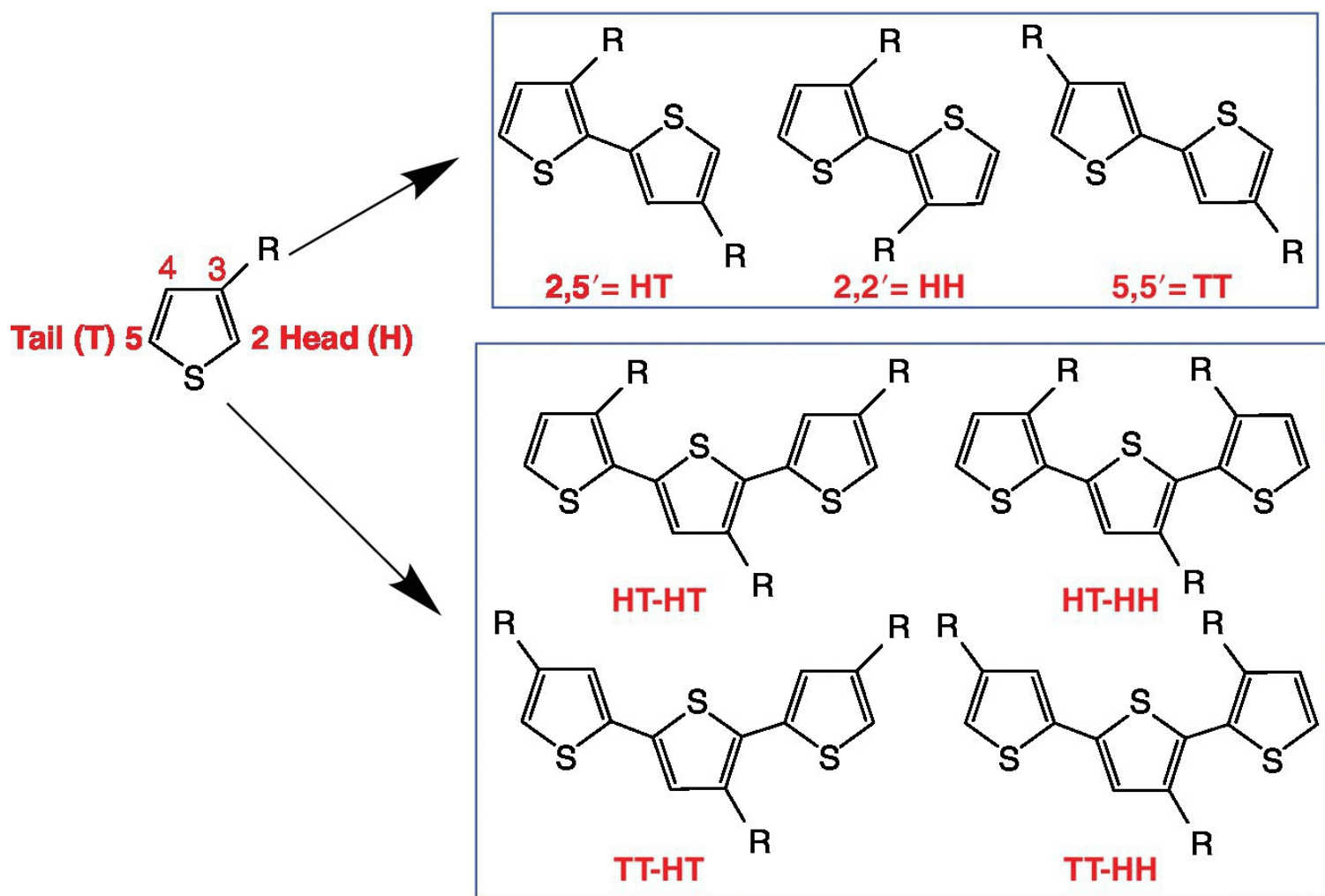
Figure 4.1 Possible regiochemical couplings of 3-alkylthiophenes.

Regioregular HT-P3HTs exhibit a supramolecular architecture consisting of a lamellar structure with two-dimensional conjugated sheets formed by interchain stacking that cannot be seen in irP3HTs [34a, 35–37]. Sirringhaus *et al.* suggested that P3HT adopts two different orientations (i.e., parallel and normal to the film) that depend on its regioregularity and processing conditions [36]. Indeed, P3HTs with high HT regioregularity (rr = 96%) but low molecular weight (M_n = 28 000 g.mol^{-1}) form lamellae with "edge-on" arrangement, while P3HTs with low HT regioregularity (rr = 81%) and high molecular weight (M_n = 175 000 g.mol^{-1}) were found to adopt a "plane-on" or flat orientation (Figure 4.2) [36]. X-ray diffraction (XRD) data of highly rrP3HT film prepared by casting from simple evaporation of a high boiling point solvent (chlorobenzene, xylene) on a glass side exhibited three highly ordered (*h00*) scattering peaks that corresponded to the lamellar stacks in the out-of-plane direction (q_z) [22c, 36, 39]. A narrow single wide-angle reflection (*010*) peak was also observed, corresponding to the π−π stacking in the in-plane direction (q_{xy}). These scattering peaks indicated a well-organized structure with edge-on geometry of the polymer. As the rr decreased, the intensities of these peaks became much weaker, indicating that a clear loss of crystallinity of the P3HT polymers. For example, for a P3HT (M_n = 9200 g.mol^{-1}, Đ = 1.33) with low regioregularity (rr = 64%), the π−π stacking peaks almost disappeared and became quite weak and broad [39b]. The quantitative effects of the regioregularity on the crystallinity and thermal properties of the P3HT were also examined by DSC [39b]. P3HT with high values of rr exhibit high melting (T_m) and crystallization (T_c) temperatures (T_m = 231°C and T_c = 200°C for P3HT (rr = 98%) with the following

features: $M_n = 20\,300$ g.mol^{-1}, $Đ = 1.08$) [39b, 40]. As the rr decreased, T_m and T_c decreased progressively until they disappeared or became almost negligible [39b]. This strong decreasing trend in both T_m and T_c is concomitant with a remarkable decrease in the interchain interaction and the decreasing degree of crystallinity [39b].

(a)
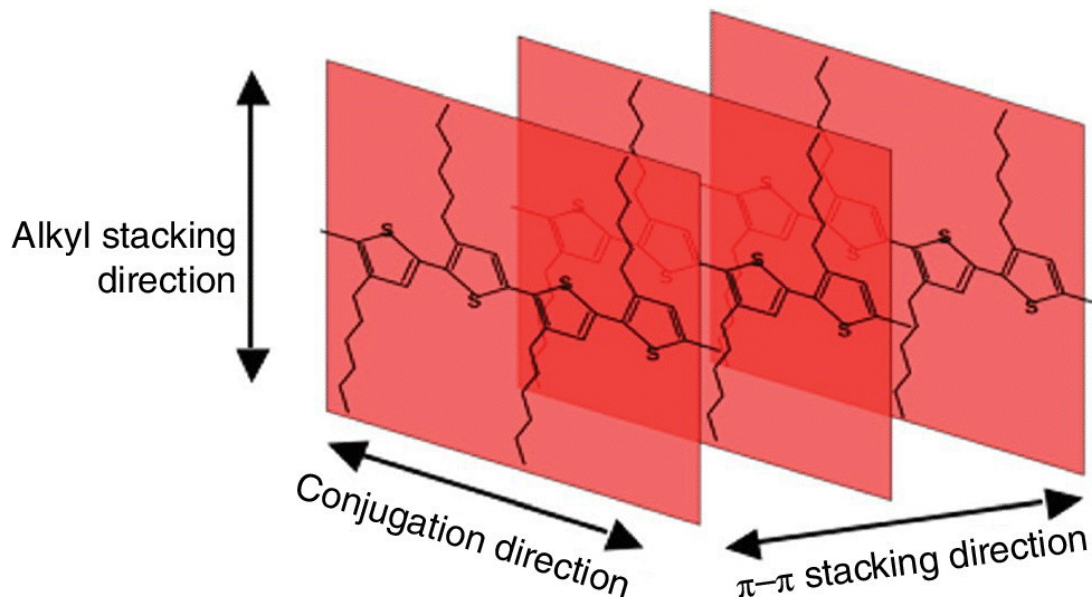
(b)
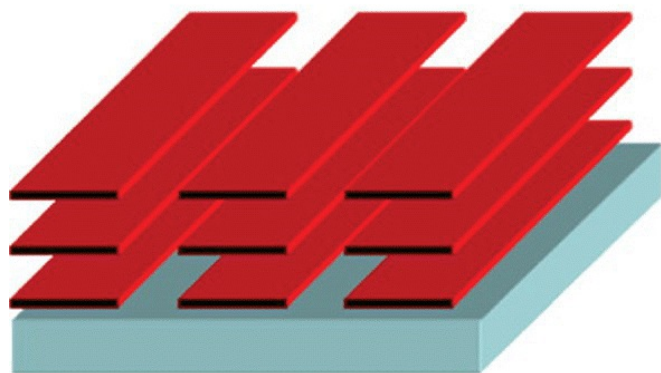
(c)
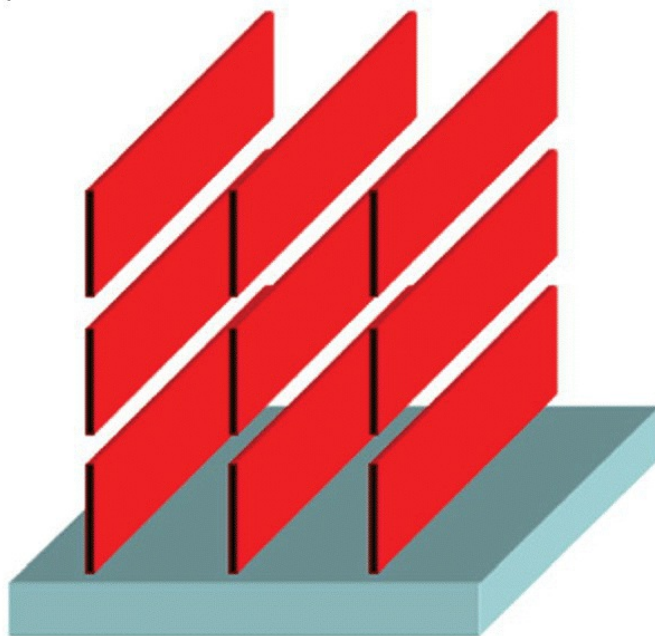
Figure 4.2 (a) Schematic structure showing the preferred arrangement of adjacent chains of regioregular HT-P3HT. (b) Plane-on orientation of P3HT with respect to an underlying surface. (c) Alternative edge-on arrangement.

Source: Salleo [38]. Reproduced with permission of Elsevier.

Electrical properties are also strongly correlated with the regioregularity. Due to their three-dimensional self-assembled superstructure, rrP3HT exhibits efficient two-dimensional hole transport [36] with high

mobilities and current density [41]. Jiang *et al.* evaluated mobilities of charge carriers in films of P3HTs with HT regioregularities of 97, 81, 70, and 54% as a function of the doping level [41c]. The difference in regioregularity of P3HT resulted in a large mobility difference, especially in the low-doping regime. At the highest doping level of ~20%, the mobility values reached 0.4 and 0.01 $cm^2.V^{-1}.s^{-1}$ for the film of P3HT 97% and P3HT 54%, respectively. Kim *et al.* reported a similar decreasing trend in hole mobilities (μ_h) for P3HT with decreasing regioregularity [39b]. These findings were attributed to the presence of regio-defects into the polymer backbone that decreased the crystalline order and thus the μ_h value.

The regioregularity also plays an important role in the bandgap control. In UV–visible (Uv-Vis) absorption, rrP3HT showed a significant redshift of the maximum absorption (λ_{max}) with respect to irP3HTs [22c, 39b]. As an example, λ_{max} in solution for rrP3HT with rr = 98% and rr = 64% were found to be 457 and 441 nm, respectively [39b]. This redshift indicates that the rrP3HT has a π–π* transition at lower energy and thus a longer π-conjugation, attributed to the more planar conformation of the regioregular polymer chains [34b]. The difference in λ_{max} between regioregular and regioirregular PTs becomes more distinct in the film. rrP3HT (rr = 98%) shows a λ_{max} at 557 nm, while rrP3HT (rr = 64%) exhibits a λ_{max} at 496 nm [39b]. The vibronic peaks (A_{0-1} and A_{0-0}) were also significantly decreased as the rr decreased [39b]. As such, the corresponding optical bandgaps ($E_g$opt) of the P3HTs were increased gradually from 1.88 eV (rr = 98 %) to 1.94 eV (rr = 64 %). The change of planarity and in molecular packing of the P3HTs influenced the highest occupied molecular orbital (HOMO) and the lowest unoccupied molecular orbital (LUMO) levels of the P3HT [39b, 42]. As the rr decreased, the HOMO and LUMO decreased progressively [39b].

Besides the HT regioregularity, P3HT molecular weight and dispersity are also important parameters to consider since they influence optical, electronic, and electrochemical properties and solid-state packing [36, 43–48]. For instance, Russell *et al.* investigated the absorption profiles of thin films prepared with P3HT of different molecular weights and spin-coated from chlorobenzene [49]. Although all rrP3HTs showed spectral tails extending to 700 nm, significant differences in λ_{max} were noticed. As molecular weight increased, λ_{max} was redshifted and the shoulder at 605 nm was more pronounced. It is interesting to note that for polymers with molecular weight higher than 10 000 $g.mol^{-1}$, the absorption profiles were similar, indicating that the effective main-chain conjugation length saturates [50]. It was suggested that the blueshift in low molecular weight P3HT (5000 $g.mol^{-1}$) was due to a less ordered structure in comparison with higher molecular weight samples [51]. Indeed, molecular weight has a considerable impact on the crystalline connectivity and ordering of pristine P3HT spin-cast films [36]. X-ray studies revealed a change in (*100*) spacing for low molecular weight P3HT, which indicated that there might be some disorder of alkyl side chains, leading to disorder in its crystal [48, 52]. This finding was also demonstrated by DSC measurements [40a, 49]. With increasing molecular weight, the melting point of P3HT increased, which indicates a higher degree of crystallinity for high molecular weight polymers. It was in particular proved that the degree of crystallinity reaches a maximum at intermediate molecular weights [49]. Polymer dispersity was also pointed out as a limiting factor for crystallinity [40a].

This crystal disorder influences the charge carrier mobility of polymer. It was reported that lowering the molecular weight results in a charge carrier mobility decrease of several orders of magnitude [45b, 46c, 49]. This drop-off was attributed to a poor connectivity between well-defined, highly crystalline grains and/or differences in backbone conformation between high and low molecular weight chains [45b, 46c, 53]. More recently, Salleo *et al.* reported that a large polymer dispersity, in particular due to the presence of low molecular weight fractions in high molecular weight P3HT, is detrimental to charge properties,

due to molecular mixing of high and low molecular weight chains, reducing the density of aggregate connecting molecules [52].

All the aforementioned considerations clearly indicate that synthetic polymerization methods that allow the formation of regioregular P3HT with desired molecular weight and narrow dispersity are required to enhance the material self-assembly ability and therefore its bulk properties. As indicated earlier, P3HT could be synthesized by either chemical or electrochemical polymerizations [21]. In this chapter, we will focus on chemical polymerizations since they offer the advantage of large-scale synthesis and provide excellent yields.

4.2.1 Metal-Catalyzed Cross-Coupling Reactions

4.2.1.1 Nickel-Catalyzed Cross-Coupling Reactions

The most commonly used methods for the synthesis of rrP3ATs are usually the following three methods: the McCullough [22c], Rieke [35], and KCTCP methods [22, 54]. More recently, Mori *et al.* reported the synthesis of rrP3ATs through C–H coupling methods [55]. All these methods allow the synthesis of rrP3ATs of comparable regioregularities. However, the Rieke method offers the advantage of being much more tolerant to functional groups carried by the monomer. Details concerning each of these methods are shown and compared in Figure 4.3.
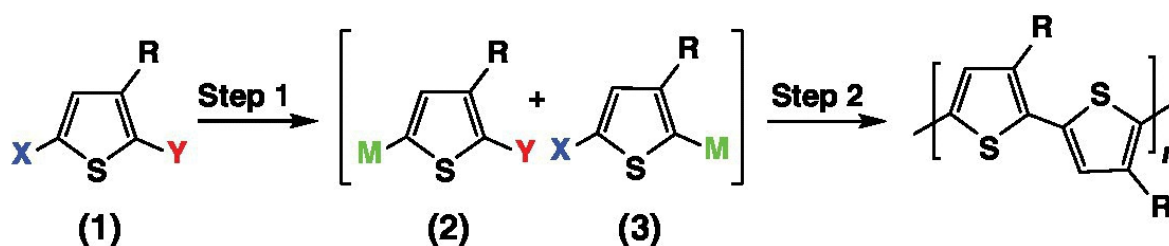
Method	X, Y	Step 1	M (ratio (2):(3))	Step 2	% of rr
McCullough	H, Br	(1) LDA/THF, −40°C, 40 min (2) MgBr$_2$.Et$_2$O(ZnCl$_2$), −60°C to −40°C, 40 min	MgBr (ZnCl) (98:2)	Ni(dppp)Cl$_2$, −5 to 25°C, 18 h	98–100
Rieke	Br, Br	Zn*/THF, −78°C to rt, 4 h	ZnBr (90:10)	Ni(dppp)Cl$_2$, 0°C to rt, 24 h	97–100
	I, Br		Zn (100:0)		
KCTCP	Br, Br	R′MgX′/THF, rt or reflux, 1 h	MgX′ (85:15)	Ni(dppp)Cl$_2$, rt or reflux, few hours	>99
	I, Br		MgX′ (100:0)		
C–H coupling	H, Br	TMPMgCl.LiCl, rt, 30 min	MgCl.LiCl (99:1)	NiCl$_2$(dppp)	97
				NiCl$_2$(dppe)	98

Figure 4.3 McCullough, Rieke, KCTCP, and C–H coupling methods for the synthesis of rrP3ATs.

The first synthesis of rrP3ATs was reported by McCullough and Lowe in 1992 [34c]. This polymerization

method consists of a two-step process. In the first step, 3-alkyl-2-bromo-5-bromomagnesiothiophene (**2**) is selectively prepared by treatment of 3-alkyl-2-bromothiophene (**1**) with lithium diisopropylamide (LDA) at −40°C, followed by the addition of $MgBr_2.Et_2O$ at −60°C. In a second step, an *in situ* polymerization of (**2**) by a Kumada cross-coupling reaction with dichloro[1,3-bis(diphenylphosphino)propane]nickel (II) ($Ni(dppp)Cl_2$) as catalyst is performed. By following this method, rr-HT-P3AT with regioregularity of 98–100% and with isolated yields between 44 and 66% were obtained [22c]. Molecular weights commonly obtained with the McCullough method are typically 20 000–40 000 $g.mol^{-1}$ ($Đ \sim 1.4$) [34, 56].

Shortly after these first studies, an alternative method was described by Chen and Rieke [35]. The main innovation of this polymerization method lies in the use of highly reactive "Rieke zinc" (Zn*) for generating the asymmetric organometallic intermediate. Thus, zinc reacts with (**1**) and leads to the formation of two regioisomers: 3-alkyl-2-bromo-5-bromozinciothiophene (**2**) and 3-alkyl-5-bromo-2-bromozinciothiophene (**3**) in a 90 : 10 ratio. The control of the regioregularity in these polymerizations was explained by the steric hindrance of the molecule during the reductive elimination step of the catalytic cycle. An alternative approach to obtain exclusively monomer (**2**) consists in using 3-alkyl-5-bromo-2-iodothiophene instead of 3-alkyl-2,5-dibromothiophene. Molecular weight commonly obtained with the Rieke method are typically 24 000–34 000 $g.mol^{-1}$ ($Đ \sim 1.4$).

To avoid the use of the specially prepared zinc active metal (Zn^*) in this reaction, Kim and Kim replaced it by a commercially available and relatively cheap zinc powder in the preparation of regioregular P3HT [57]. By using zinc dust and 2-bromo-3-hexyl-5-iodothiophene whom C–I bond is more suitable to zinc insertion [58], polymerization of organozinc was easily achieved at room temperature. Regioregular P3HTs with regioregularity up to 96% and molecular weight of $M_w = 28\,000$ $g.mol^{-1}$ ($Đ = 1.98$) were obtained. In a later contribution, the same authors replaced zinc dust by a readily available and commercially available diisopropyl zinc that allows preparation of thienylzinc monomer under mild conditions (room temperature, 1 h) [59]. The polymerization of this thienylzinc afforded P3HT with excellent HT regioregularity (>98%). M_n as high as 20 000 $g.mol^{-1}$ were achieved ($Đ = 1.4$–1.6). Recently, Higashira *et al.* reported the preparation of a zincate thiophene monomer by treatment of 2-bromo-3-hexyl-5-iodothiophene with tBu_4ZnLi_2 at 0°C (Scheme 4.3) [60]. Polymerization of zincate thiophene monomer afforded regioregular P3HTs (rr > 97% when $M_n > 10\,000$ $g.mol^{-1}$) with highly controlled molecular weights and low dispersity.
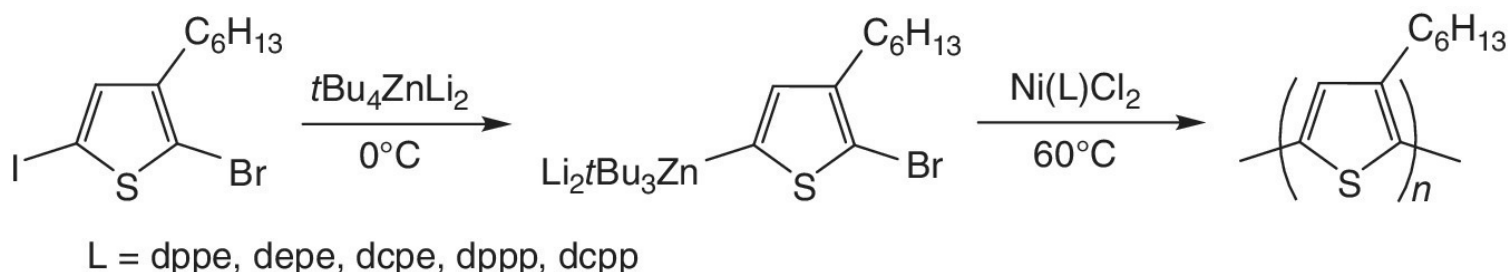
Scheme 4.3 3HT polymerization from zincate monomer with $Ni(L)Cl_2$ [L = dppe (1,2-bis(diphenylphosphino)ethane), depe (1,2-bis(diethylphosphino)ethane), dcpe (1,2-bis(dicyclohexylphosphino)ethane), dppp (1,3-bis(diphenylphosphino)propane), and dcpp (1,2-bis(dicyclohexylphosphino)propane].

Another approach named Kumada catalyst transfer condensative polymerization for the synthesis of rrP3ATs was reported [61]. Compared with the McCullough and Rieke methods, KCTCP method does not

require cryogenic temperatures or highly reactive metals ("Rieke zinc"). In this method, 3-alkyl-2,5-dibromothiophene (**1**) is treated with one equivalent of commercially available organomagnesium compounds, leading to a mixture of 3-alkyl-2-bromo-5-bromomagnesiothiophene (**2**) and 3-alkyl-2-bromo-5-bromomagnesiothiophene (**3**) in a 85 : 15 ratio [62]. This ratio is independent of the reaction time, the temperature, and the nature of the Grignard reagent. As the Rieke method, the choice of 3-alkyl-2-bromo-5-iodothiophene instead of 3-alkyl-2,5-dibromothiophene allows to obtain monomer (**2**) exclusively. This latter is polymerized *in situ* by a Kumada cross-coupling reaction with Ni(dppp)Cl$_2$ as a catalyst. In general, KCTCP method leads to rrP3ATs with a very high regioregularity above 99% due to a combination of thermodynamic and kinetic effects. Molecular weight commonly obtained with KCTCP method is typically between 20 000 and 35 000 g.mol^{-1} with low dispersities ($Đ = 1.2–1.4$) [61d].

The proposed mechanism for this polymerization reaction is described in <u>Scheme 4.4</u> [22d, 61]. The first step consists in the reaction of 3-alkyl-2-bromo-5-bromomagnesiothiophene (**1**) with Ni(dppp)Cl$_2$, leading to the organometallic nickel complex (**2**). Complex (**2**) immediately undergoes a reductive elimination to obtain an associated pair, consisting of 2,2′-dibromo-3,3′-dialkyl-5,5′-bithiophene (**3**) (TT coupling) and Ni(0)(dppp) (**4**). This step is followed by an addition of dimer (**3**) on Ni(0) (**4**), leading to nickel complex (**5**). 3-Alkyl-2-bromo-5-bromomagnesiothiophene (**1**) reacts with (**5**) through a transmetalation reaction to form complex (**6**). Reductive elimination of complex (**6**) leads then to a new associated pair based on terthiophene (**7**) and Ni(0) complex (**4**). The polymerization reaction continues to take place through successive insertions of monomer (**1**) following the catalytic cycle based on oxidative addition, transmetalation, and reductive elimination. Ni(dppp) is systematically incorporated into the growing polymer chain. Thus, Ni(dppp)Cl$_2$ is not only a catalyst but also a precursor of active species. Even though π-complex formed by Ni(0)–polymer has never been demonstrated, intermediates (**8**) and (**9**) have been identified, notably by ^{31}P NMR, which directly supports the proposed mechanism [63].
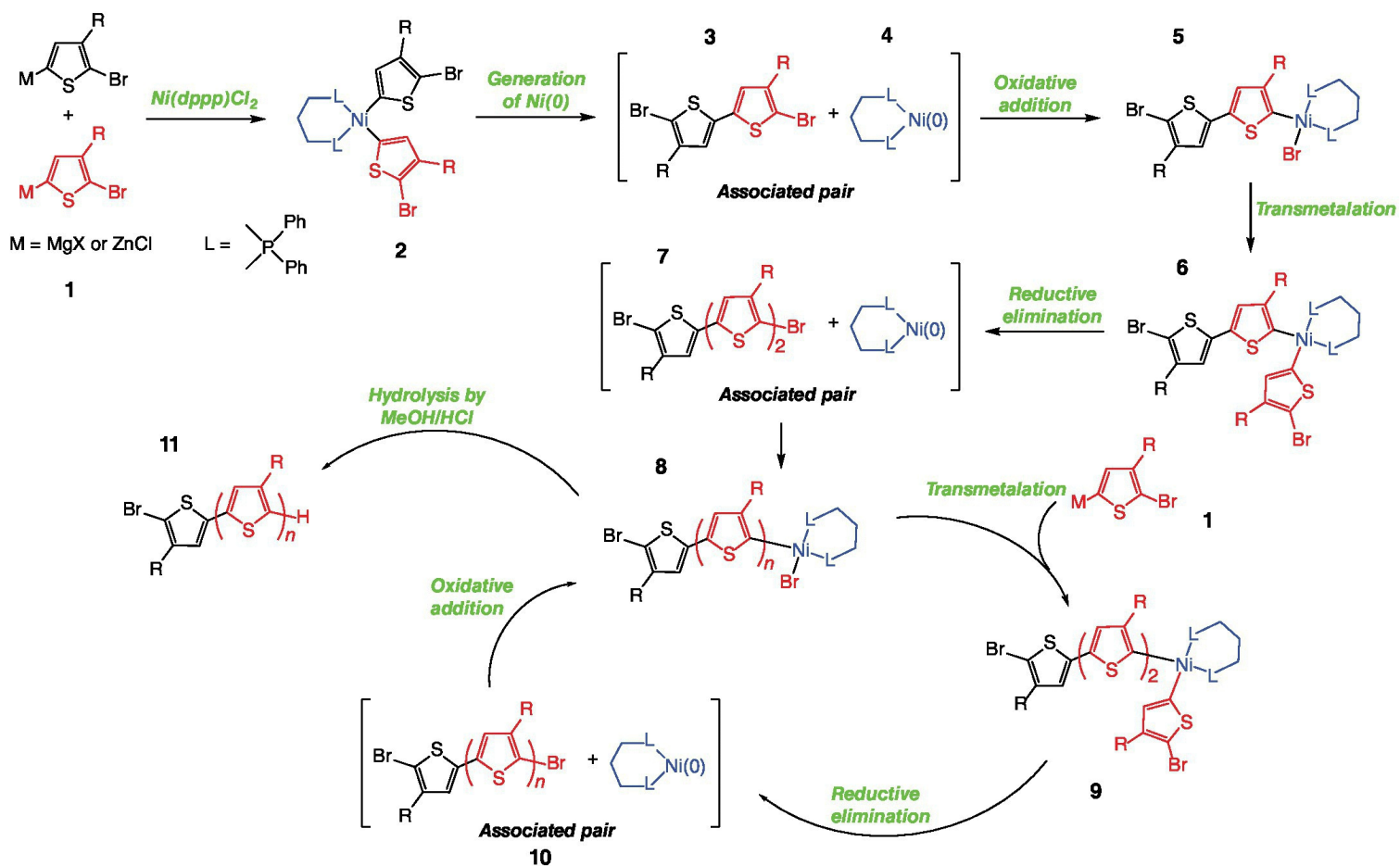
Scheme 4.4 Mechanism of the KCTCP method proposed by McCullough and Yokozawa.

Source: Yokozawa and Ohta [22]. Reproduced with permission of John Wiley & Sons.

Based on the Kumada coupling mechanism for small molecules, it was thought that the KCTCP method followed a step-growth process. However, studies carried out by McCullough and Yokozawa showed that this polymerization followed a living chain-growth polymerization mechanism since molecular weight increased linearly with the monomer conversion as well as to the feed ratio of monomer to the Ni catalyst and that the molecular weight distributions were found to be narrower ($Đ = 1.2–1.5$) than for a polycondensation route [21, 22]. The chain-growth mechanism of the polymerization was also examined by a "monomer-addition" experiment. When additional monomer was added to the polymerization mixture, a shift toward the higher molecular weight region was observed in the GPC, while the dispersity was maintained within low range [61b]. Quite interestingly, a shoulder peak in the GPC chromatogram in the high molecular region with a molecular weight twice the main peak was observed after precipitation of the samples. Yokozawa *et al.* assigned this second peak to disproportionation reactions taking place when H_2O or MeOH was used as quenching agents [61c]. This problem was solved by quenching polymerization reactions with 5 M HCl.

Due to the living nature of KCTCP polymerization, synthesis of block copolymers was achieved through the sequential addition of monomers [22]. One possible explanation to the living chain-growth nature of nickel-catalyzed cross-coupling polymerization of 3HT was proposed by Yokozawa *et al.*, suggesting that the oxidative addition was kinetically slower or thermodynamically less stable for monomer than for the growing polymer chain [64]. For a long time, it was supposed that polymerization proceeds unidirectionally from one side of the initiating TT dimer (**3**) (Scheme 4.4) due to the formation of an associated pair between the nickel(0) complex and the thiophene growing chain, which is supposed to

limit polymerization to one end of the polymer chain [65]. However, few years ago, Tkachov *et al.* showed by externally initiated 3HT polymerization from a Br-C_6H_4-Ni(dppe)-Br (dppe = 1,3-bis(diphenylphosphino)ethane) initiator that two kinds of differently terminated P3HT were formed [66]. One is the "normal" P3HT with a bromophenyl end group, whereas the other one incorporates the phenyl group inside the P3HT chain. This finding indicates unambiguously that Ni(0) is able to walk along the polymerizing chain and to insert at both sides of the initially formed symmetric TT dimer (**3**) at all times of polymerization [40a, 66]. Summer *et al.* investigated the effect of the incorporation of this TT defect within the backbone on the crystallization behavior [40a]. Based on a combination of NMR analyses and computer simulations, it was estimated that 20–30% of the polymer chains contained a TT defect at the chain end ([Figure 4.4](#)), this percentage decreasing with increasing molecular weight. The inclusion of this TT defect in the polymer chain leads to a slightly reduced degree of crystallinity compared with the "defect-free" P3HT of similar molecular weight. However, in the case of optical properties, a significant effect was reported [40a]. The defect-free P3HTs exhibited a clear trend toward longer conjugation lengths and more planar backbones as demonstrated by the higher ratio of the first and second vibronic transition A_{0-0}/A_{1-0} in UV-Vis absorption spectroscopy and the strong E_{0-0} peak in photoluminescence spectroscopy.
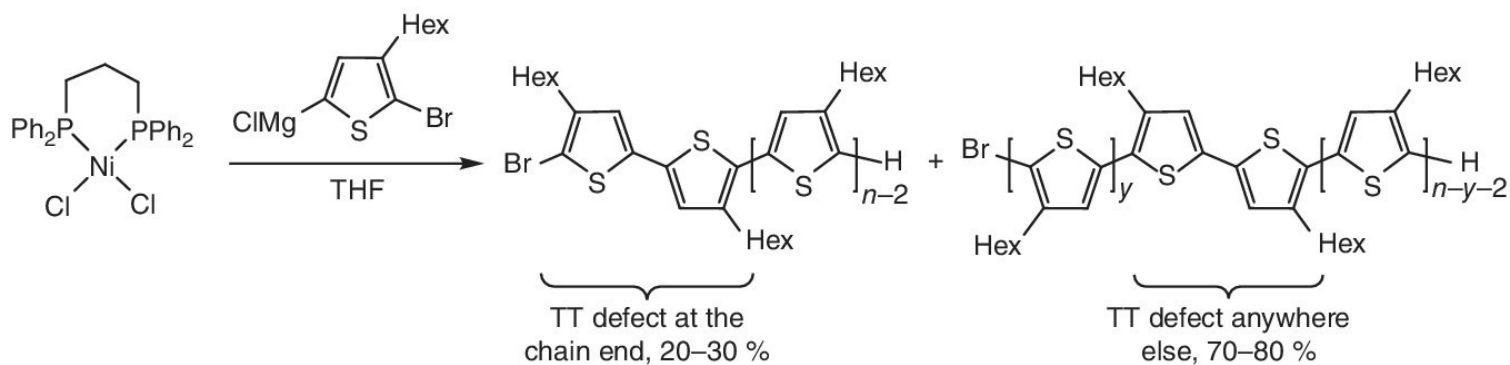
[Figure 4.4](#) Regioregular P3HT with one TT defect being distributed within the chain.

The presence of this bidirectional growth becomes more problematic in one-pot synthesis of block copolymers A and B, resulting in not only AB diblock but also BAB triblock copolymers. To overcome this problem or to synthesize "defect-free" P3HT, synthetic methods for unidirectional polymer growth based on external initiators (ArNi(dppp)X (X = Cl, Br)) were developed [22a, b]. Kiriy *et al.* first described externally initiated 3HT polymerization through the oxidative addition of Ni(PPh$_3$)$_4$ with photo-cross-linked poly(4-bromostyrene) films [67]. Unfortunately, such polymerization failed, probably because of the weak reactivity of the coordinatively saturated Ni(PPh$_3$)$_4$ complex [31, 54]. In this respect, Locklin *et al.* used Ni(COD)$_2$ (COD = 1,5-cyclooctadiene) as the source of Ni(0) and combined it with triphenylphosphine (PPh$_3$) to generate Ni(0) species for preparing surface-grafted conjugated polymers [68]. In that system, the weakly bonded COD ligands are displaced by PPh$_3$, leading to the formation of a reactive intermediate species, Ni(COD)(PPh$_3$)$_2$. Unfortunately, PPh$_3$ is an attendant ligand that offers poor results in KCTCP in comparison with its bidentate dppp and dppe counterparts. The direct incorporation of dppp or dppe into KCTCP initiators is not a trivial task, since Ni(dppp)$_2$ and Ni(dppe)$_2$ complexes are nearly inert toward oxidative addition [69]. To overcome this problem, Luscombe [70] and Kiriy [71] independently developed ligand exchange reactions allowing the preparation of surface-bound initiators carrying state-of-the-art bidentate phosphine ligands.

These initiators were prepared by reacting surface-bound aryl halides with Ni(PPh$_3$)$_4$ and Et$_2$Ni(bpy)

(bpy = 2,2′-bipyridine), followed by ligand exchange with dppe or dppp. This strategy is however very sensitive since Et$_2$Ni(bpy) decomposes quickly in the presence of air and water, making it difficult to handle. Similar exchange processes have been also developed by the group of Locklin [72]. In this method, a substrate containing an immobilized aryl halide as initiator is immersed in a Ni(COD)$_2$/PPh$_3$ or bpy solution, followed by ligand exchange with dppp. Clément *et al.* successfully applied to grow "hairy" P3HT brushes from titanium oxide nanoparticles (NPs) (Scheme 4.5) [73]. Such nickel initiators are obtained from the reaction of an aryl halide with a nickel catalyst. It was reported that the type of functional group present on the aryl halide plays a crucial role in polymerization [70, 74]. McNeil and coworkers reported that electron-donating groups (OMe or NMe$_2$) lead to polymers with low dispersity, whereas electron-withdrawing groups (CF$_3$ or F) provided polymers with higher dispersity. These differences were attributed to the variance in the rate of the reductive elimination step [74]. The electronic properties of the ligand of the initiator were also found to influence the polymerization reaction. McNeil *et al.* have modified the steric and electronic properties of the bidentate phosphine by introducing different substituents on the phosphorus atom [75]. It was notably found that the ligand steric contribution must be well balanced to avoid the derailment of the chain-growth process [74c]. In addition, electron-rich ligands outperform electron-poor ligands in terms of controlling molecular weight distribution [75]. Although bidentate phosphines are by far the most used ligands in such polymerizations, monodentate phosphines [76], carbenes [77], and diimine ligands [78] have also been used.
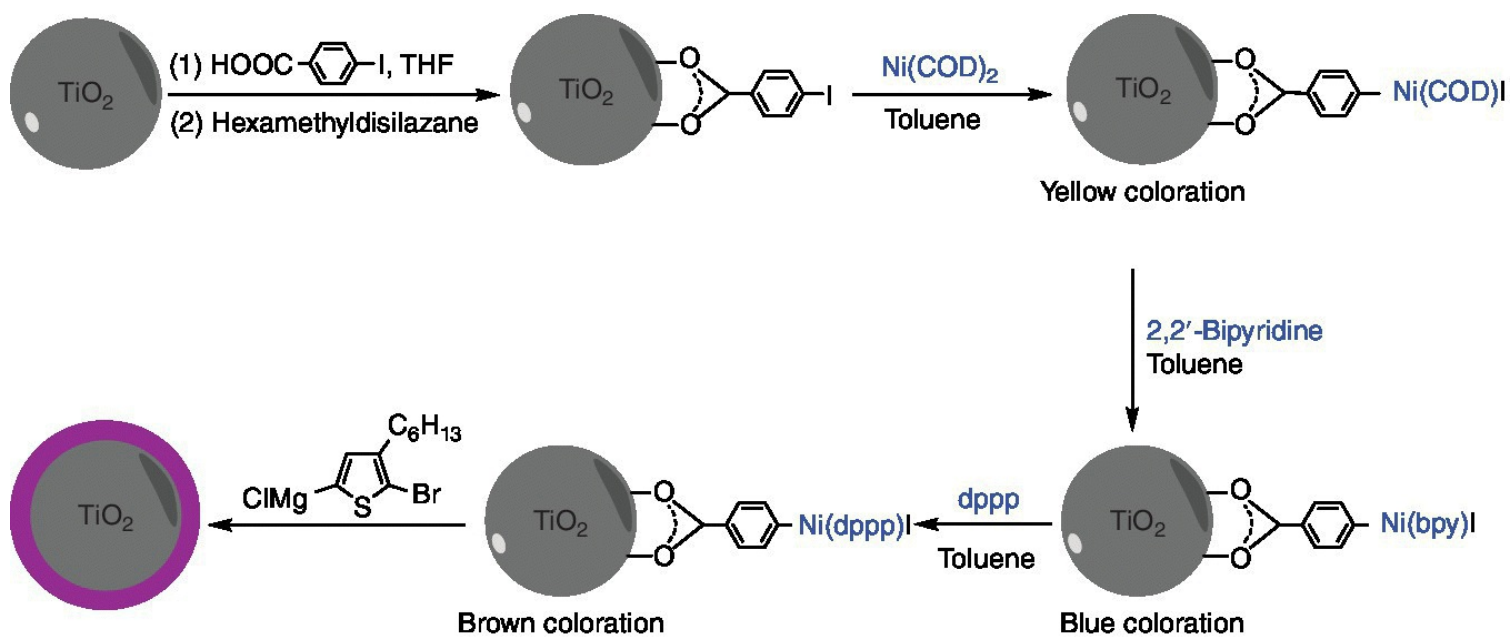
Scheme 4.5 Preparation of poly(3-hexylthiophene) brushes by a "grafting from" strategy followed by ligand exchange reactions.

Source: Boon *et al.* [73]. Reproduced with permission of American Chemical Society.

Recently, Mori and coworkers developed a C—H coupling polymerization reaction based on the use of Knochel–Hauser base (TMPMgCl · LiCl, chloromagnesium 2,2,6,6-tetramethylpiperidide lithium chloride salt) (Scheme 4.6) [55]. This method was found to be highly effective for the synthesis of oligothiophenes [79]. The treatment of 2-bromo-3-hexylthiophene with TMPMgCl · LiCl afforded the corresponding organometallic species, which were polymerized efficiently with Ni(dppe)Cl$_2$ or Ni(dppp)Cl$_2$ as catalyst [55e]. P3HTs with high regioregularities (>97%), molecular weight higher than 40 000 g.mol^{-1}, and relatively narrow dispersity ($Đ \sim 1.3$) were obtained. The same authors also investigated the polymerization of 2-chloro-3-substituted thiophenes in order to improve the atom

efficiency. Grignard monomers were generated *in situ* by using a stoichiometric amount of magnesium amide (TMPMgCl · 3LiCl) and polymerized using a nickel catalyst bearing a carbene ligand (NiCl$_2$(dppe) was not effective for this polymerization). P3HTs with controlled molecular weights (5200–29 000 g.mol^{-1}) and narrow molecular weight distributions ($Đ = 1.15$–1.31) were obtained [55d].
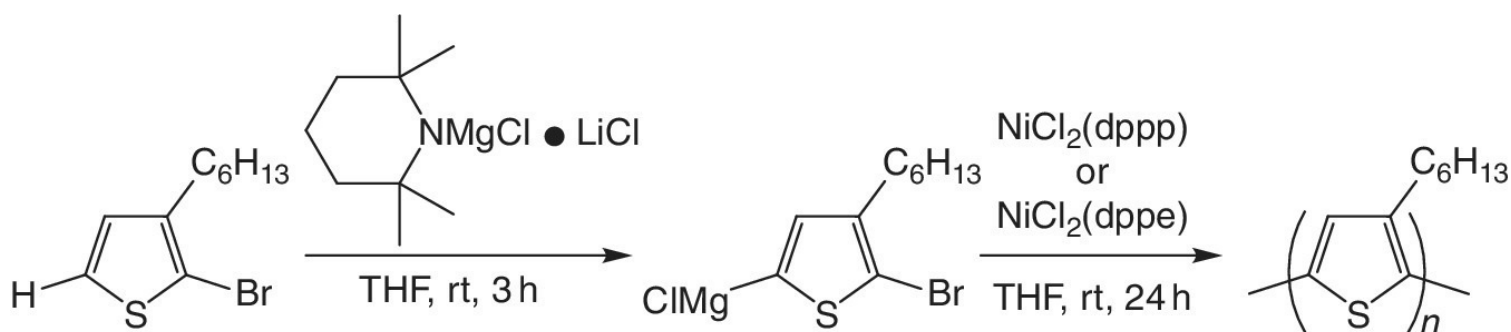
Scheme 4.6 C–H coupling polymerization applied to the generation of rrP3HT.

4.2.1.2 Palladium-Catalyzed Cross-Coupling Reactions

While nickel catalysts are probably the most common precatalysts used for Kumada and Negishi coupling reactions, palladium systems allow broadening. Thus, Stille, Suzuki, or C─H arylation coupling methods can also be used for the synthesis of rrP3HTs.

4.2.1.2.1 Stille Cross-Coupling Polymerization

Stille coupling is one of the most versatile methods for preparing highly functional semiconducting polymers via step-growth polycondensation of A–A and B–B monomers [80]. Surprisingly, few studies have been conducted on the chain-growth polymerization of organotin monomers [81–83]. Iraqi and Barker have first reported the synthesis of regioregular P3HT (rr > 96%) through the Stille reaction using 3-hexyl-2-iodo-5-(tributylstannyl)thiophene (a, Scheme 4.7) [81]. This tin-based thiophene monomer has the advantage of being air and moisture stable over its Grignard counterpart, allowing its purification. Polymerization reactions were carried out in different solvents (THF, toluene, 1,2-dichlorobenzene) at reflux temperature and in the presence of Pd(PPh$_3$)$_4$ (3 mol%) as catalyst. Molecular weights of rrP3HT prepared by this method were $M_n = 10\,000$–$16\,000$ g.mol^{-1} with $Đ = 1.2$–1.4 after purification by Soxhlet extraction. It is interesting to note that the rate of these polymerizations is slower compared with polymerization reactions involving 2-bromo-3-hexyl-5-bromomagnesiothiophene or 2-bromo-3-hexyl-5-bromozinciothiophene, explaining why lower yields were obtained (10–50%) [21b].
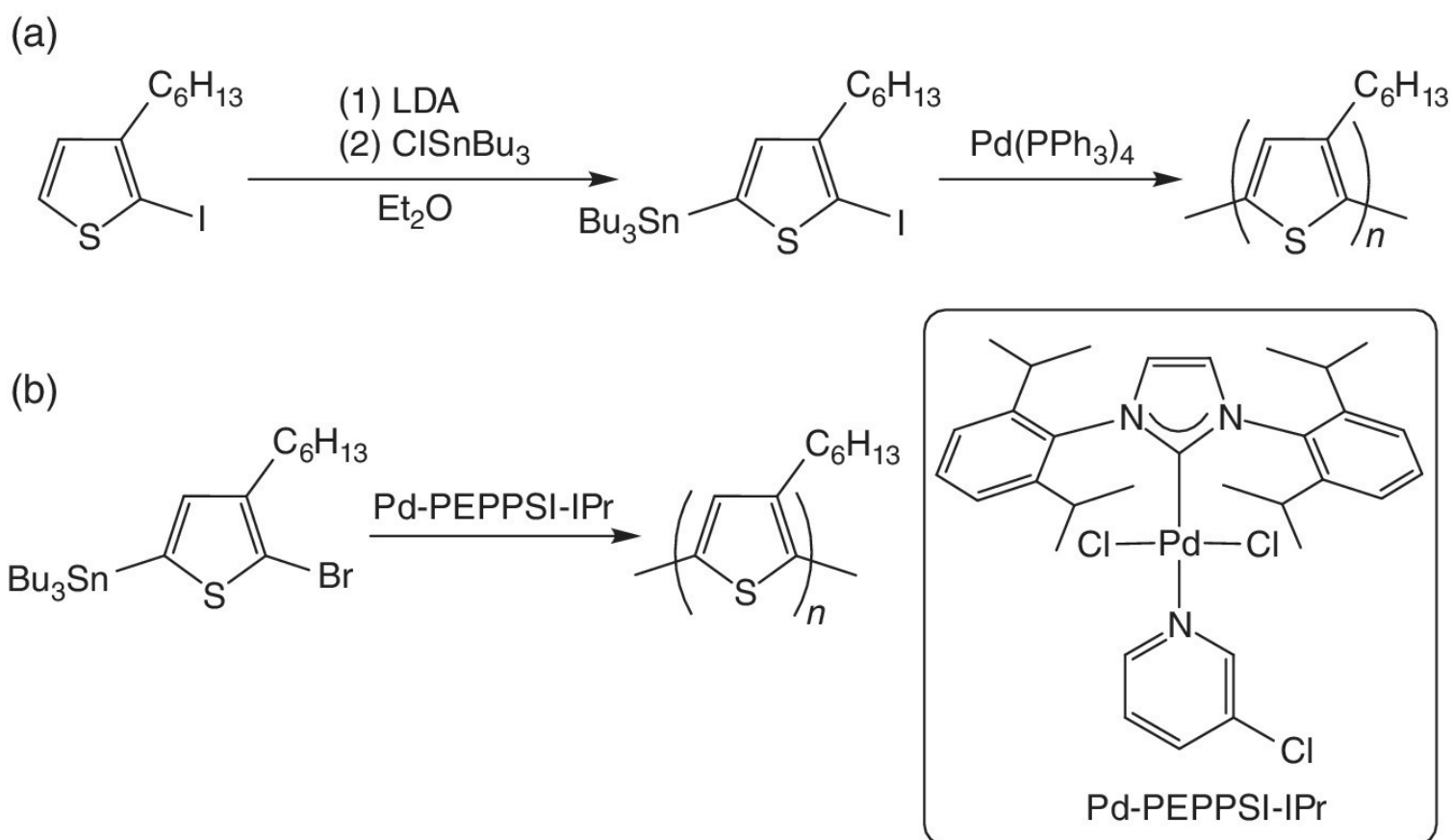
Scheme 4.7 Synthesis of HT rrP3HT by Stille coupling reactions.

More recently, Noonan and coworkers investigated the polymerization of 2-bromo-3-hexyl-5-trimethylstannylthiophene using a commercially available palladium *N*-heterocyclic carbene (Pd-NHC) complex as a catalyst (b, Scheme 4.7) [83]. A "ring walking" process was also showed for the palladium catalyst by ^{1}H NMR analysis. The polymerization proceeds in a chain-growth manner with M_n increasing linearly with monomer conversion. Regioregular HT P3HTs with molecular weights between 7000 and 73 000 g.mol^{-1} and molecular weight distributions between 1.14 and 1.53 were obtained by varying the catalyst concentration.

4.2.1.2.2 Suzuki Cross-Coupling Polymerization

Suzuki–Miyaura cross-coupling is widely used for organic synthesis and polymer synthesis since it offers several advantages such as air-stable precursors, wide functional group tolerance, high regioselectivity, and easy removal of low-toxicity by-products [84]. This polymerization can also be carried out under aqueous reaction conditions. Higgins and coworkers first reported the synthesis of P3HT by the Suzuki reaction using a range of Pd catalysts with bulky, electron-rich phosphane ligands such as P(*t*Bu)$_3$ and (*o*-biphenyl)PR$_2$ (R = *t*Bu, cyclohexyl) ligands (a, Scheme 4.8) [85].
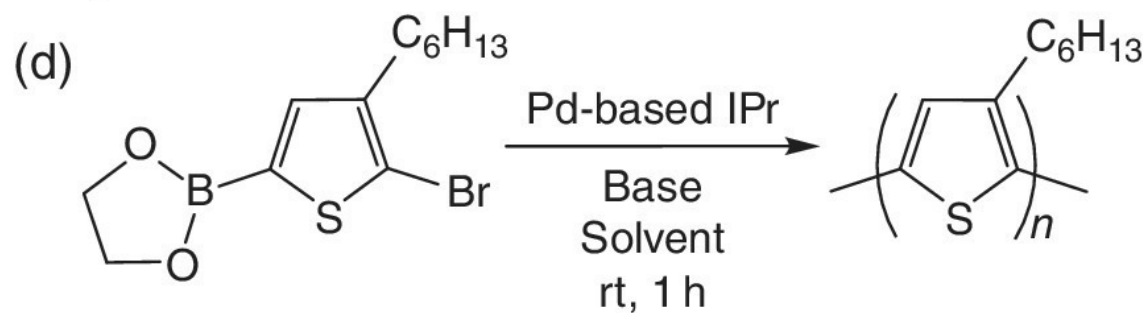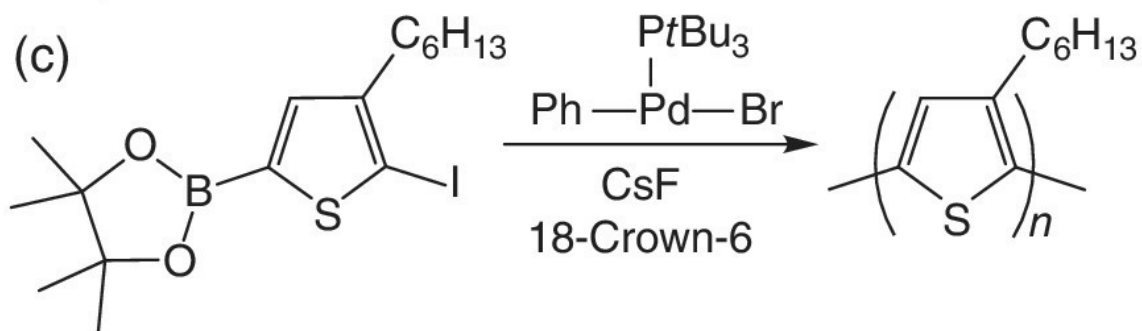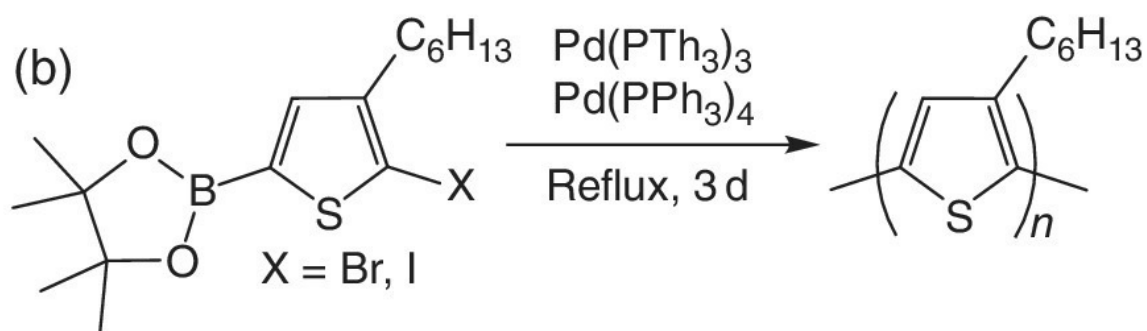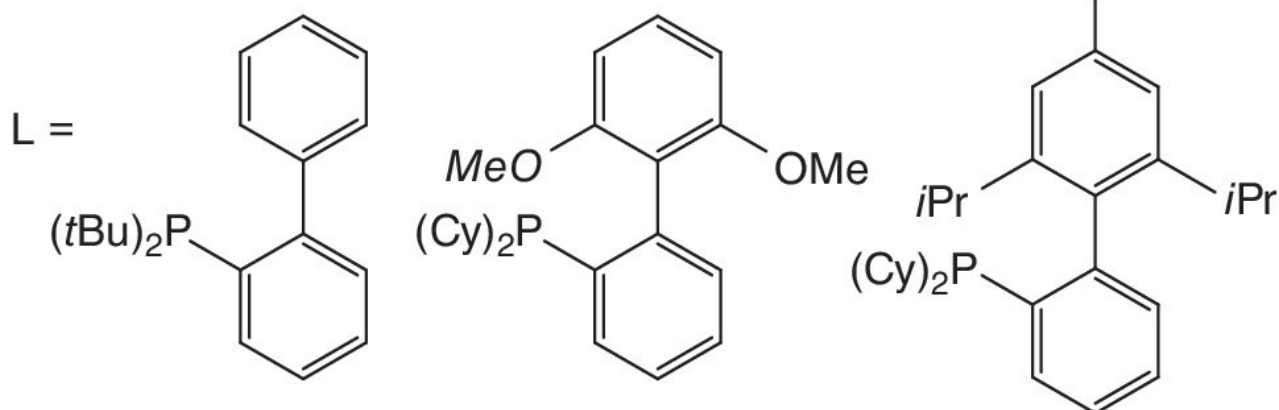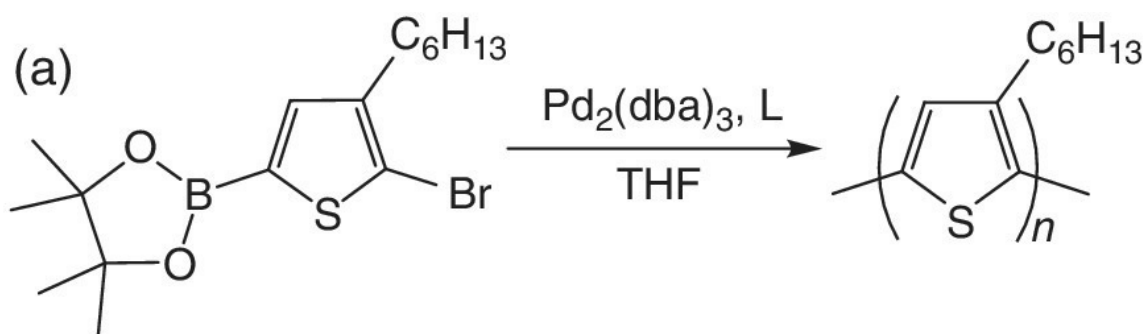
Scheme 4.8 Synthesis of rrP3HT by Suzuki–Miyaura coupling polymerizations.

Polymerization of 5-bromo-4-hexylthien-2-yl-pinacol boronate ester was carried out in the presence of $Pd_2(dba)_3$ and a phosphine ligand in THF, leading to rrP3HT (rr > 97%) with moderate molecular weights (M_w = 4500–16 900 g.mol^{-1}, Đ = 1.1–1.3) in low yields (20–30%). These unsatisfactory results were attributed to the possible protodeboronation of the starting monomer and the growing chain that can occur during the polymerization process and lead to premature chain termination [85].

To overcome this problem, Bo and coworkers reported the use of a novel zerovalent palladium catalyst precursor, tris[tri(2-thienyl)phosphine]palladium ($Pd(PTh_3)_3$), which prevents the main side reactions to occur by increasing the electron density of the palladium intermediate (b, Scheme 4.8) [86]. This catalyst was found to be superior to $Pd(Ph_3)_4$, typically used for Suzuki–Miyaura coupling polymerization of thiophene derivatives. Polymerization of 3-hexyl-5-iodothiophene-2-boronic pinacol ester afforded rrP3HT (rr > 97%) with a molecular weight of 26 000 g.mol^{-1} (Đ = 2.29) in good yield (72%).

Few years later, Yokozawa *et al.* described the preparation of P3HT by polymerization of 3-hexyl-5-iodothiophene-2-boronic pinacol ester at 0°C in the presence of a CsF and 18-crown-6 in THF using $P(tBu)_3Pd(Ph)Br$ as a catalyst (c, Scheme 4.8) [87]. Molecular weight of rrP3HT (rr > 99%) prepared by this method was M_n = 5400 g.mol^{-1} with a relatively narrow dispersity (Đ = 1.34). Further, the authors found that M_n value was controlled by the feed ratio of monomer to the Pd complex up to 11 400 g.mol^{-1}. The MALDI-TOF mass spectra showed that the obtained P3HT exhibits a phenyl group at one end and a hydrogen atom at the other, thus indicating that polymerization proceeds through a catalyst transfer mechanism. By this way, the synthesis of well-defined P3HT was not longer limited to Kumada coupling polymerization with nickel catalysts. Shi, Geng, and coworkers demonstrated that controlled Suzuki–Miyaura catalyst transfer polycondensation of thiophene could also be carried out through the use of *N*-heterocyclic carbene (NHC)-based palladium catalyst [88]. Since the electron-rich carbene ligands are strongly bound to the metal center [89], it helps the palladium to retain its ligand, which results in a longer catalyst lifetime and a consistent reactivity throughout the course of the transformation. In addition, their steric properties can be easily tuned by changing the N-substituted groups [90]. Based on these statements, they studied the polymerization of 2-(4-hexyl-5-bromanyl-2-thienyl)-1,3,2-dioxaborinane with different bis(2,6-diisopropylphenyl)imidazolin-2-ylidene (IPr)-based Pd complexes as the catalysts and found that $Pd(IPr)(OAc)_2$ is a promising catalyst for the controlled synthesis of P3HT (d, Scheme 4.8). By optimizing polymerization conditions, P3HTs with controlled molecular weights (9500–63 800 g.mol^{-1}) but broad molecular weight distributions (Đ = 1.40–1.81) due to the slow initiation process were obtained.

More recently, the influence of the boron moiety of the monomer and water in the solvent on the Pd-catalyzed Suzuki–Miyaura coupling polymerization was investigated [91, 92]. Turner and coworkers reported the preparation of highly rrP3HT (rr > 98%), by Suzuki−Miyaura polymerization using *N*-methyliminodiacetic acid (MIDA) boronate ester thienyl monomer [91]. Such MIDA boronate esters offer the advantage to be stable to protodeboronation, which is crucial for Suzuki cross-coupling reactions and possess slow release ability. By controlling the amount of water, rrP3HTs with molecular weights up to M_n = 18 700 g.mol^{-1} (Đ = 1.40–1.81) were isolated in excellent yields (up to 94%) [91]. Besides, Yokozawa *et al.* identified the presence or absence of water as a crucial parameter in the Suzuki–Miyaura coupling reaction [92]. Indeed, the polymerization of triolborate halothiophene with $Pd(o\text{-tolyl})P(tBu)_3Br$ as a catalyst afforded P3HT with a broad molecular weight distribution (Đ = 1.62–2.15) and with

different polymer end groups, whereas polymer formed in water/THF exhibited reduced dispersity ($Đ$ = 1.57) and well-controlled end groups. These results indicate that intramolecular transfer of the Pd catalyst in the Suzuki–Miyaura coupling reaction is hindered in the absence of water, while addition of a small amount of water suppresses intermolecular transfer of the catalyst, leading to controlled polymerization.

4.2.1.2.3 C—H Arylation Cross-Coupling Polymerization

C—H arylation has emerged as an important alternative for forming sp^2–sp^2 carbon–carbon bonds in organic chemistry [93]. This new cross-coupling reaction has the advantage of not using organometallic intermediates, thereby reducing synthetic steps and cost [93]. By this way, they also contribute to prevent the presence of by-products difficult to remove, which have proved to have a negative impact on device efficiency [94]. The first report on the preparation of P3HT through direct arylation was reported by Lemaire and coworkers in 1999 [95]. Polymerization reaction was carried out in DMF using $Pd(OAc)_2/K_2CO_3/Bu_4NBr$ as a catalyst. Unfortunately, only an oligomer (M_n = 3000 g.mol^{-1}) with large molecular weight distribution ($Đ$ ~ 2) and regioregularity around 90% was obtained. Later on, Thompson *et al.* introduced neodecanoic acid in the catalytic system instead of Bu_4NBr, allowing to obtain higher molecular weight P3HT (M_n = 20 000 g.mol^{-1}, $Đ$ = 2.8) [96]. The presence of this α-trialkylated carboxylic acid appeared to be crucial for the M_n enhancement of P3HT. Since $Pd(OAc)_2$-based catalytic systems were found to decompose and lead to poor reproducibility, Ozawa and coworkers tested Herrmann's catalyst as a palladium source to polymerize 2-bromo-3-hexylthiophene (Scheme 4.9) [97]. Regioregular P3HT with high molecular weight (M_n = 30 600 g.mol^{-1}, $Đ$ = 1.6) and regioregularity (98%) was obtained.
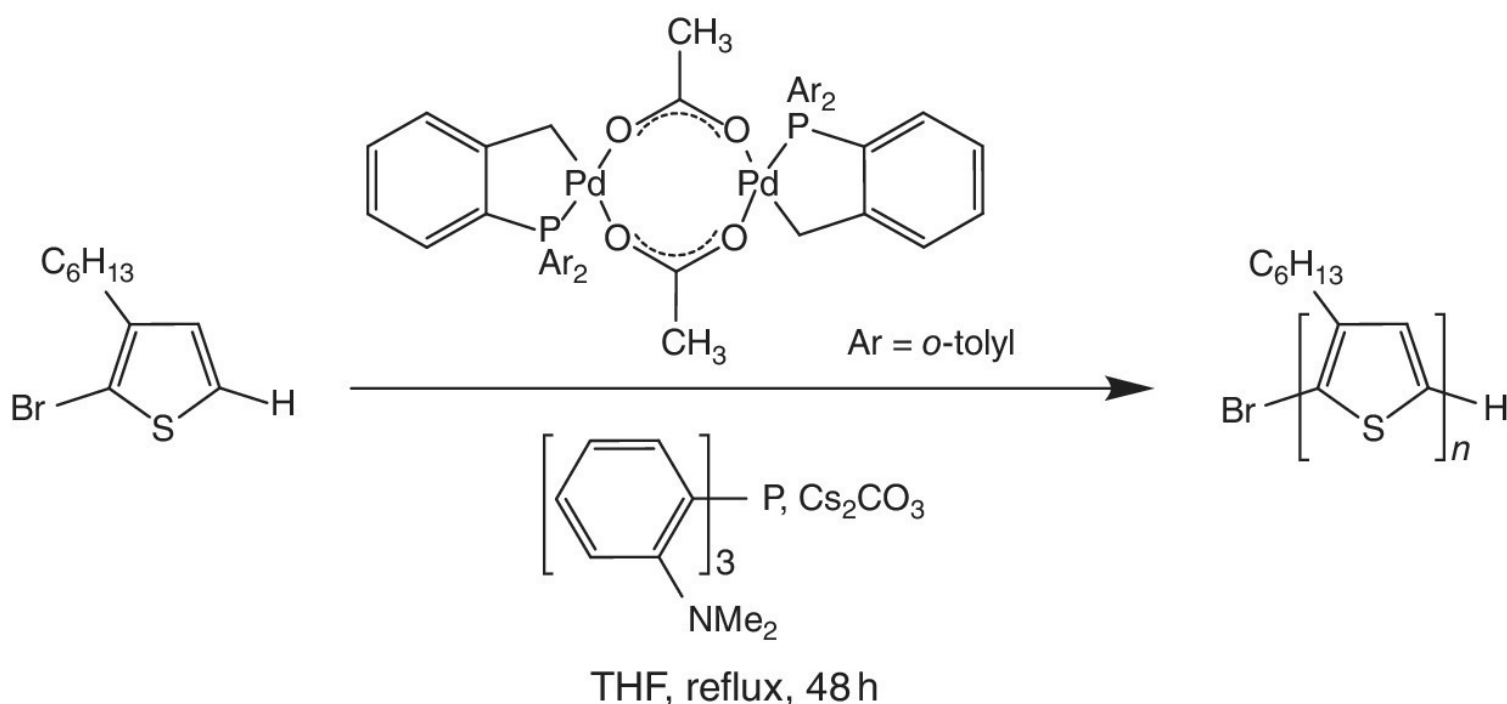
Scheme 4.9 Dehydrohalogenative polycondensation of 2-bromo-3-hexylthiophene.

Since highly thermally stable palladium catalyst seems to be advantageous to the direct arylation polymerization, Cheng *et al.* reported the use of NHC palladium complexes as catalytic systems [98]. Indeed, carbenes are well known to strongly stabilize transition metals [89, 99]. By optimizing conditions, high molecular weight rrP3HT (M_n = 26 900 g.mol^{-1}) with high regioregularity (94%) was

notably obtained by using thermally stable Pd-IPr [1,3-bis(2,6-diisopropylphenyl)imidazol-2-ylidene]chloro[3-phenylallyl]palladium(II) as the catalyst. One major problem in direct arylation polycondensation is the lack of selectivity when different aromatic C─H bonds are present [100]. 2-Bromo-3-hexylthiophene monomer exhibits two C─H bonds at C5 and C4, with C─H bond at C5 being the most reactive. Thus, the C─H arylation polycondensation of 2-bromo-3-hexylthiophene occurs not only at the 5-position but also at the unfavorable 4-position, leading to bent, hyperbranched, and/or networked structures under general conditions (Scheme 4.10) [101, 102]. To overcome this problem, Hayashi, Kiozumi, and coworkers developed heterogeneous palladium catalysts (Pd/C and Pd(OH)$_2$/C) for direct arylation of thiophene monomers (Scheme 4.10) [101]. Polymerization was carried out in different solvents (DMAc, NMP, toluene, THF) at 100°C, leading to linear and highly regioregular HT-P3HTs (rr = 97%) with high molecular weight (M_n = 18 400 g.mol^{-1}, $Đ$ = 3.11). The linear structure was evidenced by comparison of their optical properties and XRD patterns with those of similar molecular weight rrP3HT prepared by KCTCP polymerization. It was suggested that the regioselective direct arylation polycondensation may be explained by the heterogeneous-like catalyst behavior of the carbon-supported Pd.
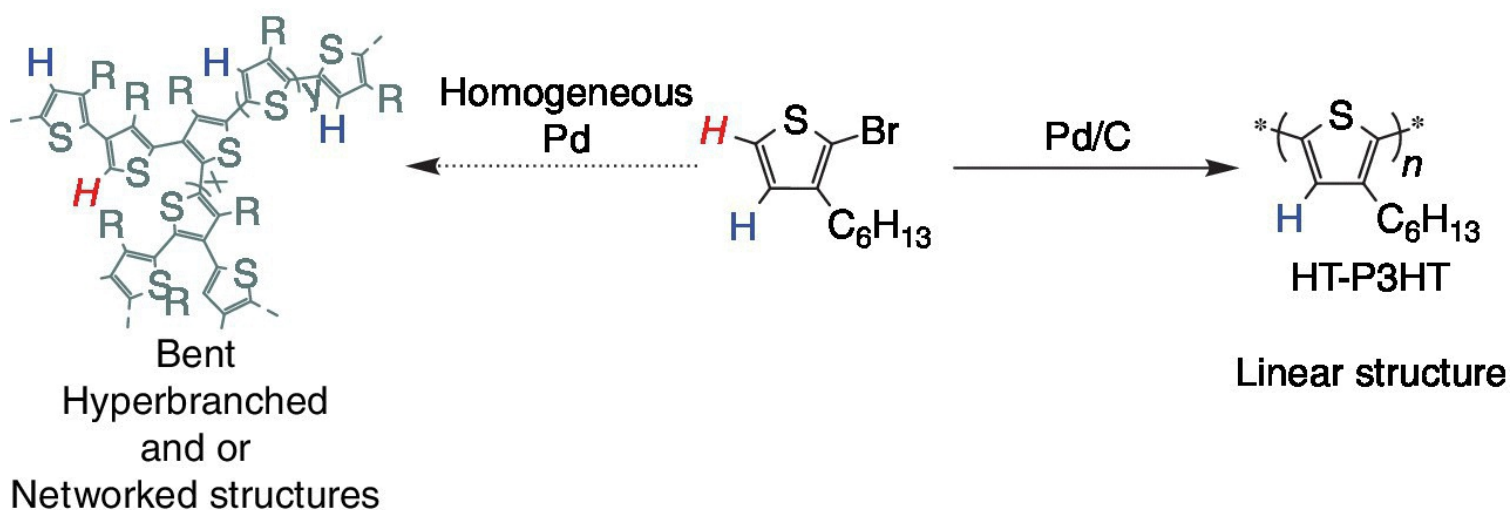
Scheme 4.10 Homogeneous and heterogeneous palladium-catalyzed direct arylation polymerization of 2-bromo-3-hexylthiophene.

Source: Hayashi *et al.* [101]. Reproduced with permission of Royal Society of Chemistry.

4.2.2 Functionalization of P3HT

In view of enhancing and fully exploiting the properties of P3HT, their facile chemical modification is required. In particular, the tailoring of P3HT properties has mainly focused on the modification of the hexyl side chains and the end groups of P3HT to expand their structure–property relationships in view of improving their utility in PV devices.

4.2.2.1 End-Group Functionalization

Three different approaches have been developed to alter end-group composition of P3HT: (a) *in situ* method mainly based on the introduction of Grignard reagents at the end of the polymerization, (b) *ex situ* method involving functional Ni-based initiators in combination with KCTCP, and (c) post-polymerization modification of end-functional P3HT relying on the conversion of aryl bromides or other groups to achieve the desired functionality [22b, c, 103]. These end-functionalized P3HT could be used as a macroinitiator for preparing block copolymers. Indeed, rod–coil block copolymers were synthesized

using "growth from" strategies such as atom transfer radical polymerization (ATRP) [104], nitroxide-mediated radical polymerization (NMP) [105], anionic polymerization [106], cationic ring-opening polymerization [107], ring-opening metathesis polymerization (ROMP) [108], and reversible addition–fragmentation chain transfer (RAFT) polymerization [105c]. Recently, rod–coil block copolymers have been also reported using a "grafting to" strategy (click chemistry) [109].

4.2.2.1.1 In Situ End-Group Functionalization

The *in situ* method offers the advantage of modifying end group(s) in a one-pot procedure. This synthetic strategy is illustrated in Figure 4.5 as well as a list of end-functional groups that can be easily introduced on P3HT. The first attempt toward *in situ* end-group functionalization was reported by Janssen and coworkers using the McCullough method. In this strategy, the polymerization was quenched with 2-thienylmagnesium bromide or 5-methylsilyl-2-thienylmagnesium bromide, leading to a mixture of H/H and mono- and dicapped polymer chains [110]. Subsequently, McCullough and coworkers described a simple and versatile *in situ* method to achieve end-functionalization of rrP3HT. This strategy involves quenching of the KCTCP polymerization with a wide range of Grignard reagents such as allyl, vinyl, aryl, and alkyl [65]. The degree of end-functionalization was found to be dependent on the nature of Grignard reagent. Indeed, when unsaturated group such as allyl, ethynyl, or vinyl-based Grignard reagent are used, only monofunctional polymers were obtained, while other Grignard reagents result in dicapped polymer chains. It was suggested that such behavior originated from the formation of nickel–π complex with unsaturated group that prevents further reaction with the aryl bromide end group. Based on this statement, Pickel and coworkers showed that adding unsaturated additives such as 1-pentene and styrene immediately before the addition of the quenching Grignard reagent decreased significantly the amount of dicapped polymer chains [111]. In addition, Thelakkat and Lohwasser demonstrated that the nature of end groups in KCTCP polymerization could be perfectly controlled by controlling the consumption of the alkyl Grignard reagent necessary to the formation of the active monomer [112]. These findings facilitated the incorporation of reactive units such as –OH, –CHO, and –NH$_2$ with the use of the adapted protecting groups as well as nitrogenous heterocyclic groups (pyridine, oxadiazole, triazole) [65, 113, 114].
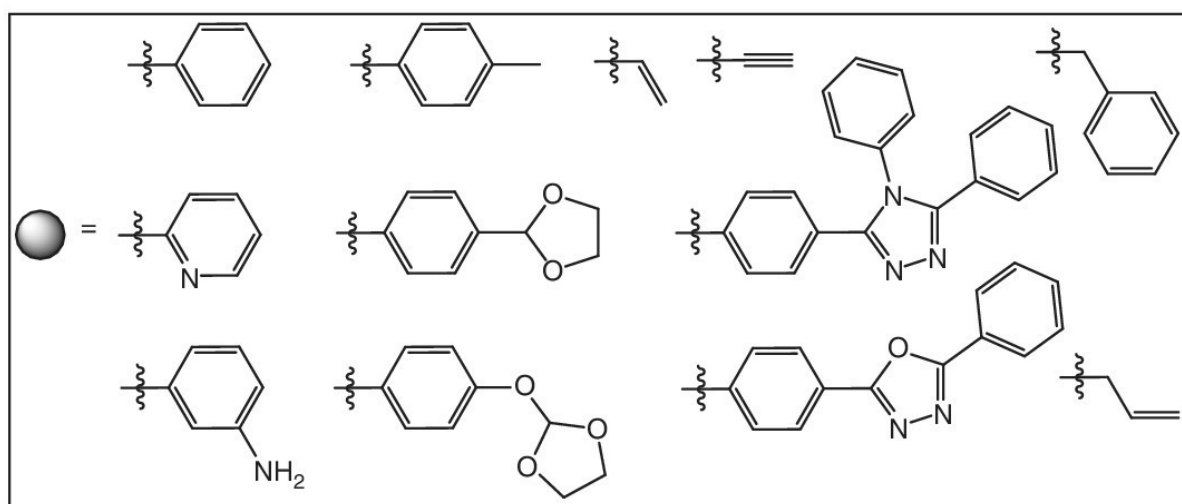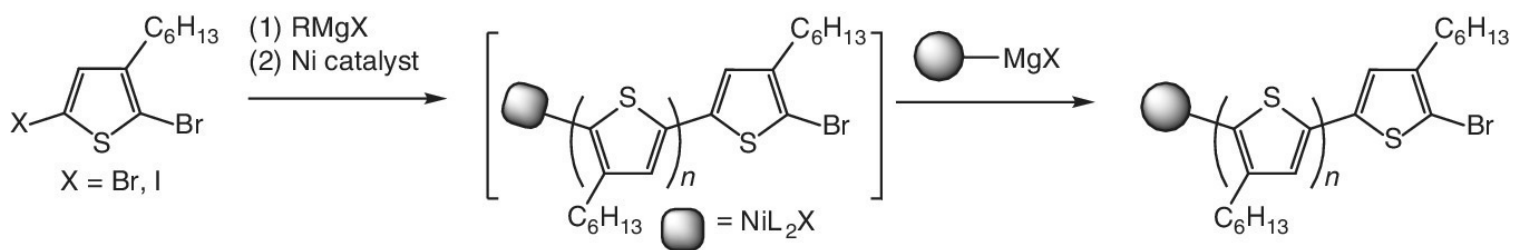
Figure 4.5 Synthetic pathway to *in situ* end-group functionalization of P3HT and comprehensive list of P3HT end-functional groups incorporated by this method.

4.2.2.1.2 Ex Situ End-Group Functionalization

The *ex situ* method consists in the polymerization of 3-hexylthiophene-based monomers from Ni initiators equipped with a functional group (Figure 4.6) [70, 109, 115–118]. As a matter of fact, a wide range of different nickel initiators incorporating (protected) alcohol, ethynyl, carboxylic acid, amine, and phosphonate functional groups have been independently developed by the groups of Kiriy [117, 118], Luscombe [70, 119], Bazan [120], and Koeckelberghs [110, 121, 122] (Figure 4.6).
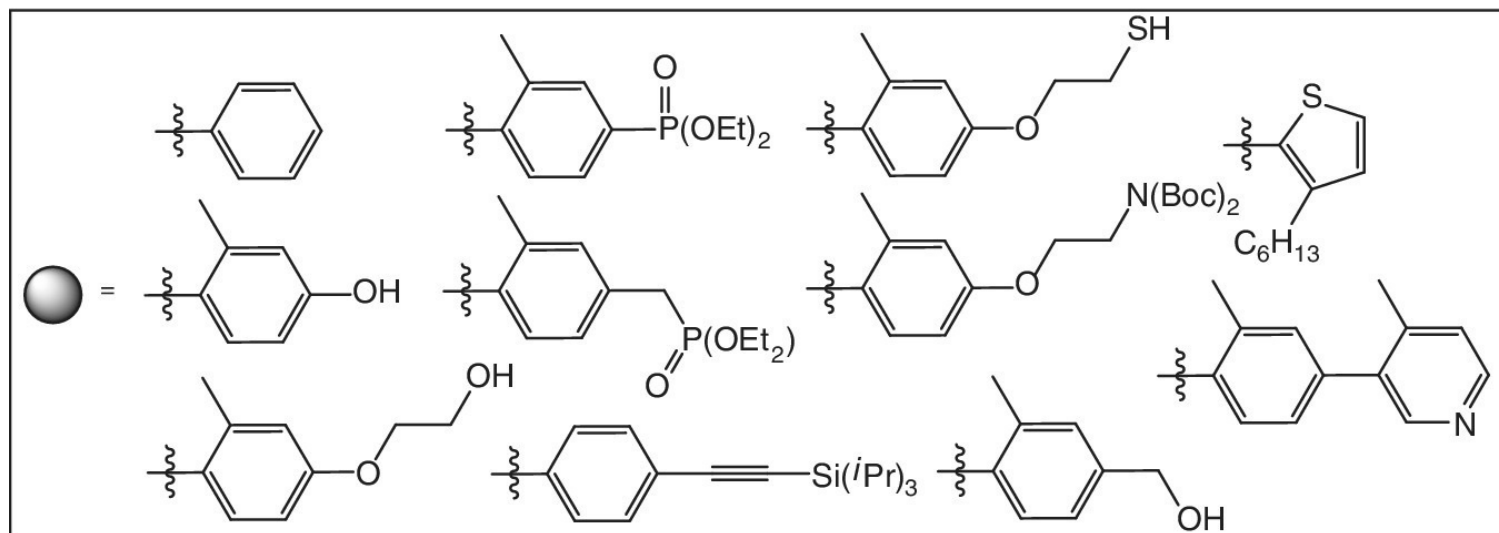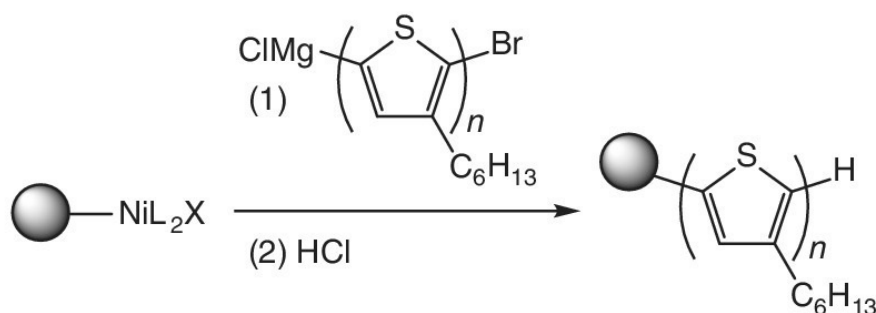
Figure 4.6 Synthetic pathway to *ex situ* end-group functionalization of P3HT and comprehensive list of P3HT end-functional groups incorporated by this method.

Indeed, Koeckelberghs and coworkers notably developed a series of phosphonic esters, pyridines, thiols, and end-functionalized P3HT, which offer the opportunity to prepare hybrid materials with inorganic particles [121]. The *ex situ* method also opens the door to the growth of conjugated polymer brushes on inorganic surfaces via a "grafting from" approach [22b, 67b, 71, 73]. While this *ex situ* method for preparing end-functionalized P3HT seems straightforward in principle, its practical implementation starting from an aryl halide has proven to be very challenging. Indeed, the initiator must exhibit high purity and be quite stable. Otherwise polymer chain ends not functionalized by the desired group may be obtained. Furthermore, since a Grignard reagent is used, the choice of compatible derivatives is limited.

4.2.2.1.3 Post-polymerization End-Group Functionalization

Compared with the previous methods, the post-polymerization modification strategy is compatible with a wide range of functional groups and allows functionalizing both chain ends, with either the same or different groups (Figure 4.7).
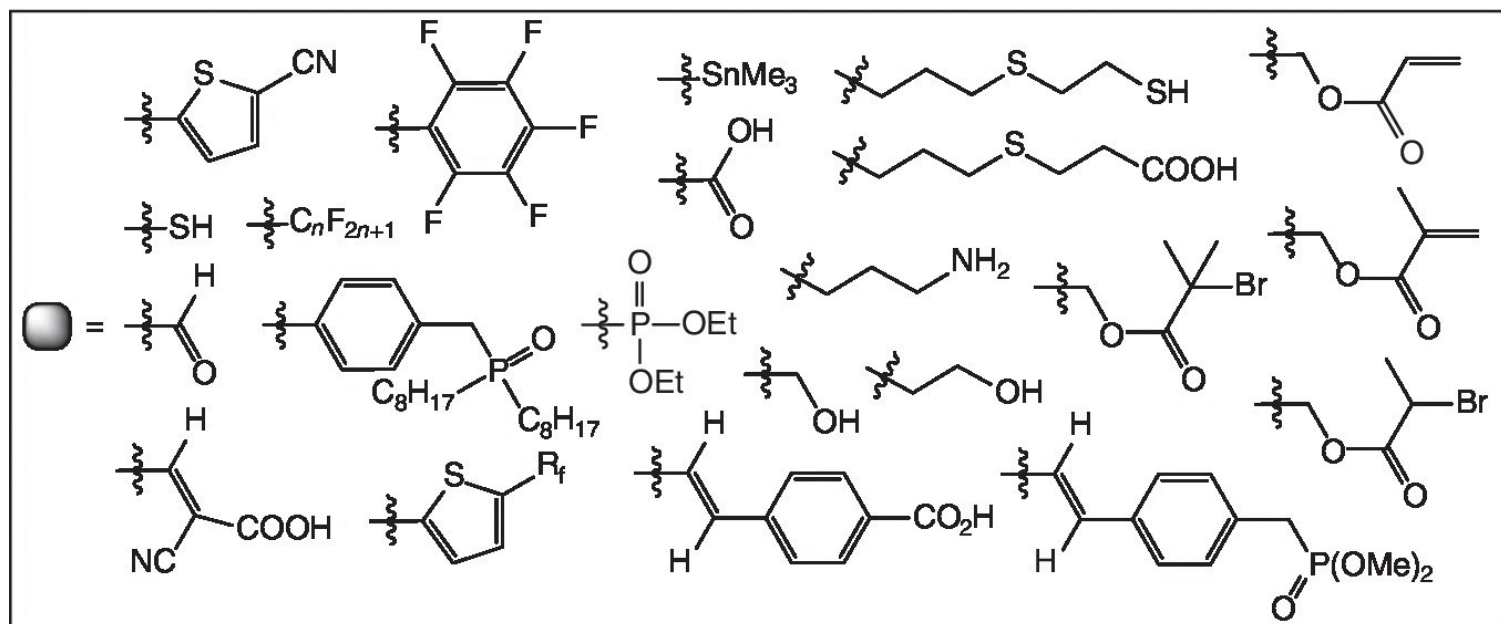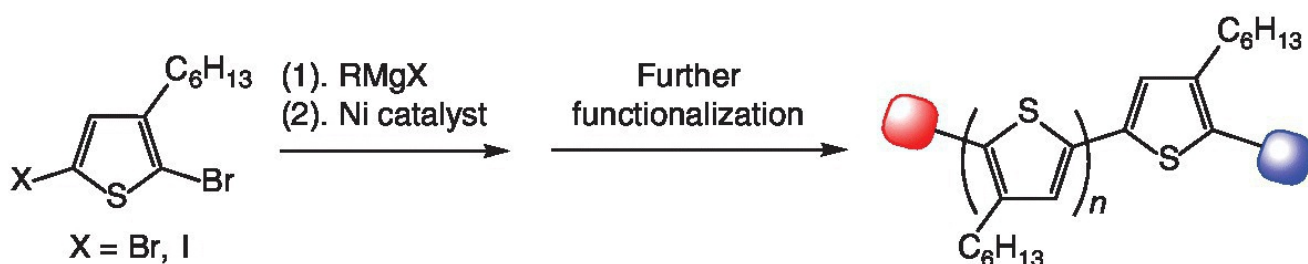
Figure 4.7 Synthetic pathway to post-polymerization end-group functionalization of P3HT and comprehensive list of P3HT end-functional groups incorporated by this method.

Regioregular P3HTs synthesized through the KCTCP polymerization have fairly pure end-group composition with a proton at one end and a bromine at the other end (H/Br) [22, 112]. McCullough and coworkers first demonstrated this strategy by selectively functionalizing one or two end groups of P3HT. Thus, thienylzinc derivatives bearing protected amino and alcohol groups were selectively introduced at one end of the P3HT chain by a Negishi coupling reaction [123]. In contrast, by selectively preparing the H/H-type P3HT, the same group converted these two end groups to aldehyde, which were subsequently reduced into the corresponding hydroxymethyl groups [104h, 124].

The carboxaldehyde end group was recently converted into cyanoacetic acid or 4-vinylbenzoic acid moieties, which allow further functionalization of metal oxide such as TiO_2 [125, 126]. Carboxylic acid moieties were also introduced by first transforming P3HT-Br via a Grignard metathesis reaction followed by treatment with gaseous CO_2 and hydrochloric acid, giving selectively and quantitatively the mono-carboxylated P3HT [127]. In a similar fashion, phosphonate ester end-functionalized P3HT was synthesized by Fréchet *et al.* by treating P3HT with *n*-butyllithium and then diethyl chlorophosphate in view of their grafting on ZnO nanowires [128]. Bromide end groups were exploited for C–C cross-coupling reactions such as Stille [129] and Suzuki–Miyaura [130] coupling reactions. Mono- and dicapped P3HT chains can also be selectively prepared by judiciously choosing the reagent. Luscombe *et al.* have notably reported the synthesis of P3HT with thiol end groups at one or both chain ends using sulfur powder or triisopropylsilanethiol as the functionalization agent, respectively [131]. Although the post-polymerization strategy seems versatile, this method requires multistep synthesis, tedious purification procedures, and specific coupling reagents.

4.2.2.2 Side-Chain Functionalization

In the past years, many efforts have been devoted to the synthesis of new conjugated polymers, in particular, focusing on the π-conjugated backbones that determine the optoelectronic properties of the resulting polymers [132]. In contrast, studies involving side-chain engineering are much less numerous, whereas side chain was found to be an important parameter to consider when designing conjugated polymers [133]. Indeed, material synthesis, processing, and device fabrication such as poor batch-to-batch reproducibility and poor thin film processability could be significantly improved by side-chain engineering [133]. The improvement of such parameters led to enhanced charge carrier mobilities of the organic field-effect transistors (OFETs) [133, 134] and higher PCEs in OPVs. [135] These effects of side chains can be due to size, density, topology (linear vs. branched), and, in the case of multiple different side chains, composition and distribution (e.g., uniform, random, etc.) [136]. From this point of view, end-functionalized side-chain PTs are particularly interesting since robust synthetic protocols (e.g., KCTCP) [21, 22] are available to allow the relatively straightforward preparation of multiple polymer topographies (homopolymers, random/block copolymers) with a high degree of control over the final structure and molecular weight.

Two strategies were developed to end-functionalize side chains of rrP3HTs. The first one involves the polymerization of thiophene monomers with protective groups at the γ end of the side chains. These protective groups allow incorporating functional groups, which are sensitive to polymerization conditions. Thus, rrP3HTs γ-functionalized with protected alcohol have been synthesized through KCTCP [136, 137]. The deprotected alcohol was then further functionalized by 2,6-bis(hexylamino)pyrimidine groups to interact with a thymine-based fullerene via hydrogen bonding interactions and thus stabilize the morphology of the active layer [137a]. In a similar fashion, rrP3HT bearing a phosphonic ester group was synthesized by the Stille method and then deprotected to lead to the corresponding phosphonic acid-functionalized P3HT [138]. This latter afforded to a supramolecular assembly when a tetraalkylammonium hydroxide salt was added to the polymer solution.

Another approach to functionalize the side chain of rrP3HTs consists in incorporating reactive groups at the γ end of the side chains that are stable toward polymerization conditions. Among the reactive groups that can be used to γ end-functionalize side chains, bromide groups are mostly used (Figure 4.8). rrP3HTs with bromohexyl side chains were first synthesized by Iraqi and coworkers using the McCullough method and then functionalized with 2-carboxyanthraquinone to give a highly redox active rrP3HT [139]. Unfortunately, the reaction afforded polymers that were functionalized in 87% yield. Few years later, McCullough described the synthesis of poly(3-(6′bromohexyl)thiophene) by using KCTCP method and the modification of the γ bromide end groups into carboxylic acid, amine, or thiols (Figure 4.8) [140]. Then, over the years, P3HTs bearing alkene [141], imidazole [142], alkoxy [143], fullerene [144], and azide [140, 145] groups at the γ end of the hexyl side chains were developed starting from poly(3-(6′-bromohexyl)thiophene) precursors. It is interesting to note that P3HT with azide groups attached to the end of the alkyl chain could improve the stability of active layer in organic solar cells [145] and allows introducing fullerene [146] and polymer side chains through "click" chemistry [147].
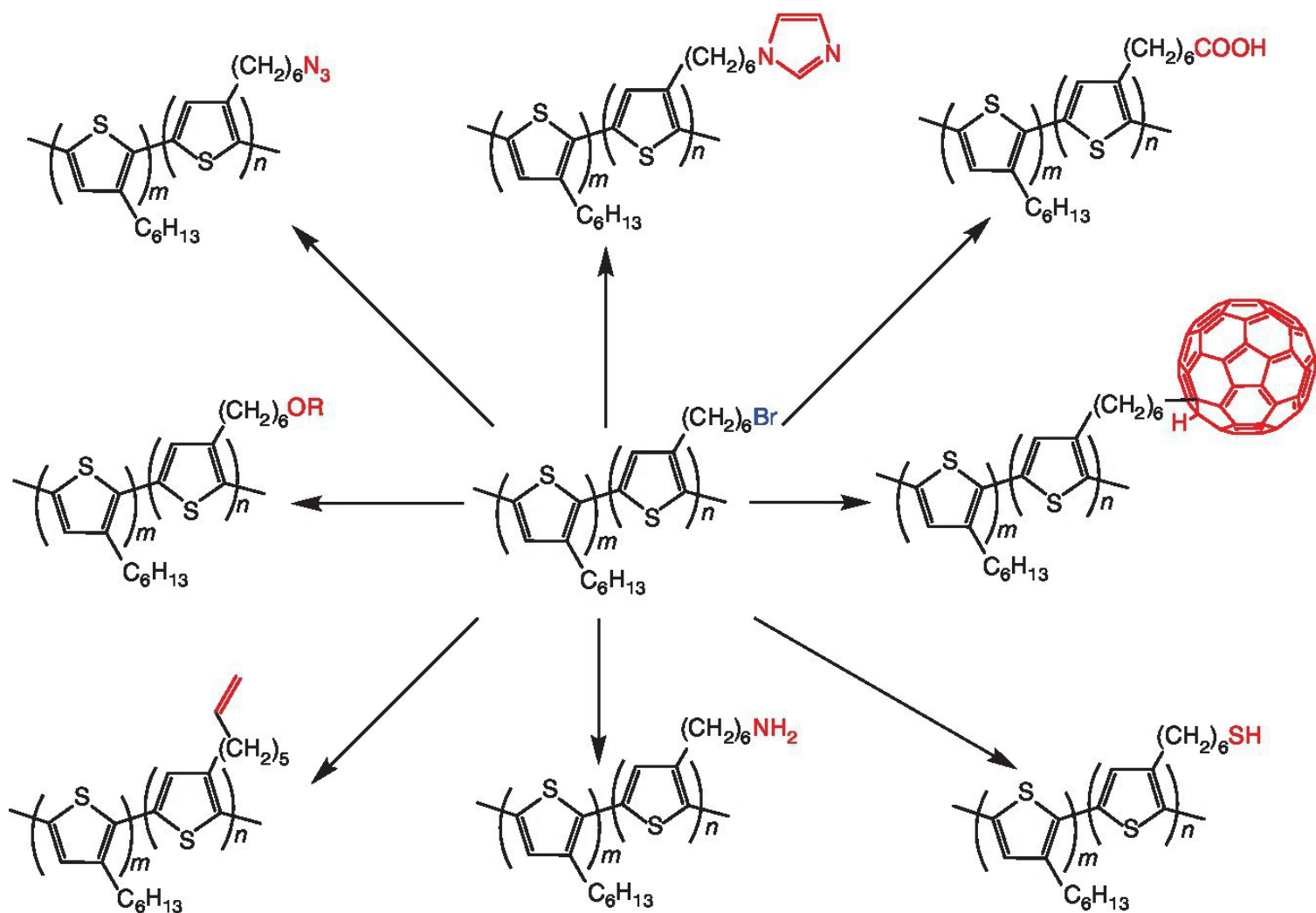
Figure 4.8 γ end-functionalized side-chain rrP3HT starting from poly(3-(6′-bromohexyl)thiophene).

4.3 Morphology Control of P3HT/PCBM Blend by Functionalization

4.3.1 Introduction

As indicated earlier, P3HT is commonly considered as a benchmark material in BHJ polymer solar cells [21]. PCEs of about 5% have been reported for single-layer devices incorporating P3HT as the electron donor material and [6,6]-phenyl-C_{61}-butyric acid methyl ester ($PC_{61}BM$) as the electron acceptor in the active layer [21]. The modest PCEs of P3HT-based solar cells were attributed to the weak absorption of P3HT in parts of the visible and the near-infrared regions of the solar spectrum [2]. The basic device structure for single-layer devices and typical current–voltage characteristics in a solar cell are described in the following (Figure 4.9).

$$\eta = \frac{P_{out}}{P_{in}} = \frac{V_{oc} \times J_{sc} \times FF}{P_{sc}}$$

FF = Fill factor
J_{sc} = Current density (mA^{-2} cm^{-2})
V_{oc} =
η = Power conversion efficiency
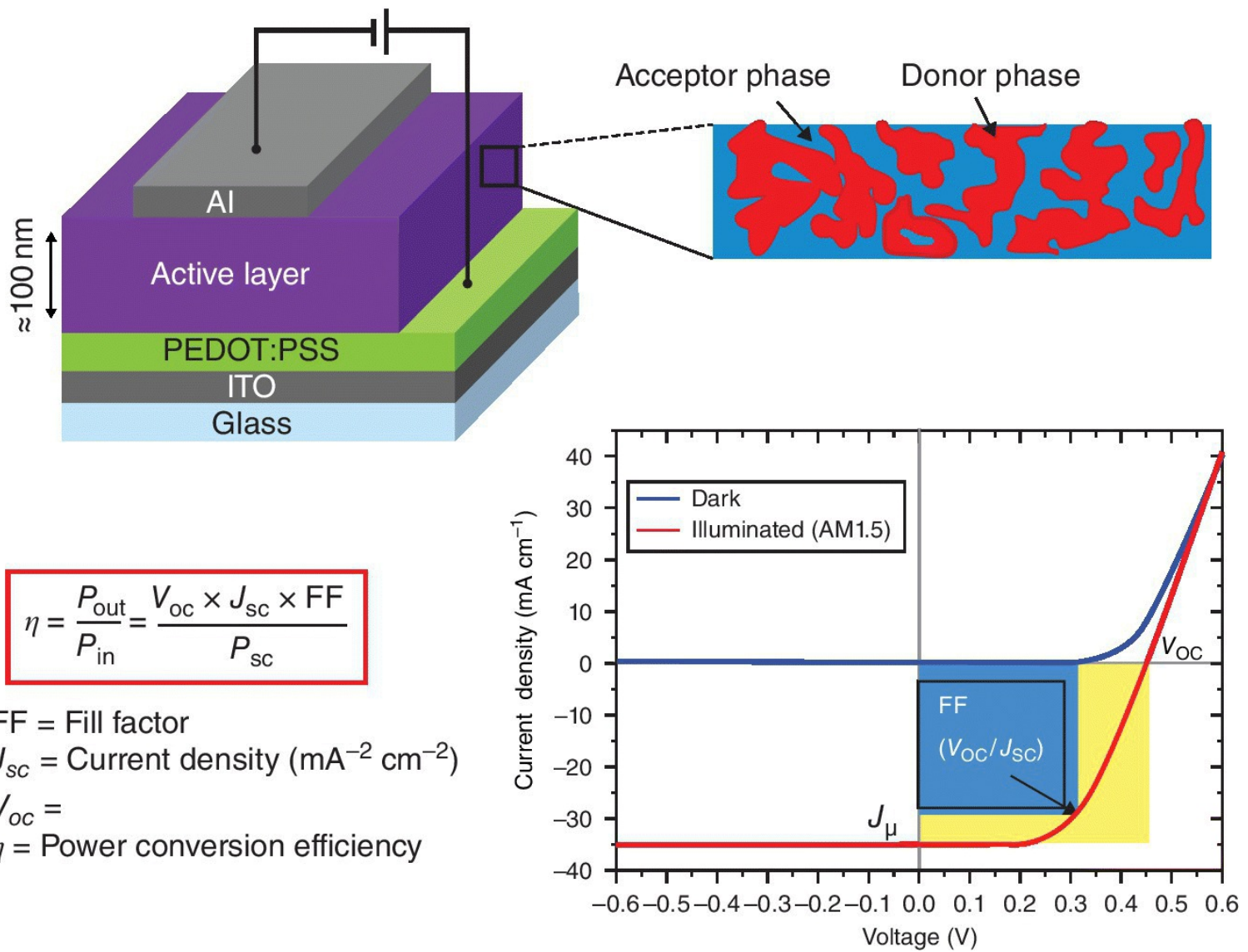
Figure 4.9 Schematic illustration of a polymer–fullerene BHJ solar cell, with a magnified area showing the bicontinuous morphology of the active layer (*top*). Typical current–voltage characteristics for dark and light current in a solar cell illustrating the important parameters of such devices (J_{SC}, V_{OC}, FF, η, or PCE) (*bottom*).

In an organic solar cell, the energy conversion proceeds through four consecutive steps as follows (Figure 4.10):

1. Absorption of light and generation of excitons in the donor domains

2. Diffusion of excitons to the D–A interface

3. Dissociation of excitons and generation of charges: hole in the donor domain and electron in the acceptor domain

4. Charge transport through their respective domains and charge collection at their respective electrodes
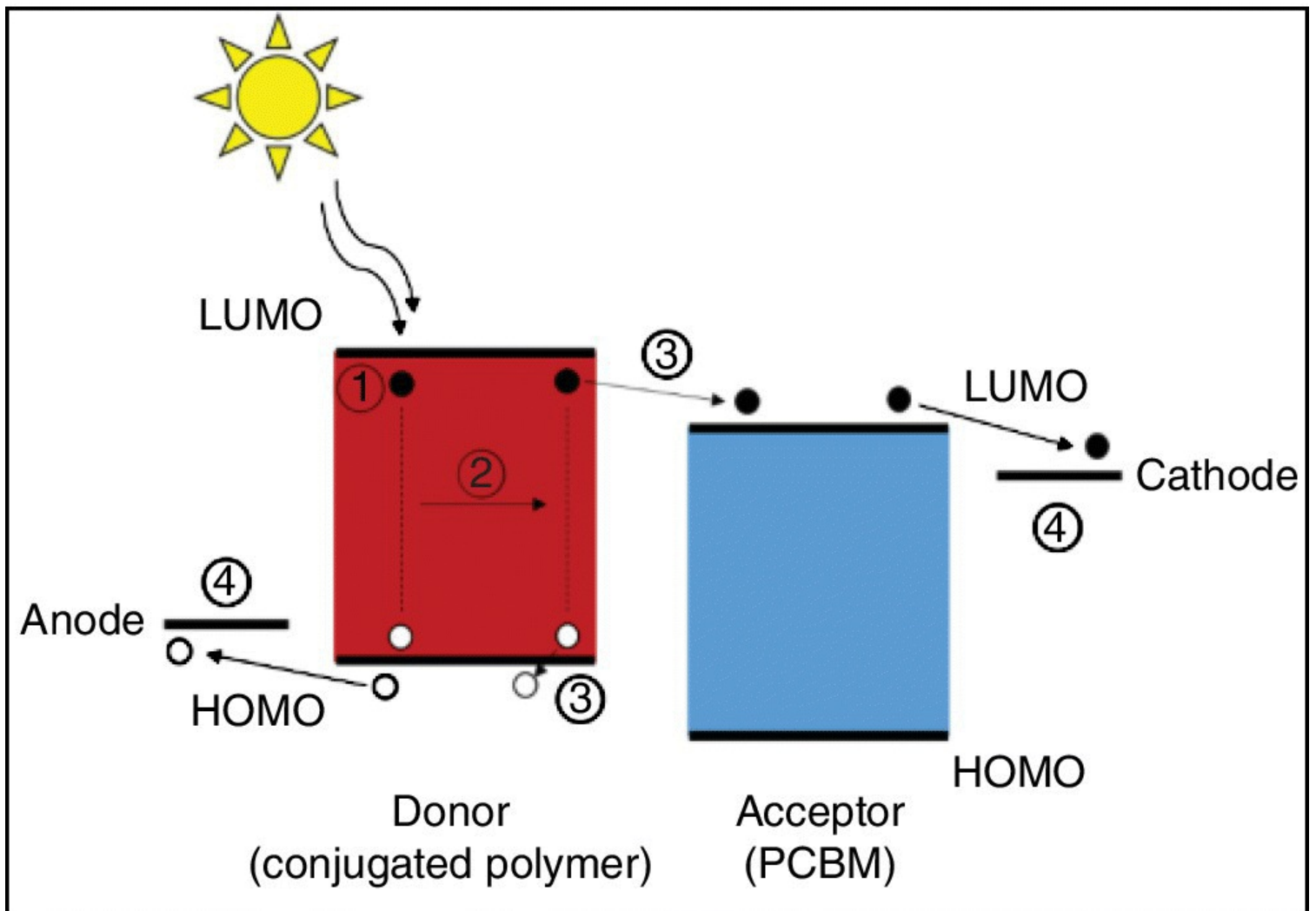
Figure 4.10 Operation principle for photoenergy conversion in OPVs.

In this process, phase separation between donor and acceptor in the blends is a crucial parameter to control for promoting the exciton dissociation at the D–A interface and the electron–hole conduction toward the electrodes. Indeed, due to the limited diffusion length of the organic materials (ca. 20 nm), organic solar cells require a high interfacial area arrangement of donor and acceptor domains to achieve efficient charge separation.

In P3HT/PCBM-based devices, despite the process optimizations including thermal and solvent annealing to afford improved morphology, the domain size and the architecture of BHJ active layer are still not well controlled [148]. Morphology achieved by mixing P3HT and PCBM are generally thermodynamically unstable in time, leading to the deterioration of the device during fabrication and/or extended use [148]. Specifically, macrophase separation of blend components can occur upon post-processing and extended device operation, resulting in significant changes compared to the as-deposited thin film morphology. Additional instability can also arise from the diffusion of PCBM. During device preparation and use, concentration gradients, depletion from active areas, and sometimes aggregation/crystallization of PCBM can occur, thus decreasing the interfacial area available for charge separation and impairing the device performance. Consequently, developing methods to precisely control the morphology at the nanoscale is a key challenge toward efficient organic solar cells.

Recently, it was shown that modifying the molecular structure by adding various functionalities in end or side chains of P3HT-based polymers could improve the morphology of the P3HT/PCBM blend and thus

the device performance. Moreover, block copolymers have emerged as the most promising candidates for OPV applications due to their capability to form well-defined and controllable nanostructures by adjusting the polymer structure in bulk or thin films through microphase separation [149]. Since then, many studies have explored block copolymers as a template for the optoelectronically active structures, as the main component in the active layer for OPVs, and as compatibilizer to improve the blend structure [150].

In this section, some significant examples illustrating the improvement of the morphology of P3HT–fullerene blends through the end- and side-chain functionalization of P3HT-based polymers will be provided.

4.3.2 End-Group Functionalization

End-group-functionalized P3HTs, in particular native bromine end groups, were first considered as impurities in the active layer. Indeed, introducing bromine end groups even in load loading percentage, that is, 2 mol%, resulted in a decrease of PCE due to disorder of chain packing, trapping of charge carriers, quenching of photogenerated excitons, and disturbance of film morphology [19, 151].

Bazan, Heeger, and coworkers reported that modifying the nature of the end chains of a narrow bandgap conjugated polymer by thiophene groups resulted in an improvement of the device performances by making the device less sensitive to active layer thickness and thermal degradation [152]. In a similar fashion, end-functionalized P3HTs were also found to be able to improve morphology in P3HT–fullerene blends and thus the efficiency and stability of OPV devices [153]. Moreover, as already discussed earlier, the development of controlled polymerization of rrP3HTs affords not only the opportunity to develop various end-functionalized P3HTs but also P3HT-based block copolymers [154]. The synthesis of block copolymers is a particularly attractive approach for controlling phase separation and interfaces since they can produce numerous phase-separated nano- or microstructures [155].

4.3.2.1 Fluorinated Chain Ends

Inducing hydrophilic–hydrophobic repulsive interactions in the boundary between the relatively hydrophilic PCBM and the relatively hydrophobic P3HT was reported to be a successful approach to control the morphology and thus to maximize the interfacial area in blends [129a, 153, 156]. Thus, modifying the bromine end group by the hydrophobic perfluoro end groups ($-CF_3$) induced morphology differences (**1** and **4**; [Figure 4.11](#)) [153]. The phase separation of the active layer in both vertical and horizontal directions was shown to be controlled by the surface-energy matching between donor and acceptor materials. Indeed, in comparison with hydroxy end-functionalized P3HT (40.3 mJ.m^{-2}), CF_3 end-capped P3HT was found to show surface energy (34.3 mJ.m^{-2}) similar to that of PCBM (34.2 mJ.m^{-2}), leading to more homogeneous blends as shown in transmission electron microscopy (TEM) images ([Figure 4.12](#)) and improved charge separation efficiency [153]. This better morphology control led to one of the best efficiency (4.5%) reported for P3HT/PC$_{61}$BM-based BHJ solar cells (Entry **1**, [Table 4.1](#)).
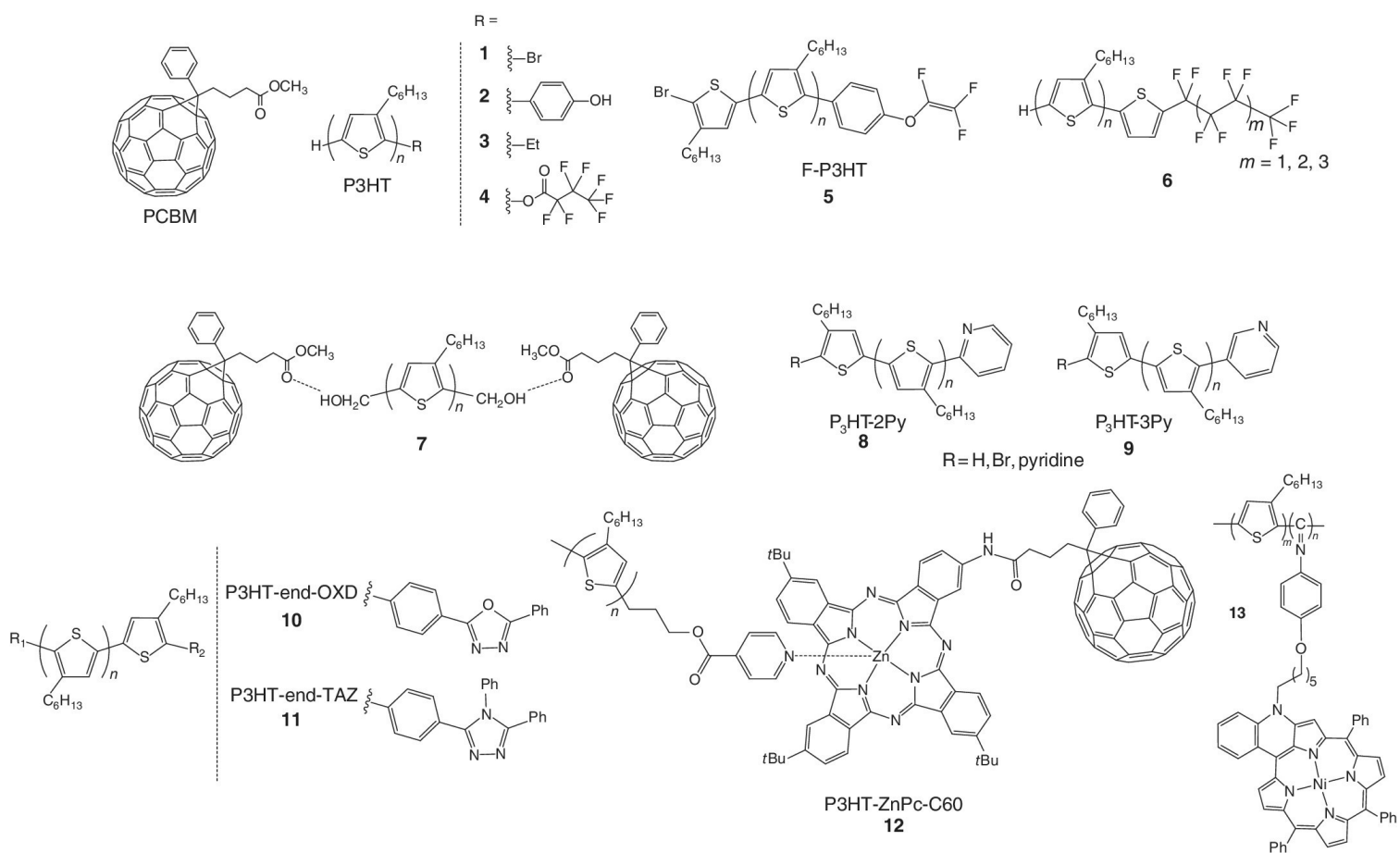
Figure 4.11 Structures of end-functionalized P3HT derivatives: homo- and copolymers.
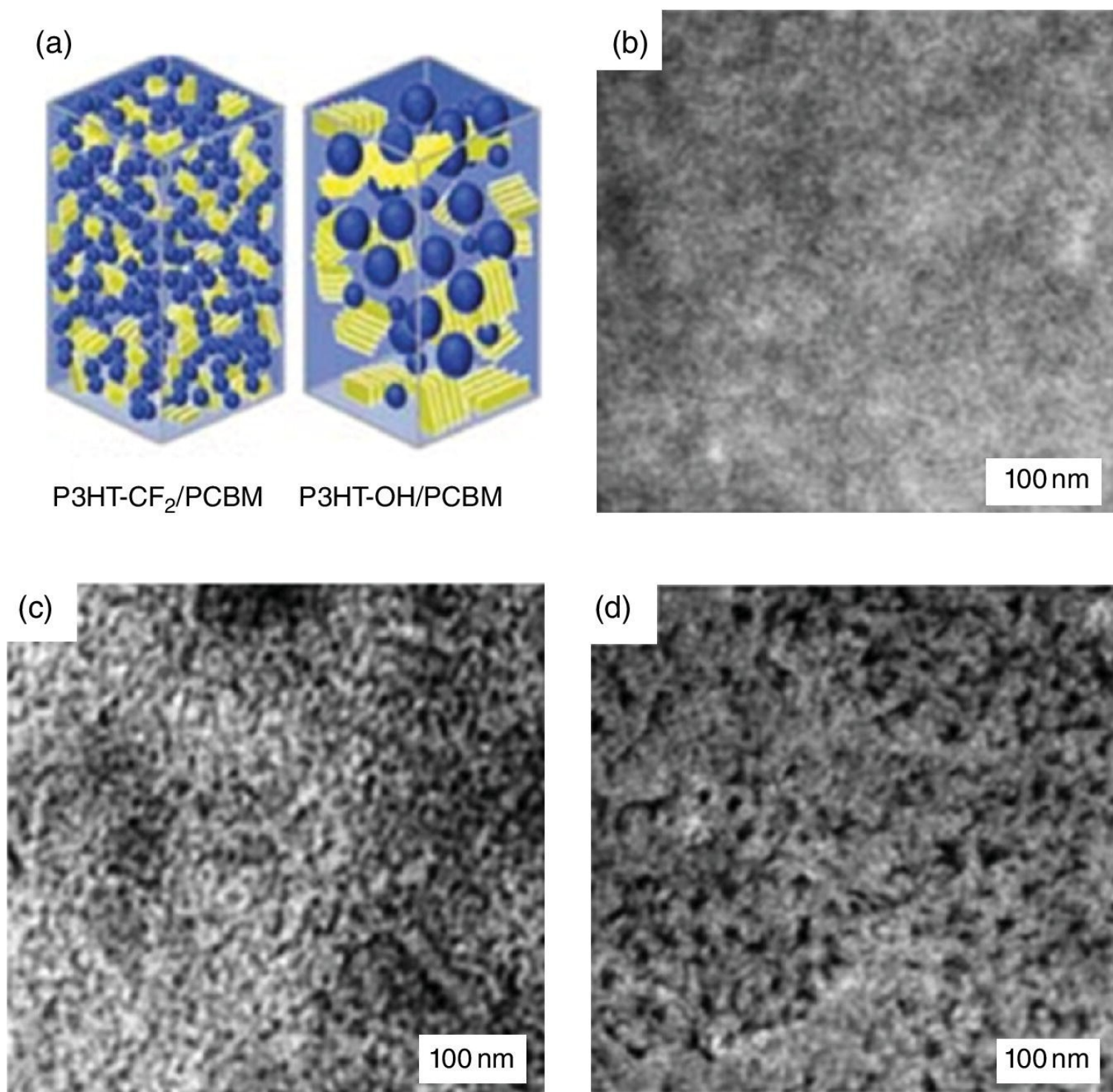
Figure 4.12 (a) Schematic diagram of the P3HTCF$_3$/PC$_{61}$BM and P3HTOH/PCBM blend films. TEM images of the end-functional-group-modified P3HT/PC$_{61}$BM film morphology: P3HTCF$_3$/PC$_{61}$BM (b), P3HTBr/PC$_{61}$BM (c), and P3HTOH/PC$_{61}$BM (d).

Source: Kim *et al.* [153]. Reproduced with permission of John Wiley & Sons.

Table 4.1 Bibliographic data of end-functionalized P3HTs extracted from the literature.

Entry	Device structure	Ratio	PCE (%)	Reference
1	**P3HTBr** : PC$_{61}$BM	1 : 1	3.2	[153]
	P3HTOH : PC$_{61}$BM	1 : 1	2.1	

	P3HTCH$_3$: PC$_{61}$BM	1 : 1	4.0	
	P3HTCF$_3$: PC$_{61}$BM	1 : 1	4.5	
2	**F-P3HT** : PC$_{61}$BM	1 : 1	*Impossible to spin-coat*	[156]
	P3HT : **F-P3HT** : PC$_{61}$BM	2 wt%	3.63	
		10 wt%	3.48	
		30 wt%	3.36	
3	**P3HTC$_4$F$_9$** : PC$_{61}$BM	1 : 1	1.3	129a
	P3HTC$_6$F$_{13}$: PC$_{61}$BM	1 : 1	0.63	
	P3HTC$_8$F$_{17}$: PC$_{61}$BM	1 : 1	0.32	
4	P3HT : **HO-P3HT-OH** : PC$_{61}$BM	95 : 5 : 100	4.06	[157]
		90 : 10 : 100	3.76	
		85 : 15 : 100	3.53	
		80 : 20 : 100	3.37	
5	P3HT : **P3HT-2-Py-1** : PC$_{61}$BM	2.5 wt%	4.2	[158]
	P3HT : **P3HT-3-Py-1** : PC$_{61}$BM	2.5 wt%	4.3	
6	**P3HT-OXD** : PC$_{61}$BM	1 : 1	4.24	[114]
	P3HT-TAZ : PC$_{61}$BM	1 : 1	0.50	
7	**P3HT : ZnPc** : PC$_{61}$BM	0.5 : 0.5 : 1	2.25	[159]
	P3HT-ZnPc : PC$_{61}$BM	1 : 1	3.27	
	P3HT-ZnPc-C$_{60}$: PC$_{61}$BM	1 : 1	3.56	
8	**14** : PC$_{61}$BM	1 : 1	Poor performances	162
	P3HT : PC$_{61}$BM : **14**	17 wt%	3.1%	
9	P3HT : PC$_{61}$BM : **P3HT-*b*-C$_{60}$**	1.25 wt%	2.29 (after 0 min)	[160]
			2.85 (after 15 min)	
			0.99 (after 360 min)	
		2.5 wt%	2.24 (after 0 min)	
			3.19 (after 15 min)	
			1.50 (after 360 min)	
		5 wt%	1.93 (after 0 min)	
			2.63 (after 15 min)	
			1.42 (after 360 min)	
10	P3HT : PC$_{61}$BM : **P3HT-*b*-P(S$_8$A$_2$)-C$_{60}$**	5 wt%	3.5%	[161]
		10 wt%	3.1%	

		20 wt%	Lower, not notified	
11	P3HT : PC$_{61}$BM : **P3HT-C$_{60}$**	2.5 wt%	3.76 (after 10 min)	[162]
			2.71 (after 24 h)	

Blends incorporating P3HT modified with phenyl-O-CF=CF$_2$ end group as an additive were also found to show slightly better device performance [156]. Despite the introduction of a fluorinated bulky end group (**5**; Figure 4.11), due to repulsive interactions after blending PC$_{61}$BM, the size of the PCBM-rich domains increased while maintaining the P3HT crystallinity. As a result, efficient exciton dissociation was achieved due to the maximization of continuous interfacial area between the donor and the acceptor as well as bicontinuous networks of donor and acceptor domains, resulting in better percolation pathways for charge transport (Entry **2**, Table 4.1).

Nevertheless, a negative correlation between the length of perfluoroalkyl chain and OPV performances was reported by Mao and coworkers (**6**; Figure 4.11) [129a]. PV performance systematically decreased with increasing perfluoroalkyl end-group length from –C$_4$F$_9$ to C$_8$F$_{17}$, in particular the short-circuit current density (J_{SC}) and series resistance, pointing out the lower charge carrier mobility and the poor morphology (Entry **3**, Table 4.1). While the morphology of blends did not show any significant change by atomic force microscopy (AFM), wider nanofibril P3HT (20 nm) domains were observed using energy-filtered transmission electron microscopy (EF-TEM). This finding indicates that perfluoroalkyl chains probably segregated with each other, leading to short P3HT nanofibril domains, despite good nanoscale phase separation. While small amounts of short fluorinated end groups may be advantageous for solar cell performance, large amounts of long fluorinated end groups are detrimental to device performances within P3HT/PC$_{61}$BM blends.

4.3.2.2 Hydrophilic Chain Ends

Hydrophilic end groups such as hydroxyl groups (**HO-P3HT-OH**) have been proved to stabilize the P3HT/PC$_{61}$BM blend through hydrogen bonding interactions with ester group of PCBM (**7**; Figure 4.11) [157]. When this material was used as a compatibilizer, aggregation of PCBM crystals in the annealed P3HT/PC$_{61}$BM film was reduced, and the surface roughness of the P3HT/PC$_{61}$BM film also became smoother. Due to the increase of miscibility, PCBM was finely dispersed in the blend film, resulting in an increase of interfacial area between P3HT and PCBM and thus current density. In addition, thermal stability of the corresponding solar cell devices was improved significantly since the morphology of the active layer remained stable even after annealing at 150°C for 1 h, compared with the P3HT/PC$_{61}$BM reference (Figure 4.13). Polymer solar cell with a PCE of 4.06% was obtained by adding 5% of **HO-P3HT-OH** in the P3HT/PC$_{61}$BM active layer (Entry **4**, Table 4.1). However, PCE performance decreased gradually by increasing the amount of **HO-P3HT-OH** in the blend, indicating that the miscibility should be judiciously adjusted to keep the bicontinuous phase morphology.
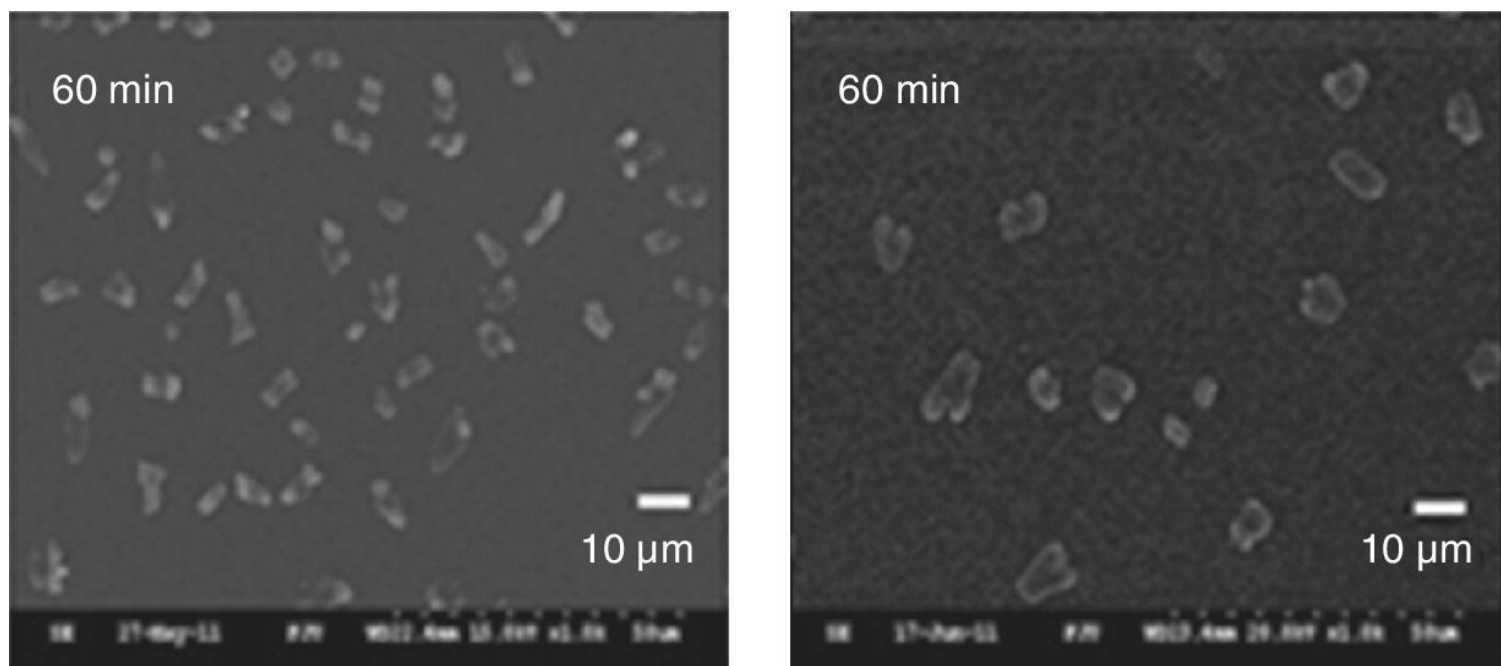
Figure 4.13 Scanning electron microscopy (SEM) images of P3HT/PC$_{61}$BM (left) and P3HT/PC$_{61}$BM:10% HO-P3HT-OH (right) films after thermal annealing at 150°C for 1 h.

In a similar fashion, P3HT/PC$_{61}$BM blends were also compatibilized by pyridine end-functionalized P3HTs (**8** and **9**; Figure 4.11) [158]. Small-angle neutron scattering (SANS) studies demonstrated that the presence of pyridine-based compatibilizer modified the average domain size and thus the specific interfacial area between the PCBM and P3HT-rich phase in blends. Surprisingly, the morphology was found to significantly depend on the pyridine position. Indeed, **2-Py** end-functionalized P3HT exhibited increased crystallinity and decreased specific interfacial area and domain size, whereas **3-Py** end-functionalized P3HT exhibited very little change. Nevertheless, these morphological changes led to BHJ structures with improved PV activity (Entry **5**, Table 4.1).

4.3.2.3 Aromatic Chain Ends

Since exciton diffusion length (around 20 nm in conjugated polymers) depends on both mobility and lifetime of exciton, increasing exciton lifetime could be effective to extend exciton diffusion length. To this end, Chi-Min Chen and coworkers introduced electron-deficient moiety (EDM) end groups on P3HT, which allowed an increase of the exciton lifetime from 411 ps for P3HT with H/Br end groups to 524 ps for P3HT with oxadiazole (OXD) units (**10** and **11**; Figure 4.11) end groups [114]. Adding OXD end groups not only improved exciton lifetime but also enhanced absorption coefficient and promoted slightly lower HOMO level. Chain ordering was increased in the blend with PC$_{61}$BM, resulting in more efficient charge carrier transport and thus improved PCE (4.24%) (Entry **6**, Table 4.1). Nevertheless, as already discussed earlier, the type of end-functionality added to P3HT chain ends is a critical factor for OPV efficiency. Compared with **P3HT-OXD**, triazole end-functionalized P3HT (**P3HT-TAZ**) exhibited modest PCE (0.50%) due to the steric hindrance of the TAZ groups that disturb the interchain packing [114].

As promising photosensitizers, porphyrin and phthalocyanine derivatives have been widely used for the functionalization of P3HT-based polymers to enhance the absorption spectra of blend films and the intermolecular charge transfer. By successfully linking a zinc phthalocyanine dye (**ZnPc**) to the chain end

of P3HT through the formation of a coordination complex, the photocurrent generation by both direct photoexcitation and effective charge separation was enhanced (**12**; Figure 4.11) [159]. Contrary to phthalocyanines directly blended with P3HT and PCBM, end-functionalization avoided the self-aggregation of **ZnPc** dyes, which were preferentially located at the interface between P3HT and $PC_{61}BM$, without disturbing the P3HT crystallization (a, Figure 4.14). This result also remained true when 10 mol% of isocyanide porphyrin was incorporated as a P3HT end group (**13**; Figure 4.11) [163]. Well-aligned fibrils over few micrometers in length were observed (b, Figure 4.14), and characteristic crystalline ordering of P3HT was confirmed by the position of the (100) lattice peak in the XRD spectrum. Moreover, when the fullerene was directly functionalized by this **ZnPc** dye, the interfacial tension was decreased, affording to the reduction of the domain size in the $P3HT/PC_{61}BM$ blend [159]. Devices achieved better efficiencies with 20% enhancement of the short-circuit current compared with $P3HT/PC_{61}BM$ reference (Entry **7**, Table 4.1).
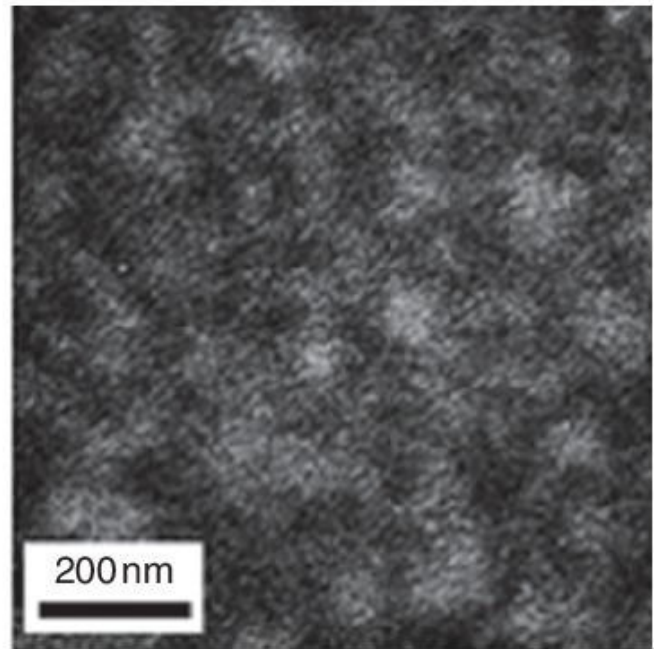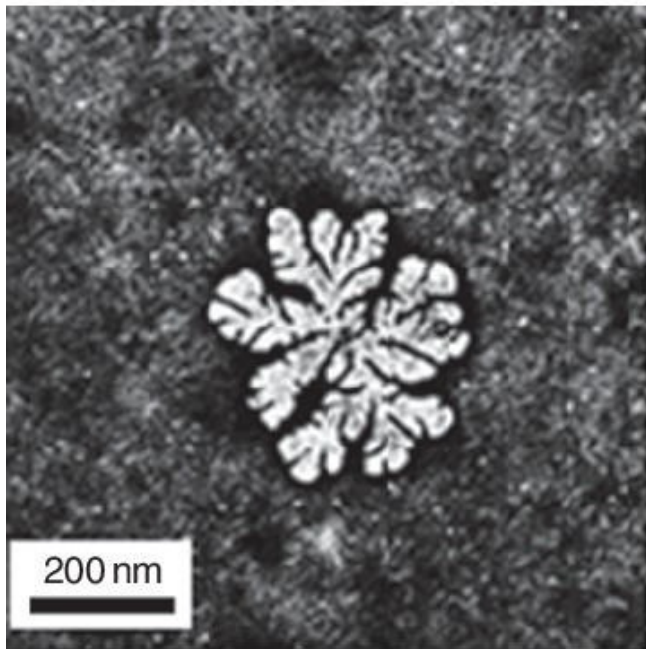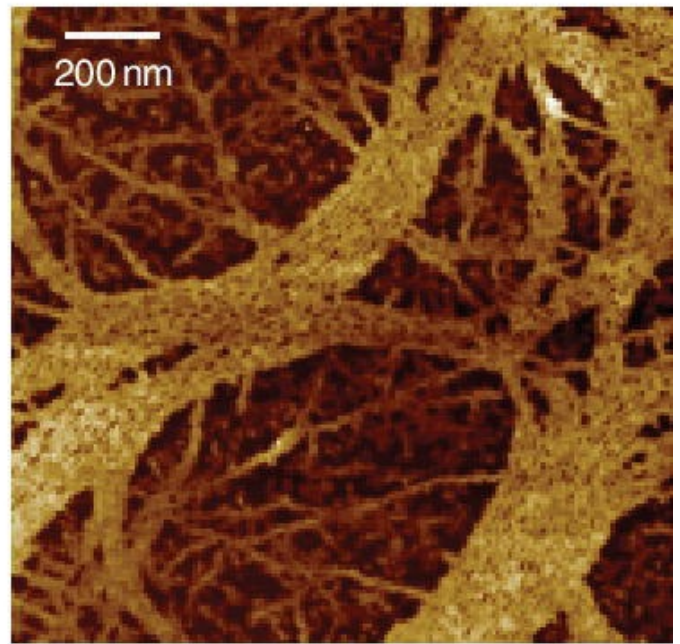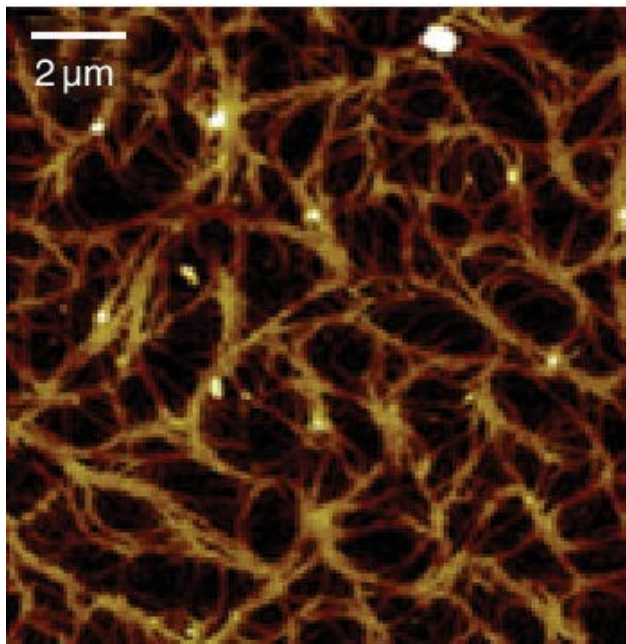
Figure 4.14 (a) TEM images of P3HT/ZnPc/PC$_{61}$BM (left) and P3HT-ZnPc/PC$_{61}$BM (right) after thermal annealing at 150°C for 5 min.

Source: Lee *et al.* [159]. Reproduced with permission of Royal Society of Chemistry.

(b) 10×10 µm^2 (left) and 2×2 µm^2 (right) peak force AFM height image of 13 drop-cast from xylene onto a mica substrate.

Source: Chevrier *et al.* [163]. Reproduced with permission of Royal Society of Chemistry.

4.3.2.4 Fullerene Chain Ends: Compatibilizer Case

Block copolymers have been successfully applied in conjugated polymer–fullerene solar cells as compatibilizers to improve the morphological control and stability of immiscible materials such as P3HT and fullerene. By having at least two blocks (one similar to donor polymer and the other to fullerene), block copolymers decrease the interfacial energy due to their preferential location at the interface, thus improving the miscibility of such systems. Many research groups have synthesized block copolymers based on different functional blocks, for example, perylene tetracarboxydiimide (PDI), polystyrene (PS), and polyethylene oxide (PEO), for compatibilizer applications [164].

The first graft-block-type copolymer based on pendant P3HT units in one segment and pendant fullerene derivatives in the other segment was reported by Fréchet *et al.* in 2006 (**14**; Figure 4.15) [165]. Although this copolymer showed poor performance as employed in the active layer, it improved the stability of P3HT/PC$_{61}$BM-based BHJ solar cells when used as compatibilizer. By using covalent approach, fullerene could be load in such copolymers at high content of about 50%. Upon addition of **14**, morphology of the P3HT/PC$_{61}$BM blend was not affected until the subsequent annealing that produced micrometer-order band-type morphology. Besides, phase segregation was not detected by adding 17 wt% of **14** in blends, significantly improving the thermal stability of the P3HT/PC$_{61}$BM device (Entry **8**, Table 4.1).

$m = 25$
$n = 2–10$
$p = 25$

14

15

16
P3HT-*b*-P(S$_x$A$_y$)-C$_{60}$

17

18
P3HT-*b*-PPC$_{71}$BM

P3HT-C$_{60}$
19

C$_{60}$-P3HT-C$_{60}$
20
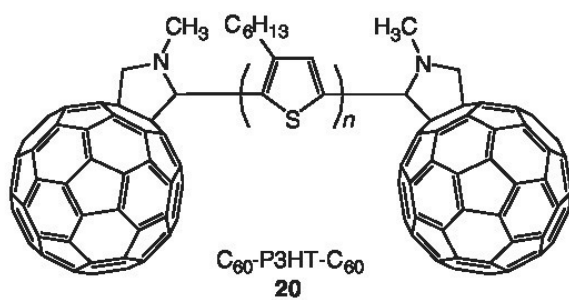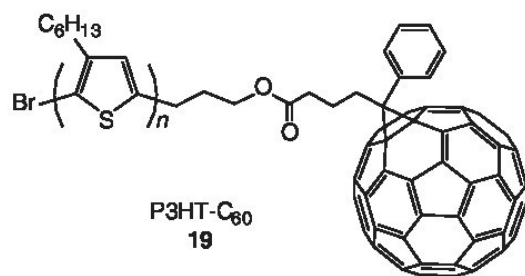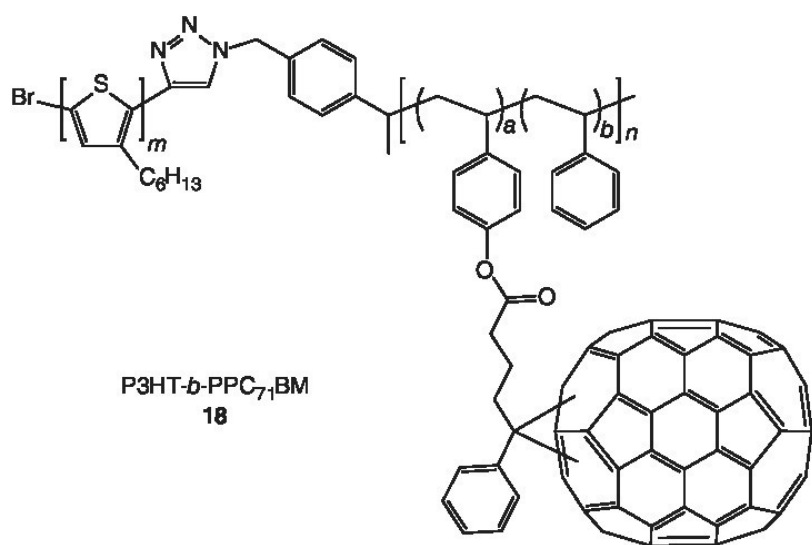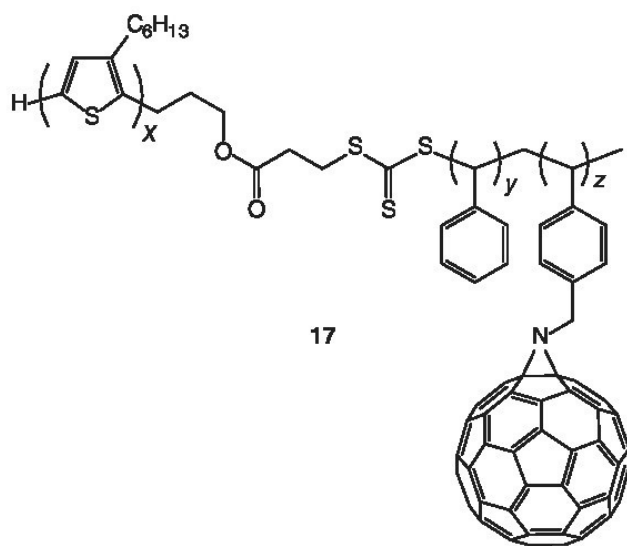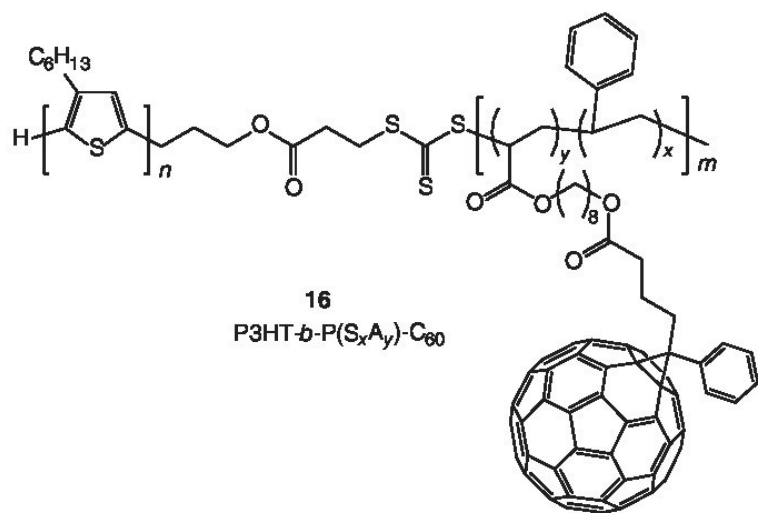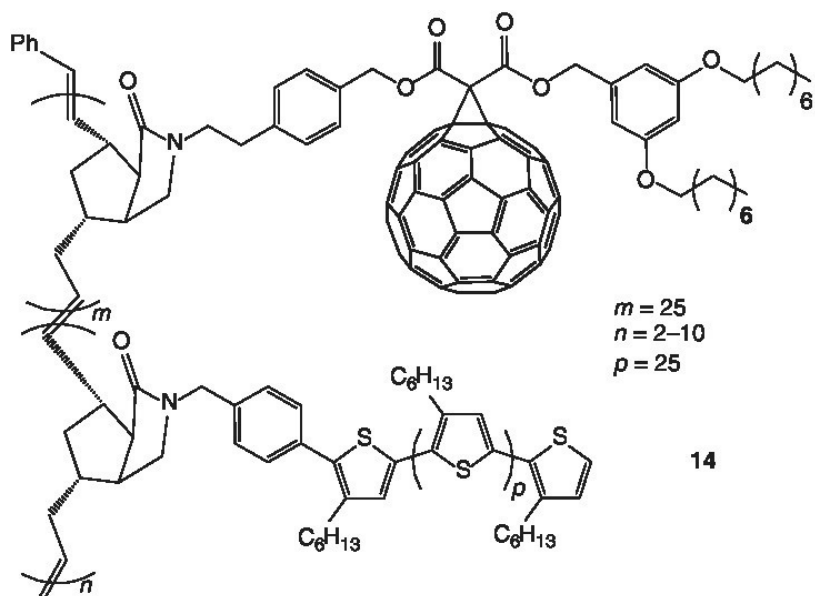
Figure 4.15 Structures of fullerene end-functionalized P3HT derivatives.

A well-defined diblock copolymer (**P3HT-*b*-C$_{60}$**) based on a regioregular P3HT and fullerene has also been employed as a compatibilizer in P3HT/PC$_{61}$BM-based BHJ solar cells [160]. The diblock copolymer (**P3HT-*b*-P(MMA-*r*-HEMA)**) was functionalized by fullerene derivative having carboxylic acid functionality, [6,6]-phenyl-C61-butyric acid (PCBA) (**15**; Figure 4.15). The addition of a small amount of **P3HT-*b*-C$_{60}$** improved the high temperature stability of device performance due to the interfacial tension decrease between P3HT and PCBM phases. The phase size of the P3HT/PC$_{61}$BM blend increased with extending annealing time, while the blend with the compatibilizer kept a well-defined bicontinuous network morphology. Moreover, the diblock copolymer suppressed the rate of domains agglomeration, resulting in an improved long-term stability of device performance (Entry **9**, Table 4.1).

Heeger and coworkers have also reported rod–coil block copolymers consisting of P3HT donor and C$_{60}$ acceptor chromophores (**P3HT-*b*-P(S$_x$A$_y$)-C$_{60}$**) (**16**; Figure 4.15) [161]. In thin films, the resulting block copolymer self-assembled into well-defined nanofibrils. Furthermore, by adding a small amount of the diblock copolymer to P3HT/PC$_{61}$BM blend, the interfacial morphology between the two immiscible components was also altered, resulting in a significant phase segregation difference. Upon addition of 5% diblock copolymer as compatibilizer, J_{SC} was significantly enhanced, leading to about 35% increase in PCE compared with the reference P3HT/PC$_{61}$BM cell fabricated without the compatibilizer (Entry **10**, Table 4.1). In a similar fashion, Nguyen *et al.* reported the synthesis of a triblock copolymer consisting of a rigid donor PT block with a shorter coil PS block containing a C$_{60}$ pendant group (**17**; Figure 4.15) [166].

The third coil block based on PS acted as a spacer and a solubilizing moiety. Quenching of photoluminescence indicated the presence of a strong light-induced charge transfer between P3HT and fullerene blocks attached covalently. Thanks to conducting AFM, it was also found that thin films of **18** were fairly electrically homogeneous and that similar hole and electron mobilities to those of P3HT/PCBM BHJ films were obtained. Very recently, PC$_{71}$BM-grafted D–A block copolymers were reported by Thelakka and coworkers (**18**; Figure 4.15) [167]. By covalently grafting PC$_{71}$BM, the block copolymer exhibited enhanced absorption in the entire visible range between 300 and 600 nm and ordered morphology with phase separation in the range of 10–20 nm, suitable to exciton diffusion. More importantly, this ordered morphology observed in bulk and thin films was found to be independent of the processing method, that is, from solution evaporation or by melt crystallization.

Although the block copolymer compatibilizer could control the nanometer-scale morphology and improve the long-term thermal stability of BHJ solar cells, its synthesis is tedious due to the multiple post-polymerization steps and the low solubility of fullerenes. Furthermore, the presence of a substantial amount of insulating moieties is required for introducing C$_{60}$ in the other block. To overcome these limitations, fullerene end-functionalized P3HT have been synthesized (**19** and **20**; Figure 4.15) [162, 168]. In both cases, adding C$_{60}$ as end group of P3HT impacted the P3HT thermal properties. Both C$_{60}$-functionalized P3HTs exhibited decreased melting and crystallization temperatures compared with pristine P3HT due to the bulky C$_{60}$ group, which acts as an impurity in P3HT crystallite. Nevertheless, the P3HT crystallinity remains approximately the same as that of the pristine P3HT [168]. When used as compatibilizer in P3HT/PC$_{61}$BM blends, P3HT-C$_{60}$ eliminated macrophase separation and improve long-term stability by avoiding the formation of PCBM aggregates and promoting smaller domain size (Figure

). Indeed, the PCE of the P3HT/PCBM device without compatibilizer decreased below 1% of PCE after annealing at 150°C for 2 days, whereas PCE was maintained at around 3% with 2.5 wt% compatibilizer (Entry **11**, Table 4.1) [162].
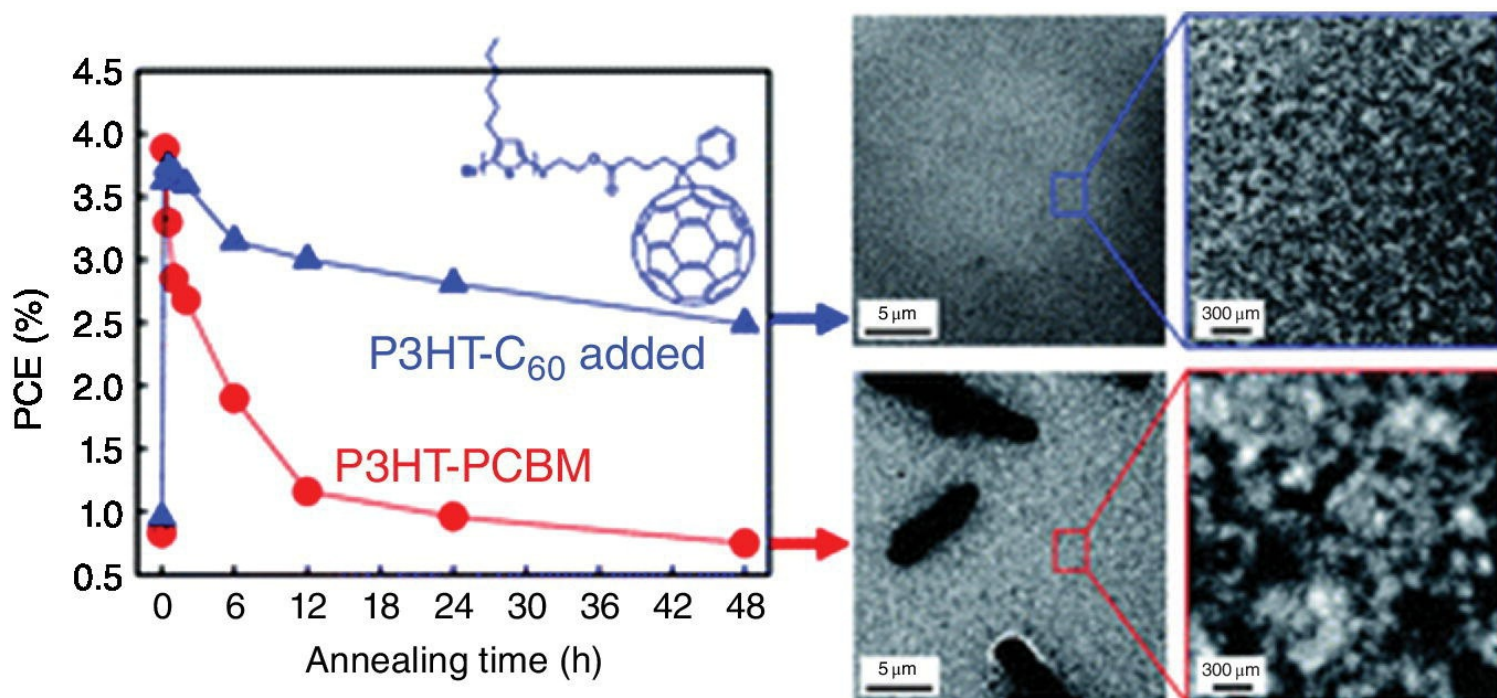
Figure 4.16 Power conversion efficiencies of P3HT/PC$_{61}$BM and P3HT/P3HT-C$_{60}$/PC$_{61}$BM blends as a function of annealing time at 150°C.

Source: Lee *et al.* [162]. Reproduced with permission of Royal Society of Chemistry.

4.3.3 Side-Chain Functionalization

The introduction of functional moieties in the P3HT side chains also offers a potential pathway toward morphology control and stability of P3HT–fullerene active layer blends applied in BHJ organic photovoltaics.

4.3.3.1 Thermal and Photo-Cross-Linking

The cross-linking strategy is a powerful solution for achieving morphology stability of BHJ solar cells by locking in the active layer morphology. The first cross-linkable P3HT (regioregular poly(3-(5′-hexenyl)thiophene) (**P3HNT**)) crystallized and generated nanoscale phase-separated structures in a similar manner to P3HT/PC$_{61}$BM films (**21**; Figure 4.19) [141]. The thermal treatment induced a cross-linking reaction of vinyl group at the side chains, preventing the diffusion of PCBM into the film (Figure 4.17) and leading to more stable device performance for **P3HNT** than for P3HT (Entry **1**, Table 4.2).
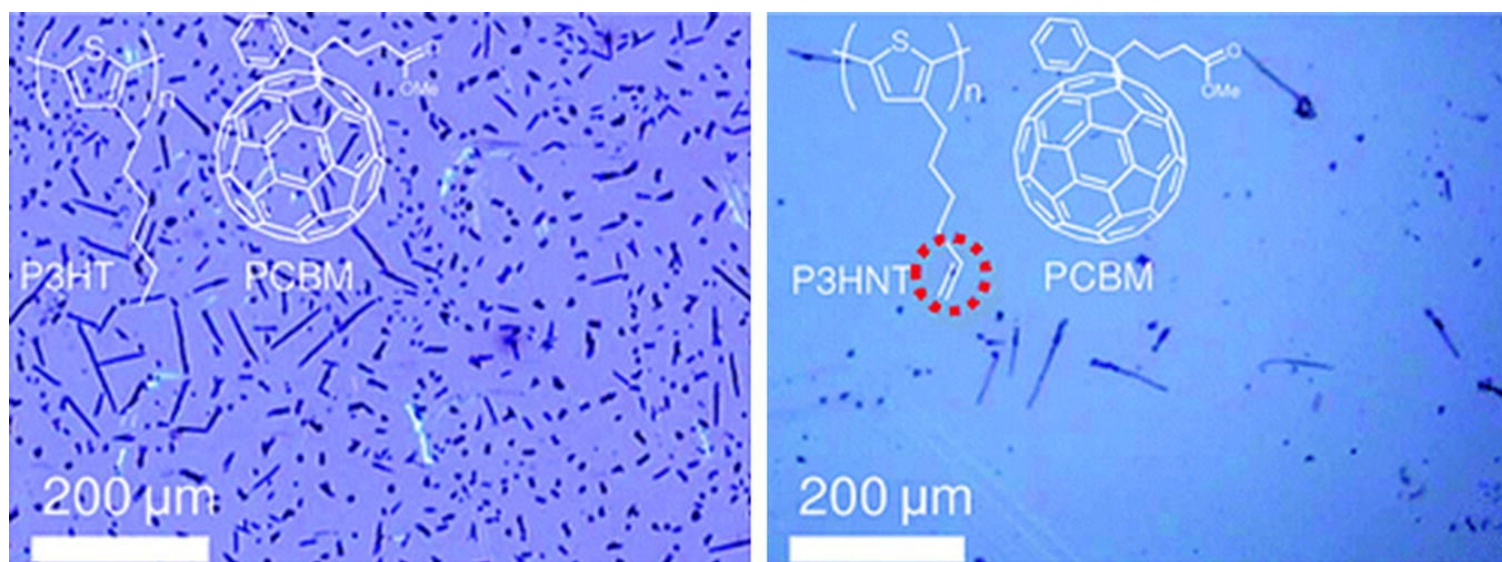
Figure 4.17 Optical microscope images of P3HT/PC$_{61}$BM (left) and **P3HNT**/PC$_{61}$BM (right) films after thermal annealing at 150°C for 10 h.

Source: Miyanishi *et al.* [141]. Reproduced with permission of American Chemical Society.

Table 4.2 Bibliographic data of side-functionalized P3HTs extracted from the literature.

Entry	Device structure	Ratio	PCE (%)	Reference
1	**P3HNT** : PC$_{61}$BM	1 : 0.8	3.16	[141]
2	**P3HT-*r*-P3HTBr (95-5)** : PC$_{61}$BM	1 : 1	3.38	[169]
	P3HT-*r*-P3HTBr (90-10) : PC$_{61}$BM	1 : 1	3.35	
	P3HT-*r*-P3HTBr (80-20) : PC$_{61}$BM	1 : 1	3.11	
3	**P3HT-N5** : PC$_{61}$BM	1 : 1	1.2 (110°C)	[170]
4	**P3HT-Ox10** : PC$_{61}$BM	1 : 1	0.56 (nanostructured bilayer)	[171]
5	**Random 5**	Single component	0.48	[172]
	Block 5		1.70	
6	**Random 6**	Single component	0.45	[173]
	Block 6		2.13	
7	**28** : P3HT:PC$_n$BM	0.25 wt%	3.4	[143]
	29 : P3HT:PC$_n$BM		3.4	
	30 : P3HT : PC$_n$BM		3.1	
	31 : P3HT : PC$_n$BM		3.3	
	32 : P3HT : PC$_n$BM		3.2	
	33 : P3HT : PC$_n$BM		3.8	
	33 : P3HT : PC$_n$BM	2.5 wt%	3.4	
		10 wt%	0.47	

8	34 (9/1) : PC$_{61}$BM	1 : 1	2.49	[174]
	34 (7/3) : PC$_{61}$BM		1.98	
	34 (1/1) : PC$_{61}$BM		1.97	
	35 (9/1) : PC$_{61}$BM		2.43	
	35 (7/3) : PC$_{61}$BM		2.13	
	35 (1/1) : PC$_{61}$BM		1.61	
9	36 (9/1) : PC$_{61}$BM	1 : 1	2.04	[174]
	36 (7/3) : PC$_{61}$BM		1.14	
	36 (1/1) : PC$_{61}$BM		0.47	
10	38 25% : PC$_{61}$BM	1 : 1	1.08	[175, 176]
	38 15% : PC$_{61}$BM		0.14	
	38 10% : PC$_{61}$BM		0.028	
	38 5% : PC$_{61}$BM		0.012	
11	P3HTIm-1Zn : PC$_{61}$BM	1 : 0.6	0.15	[142]
	P3HTIm-2Zn : PC$_{61}$BM		0.24	
12	PT-1 : PC$_{61}$BM	1 : 1	1.86	[177]
	PT-Pc : PC$_{61}$BM	1 : 1	0.32	
	PT-Pc : PC$_{61}$BM	1 : 2	0.41	
13	P3HT-*b*-P3TODT : PCBA	3 : 2	2.04	[178]

Thermal treatments used to induce cross-linking reactions of cross-linkable P3HTs may be problematic because they can interfere with the thermal annealing process required for controlling the morphology and thus the device performance. Hence, many research groups have synthesized photo-cross-linkable P3HTs. Indeed, by carefully controlling the monomer ratio in the random copolymer **P3HT-*r*-P3HTBr**, UV-photo-cross-linkable layer was achieved while maintaining the π–π stacking interactions operating in P3HT (**22**; Figure 4.19) [169]. Unlike the devices prepared from P3HT/PC$_{61}$BM blends, photo-cross-linkable **P3HT-*r*-P3HTBr**-based devices were stable even after annealing at 150°C for 2 days exhibiting PCE around 3% (Entry **2**, Table 4.2). However, although high efficiencies were reported for these devices, suggesting that the cross-linking byproducts are not necessarily detrimental to device performance, the fate of the bromine functional group after cross-linking reaction remained ambiguous. To avoid this potential problematic, azide groups, known to have a minimal impact on the polymer properties, were attached to the side chain of P3HT (**23**; Figure 4.19) [170]. Azide photo-cross-linkable PT-based devices showed excellent performance with high solvent and thermal resistance. OFETs of these copolymers exhibited similar charge carrier mobility to that of P3HT, demonstrating that azide groups do not degrade the electronic properties of P3HT. Cross-linking slightly compacted the PT chain lamellar stacking while increasing the polymer crystal coherence length by 20%. Optimized solar cells having cross-linked active blend layers retained 65% of their initial PCE after 40 h of thermal annealing at 110°C (Entry **3**, Table 4.2), while devices using uncross-linked PT underwent significant phase

separation and retained less than 30% of their initial efficiency.

Active layer structure can also be controlled through a cross-linking approach. A columnar-grain morphology was thus obtained by copolymerizing a 3-hexylthiophene monomer with 10% molar of a cross-linkable oxetane-functionalized thiophene monomer (**24**; Figure 4.19) [171]. Optical and electrochemical properties of this cross-linkable polymer were analogous to those of P3HT, although a noticeable absorption decrease was observed upon cross-linking for **P3HT-Ox10**. By using this copolymer, OPVs with nanostructured D–A interface could be fabricated using low-cost and solution-based method, allowing the PCBM deposition from solution on top of the polymer layer (Figure 4.18). The obtained morphology was very close to the optimal architecture type for OPV operation since well-defined domains of electron donor were formed perpendicular to the cell substrates. Unfortunately, despite this excellent nanomorphology, **P3HT-Ox10**-based BHJ solar cells exhibited lower performance than those with pristine P3HT (Entry **4**, Table 4.2).
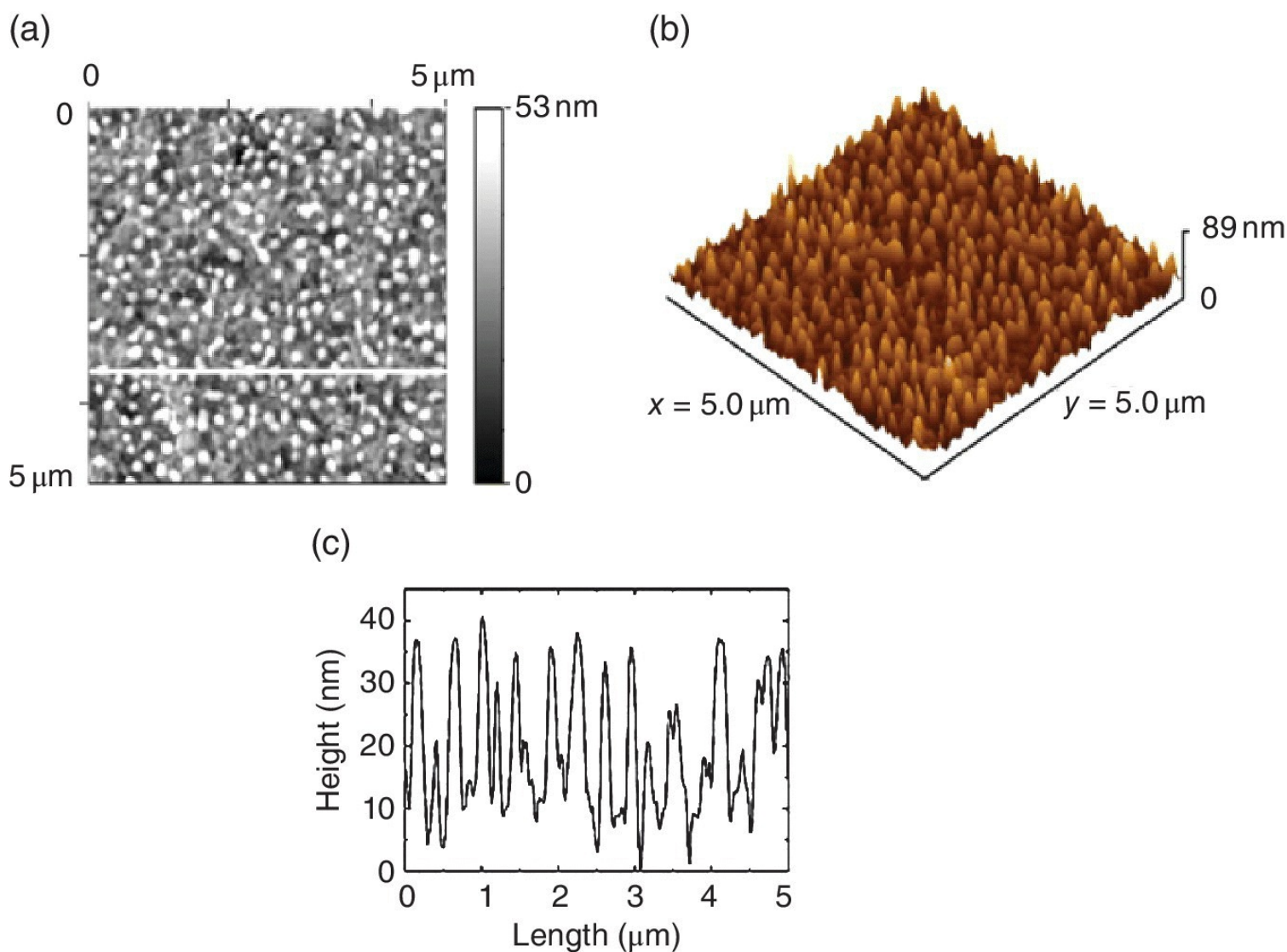
Figure 4.18 (a) AFM topographic image (5 μm × 5 μm) and (b) corresponding 3D projection showing a columnar structured film of cross-linked **P3HT-Ox10**; (c) sectional view along a line in the AFM image.

Source: Brotas *et al.* [171]. Reproduced with permission of Elsevier.

4.3.3.2 Fullerene Side-Functionalization on Polythiophene Block Copolymers

Single-component systems present potential advantages over the mixed BHJ systems such as the

simplicity of the fabrication process and the construction of thermodynamically stable nanostructures, which can be tuned through molecular modifications.

Poly-(3-alkylthiophene)-based random and diblock copolymers with a fullerene-attached block were applied in single-component polymer solar cells (**25**; Figure 4.19) [172]. Contrary to random copolymers, P3HT–fullerene diblock copolymers showed microphase separation characteristic from most of the PT diblock copolymers. Crystalline P3HT domains were also evidenced by UV-Vis spectroscopy, where a redshift and a shoulder around 610 nm in absorption were observed in the diblock copolymer. In the random copolymer, the absence of ordered structures, due to the strong aggregation tendency of the fullerenes distributed statistically on the side chains, caused lower efficiency than diblock copolymer even after thermal annealing (Entry **5**, Table 4.2). Moreover, the block structure was also clearly important to improve the device stability: after 80 h at 130°C, no PCBM aggregation was observed compared with P3HT/PC$_{61}$BM blend reference, resulting in a small change in PCE from 1.59 to 1.50%.
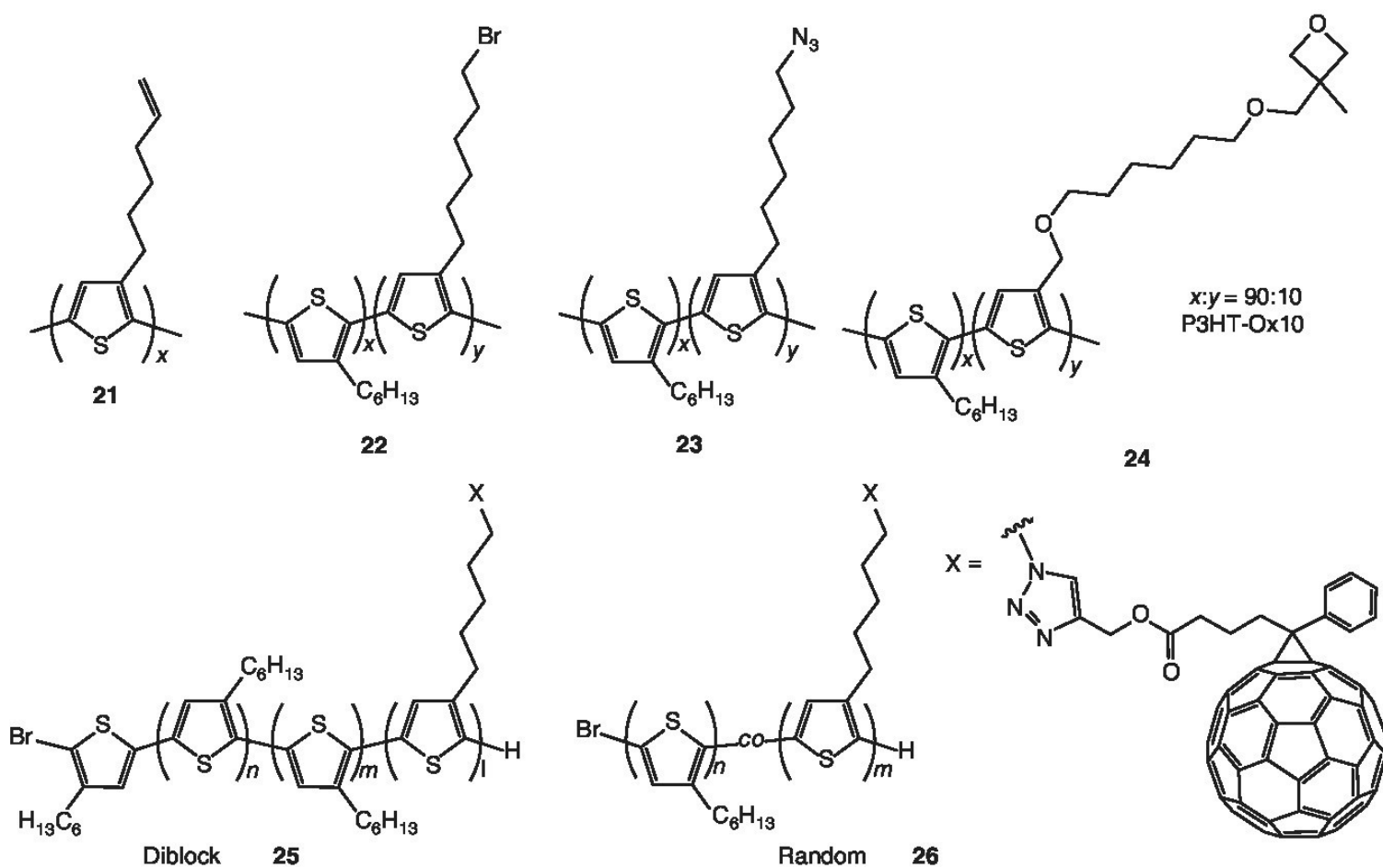
Figure 4.19 Cross-linker and fullerene side-chain-functionalized P3HTs.

In 2012, Tajima *et al*. synthesized regioregular PT-based block and random copolymers with pendant fullerene units (**26**; Figure 4.19) [173]. After the synthesis of P3AT-based copolymers using KCTCP polymerization, conversion of the bromide into azide group affords the attachment of fullerene via Cu(I)-catalyzed click reaction. It was found from the XRD that the copolymer **26** exhibits similar diffraction patterns than P3HT/PCBM blend mixture, suggesting a lamellar nanostructure, similar to P3HT. OPVs fabricated using **26** demonstrated relatively high PCEs, due to the formation of a nanophase separation, similar to that of the P3HT/PC$_{61}$BM blend mixture (Entry **6**, Table 4.2). The incorporation of P3HT-C$_{60}$ block copolymers as compatibilizer in P3HT/PCBM BHJ solar cells also afforded to the formation of a self-organized nanostructure and the enhancement of the interchain interactions in P3HT domains [179].

PCE of 2.56% was obtained upon addition of 20% P3HT-C$_{60}$ diblock copolymer.

4.3.3.3 Cooperative Self-Assembling

Most of the existing D–A block copolymers incorporating fullerene acceptor moieties include fullerene covalently attached to one block. However, fullerene loading percentages in these copolymers are generally low and difficult to control due to the limited solubility and the strong aggregation tendency of fullerenes. In parallel to these works, non-covalent approaches have been developed to easily attach fullerenes with a controllable molar ratio [143, 180].

4.3.3.3.1 Aromatic π-Stacking

Aromatic π-stacking interactions can be used to mediate interactions between donors and acceptors and thus their self-assembling and electronic properties. For example, P3HT-based side-chain copolymers functionalized with pyrene groups were combined with a pyrene-containing fullerene derivative to promote π-stacking interactions between donor and acceptor (**27**; Figure 4.20) [180].
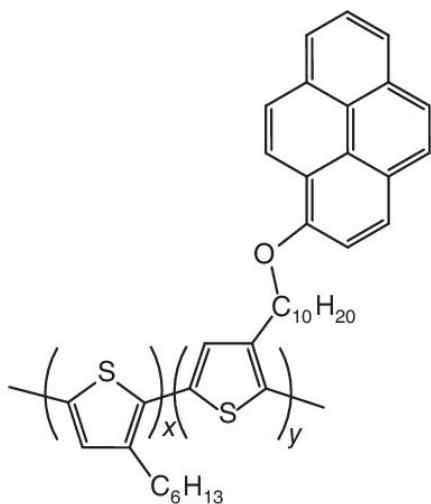
P3HT-b-P3TPy(3:1),   x:y = 3:1
P3HT-b-P3TPy(10:1), x:y = 10:1
P3HT-b-P3TPy(14:1), x:y = 14:1

PCBPy

27

28

29

30

31

32

33

x/y = 9/1, 7/3, 1/1

x/y = 9/1, 7/3, 1/1

34

35

36
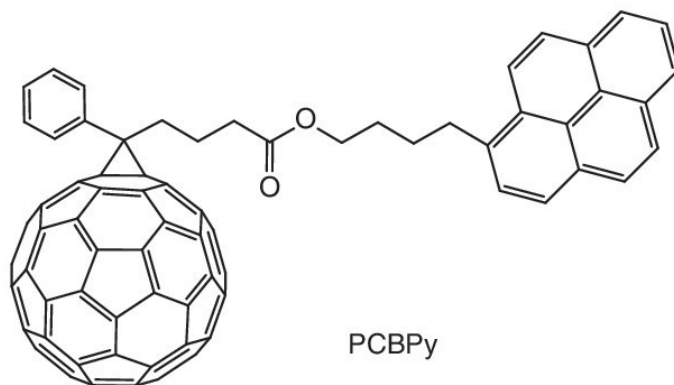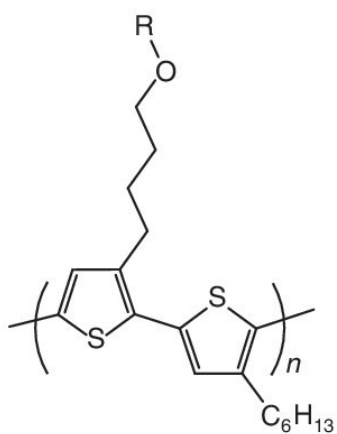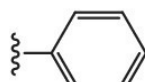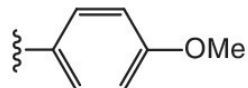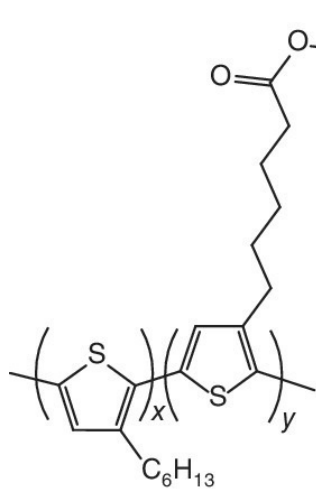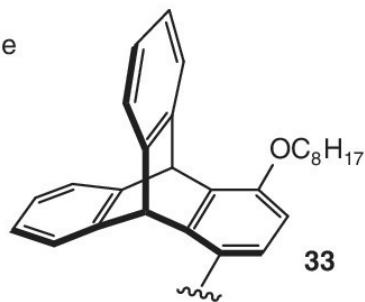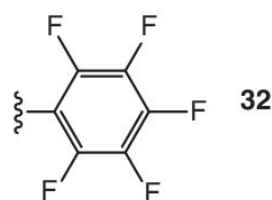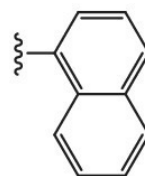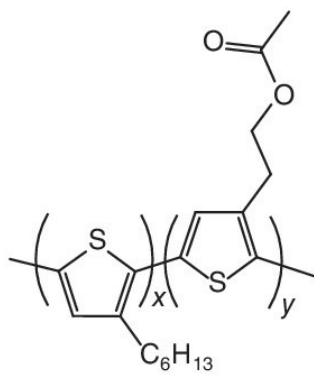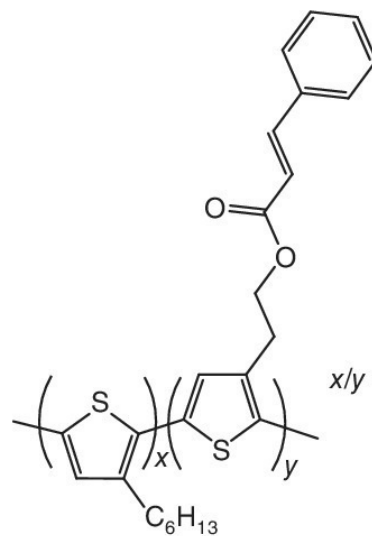
Figure 4.20 Aromatic side-chain-functionalized P3HTs.

Although pyrene are bulky groups, UV-Vis, photoluminescence, and XRD results demonstrated that their introduction on the side chains of P3HT-based copolymer does not affect the conjugation length and the high crystallinity of the P3HT block. This cooperative introduction results in a strong decrease in luminescence, indicating a fast photoinduced charge transfer between the donor and the acceptor, compared with the P3HT/PCBM blend reference. Cooperative π-stacking between functionalized P3HT and PCBM was evidenced by the presence of an XRD peak at 2θ = 2.5° (d = 3.53 nm) and confirmed by DFT calculations. Nevertheless, the obtention of an ordered morphology was strongly dependent on the amount of pyrene. At low pyrene loading (14 : 1), functionalized P3HT and PCBM tended to cooperatively self-assemble into lamellar structure with 10–20 nm wide domains with alternate pyrene-functionalized fullerene-rich and fullerene-poor regions. In contrast, too high content of pyrene functionalities in the copolymer promoted pyrene mesogen structures over PT interchain interactions.

A series of AB-alternating side-chain-functionalized P3HT containing aryloxy groups such as phenoxy, 4-iodophenoxy, 4-anisyloxy, 1-naphthoxy, triptycenoxy, and perfluorophenoxy groups were also reported by Swager *et al.* (**28–33**; Figure 4.20) [143]. The side-chain-functionalized polymers displayed the same photophysical properties as P3HT. The presence of these functionalities up to 10 wt% of polymers did not disturb the formation of P3HT lamellar structures. At low loading (0.25 wt%), adding them as additives in BHJ solar cells significantly increased the PCE compared with P3HT/PC$_n$BM reference (Entry **7**, Table 4.2). However, higher additive loadings (>5 wt%) led to detrimental nanoscale phase separation within the active layer, resulting in low PCE solar cells (0.47% at 10 wt%). Among these functionalizations, perfluorophenoxy-functionalized P3HT was the most effective additive and yielded a 28% increase in PCE when incorporated into the P3HT/PC$_{61}$BM BHJ solar cell. The additive was selectively localized at the interface P3HT/PC$_{61}$BM so that the functional groups could interact with the fullerene phase. It is admitted that these side-chain aromatic moieties introduced a dipole at the polymer–fullerene interface, which decreased the rate of recombination and, therefore, improved charge collection across the active layer in a BHJ solar cell.

As illustrated earlier, the copolymer composition has to be judiciously adjusted to improve the solar cell efficiency as well as the nature of the side-chain group. rrP3HT-based random copolymers have been obtained with 10, 30, and 50% of cinnamoyl-functionalized side chains after modification of ester side chains (**36**; Figure 4.20) [174]. When smaller ester-functionalized side chains were introduced (**35**; Figure 4.20), moderate modification of the self-organization and π–π stacking of the conjugated backbone was observed. In this case, the optical, thermal, and electronic properties of the copolymer and the PCE in BHJ organic solar cells were found to depend less strongly on the percentage of functionalized side chains in the copolymer **35** (Entry **8**, Table 4.2). In contrast, for copolymers with longer ester-functionalized side chains (**34**; Figure 4.20), a decrease in external quantum efficiency (EQE), J_{sc}, and hole mobility was observed with more than 10% of functionalization due to the less perfect crystalline structure and the lower content of crystalline regions in the polymer phase. Thus, by limiting the amount of functionalized chains below 10%, solar cell performance comparable with pristine P3HT (2.48%) was obtained (Entry **9**, Table 4.2).

4.3.3.3.2 Porphyrins and Phthalocyanines

As already discussed for the end-functionalization, another way to improve the photocurrent generated in a solar cell consisted in introducing porphyrin chromophores to increase the intermolecular charge transfer. When porphyrins were directly blended with P3HT and PCBM, their self-aggregation led to self-

quenching of the excited states and decreased performances [181]. To avoid this negative effect, side-chain coordination strategies were also developed. In this context, PT random copolymers bearing porphyrin in the side chains were prepared through post-functionalization (**37–38**; Figure 4.21) [175, 176].

Poly(T6TPP)

37

Poly(T6Br-co-T6TPP)

38

P3HT-1Zn : R = C$_6$H$_5$

39

P3HT-2Zn : R = C$_6$F$_5$

40

O—R

ξ—H

ξ—Et

ξ—$\equiv$—H

41

P3HT-b-P3TODT

bis-PCPBA

42

P1

m/n = 6/1

x/y = 1/1

43

PCBM

44
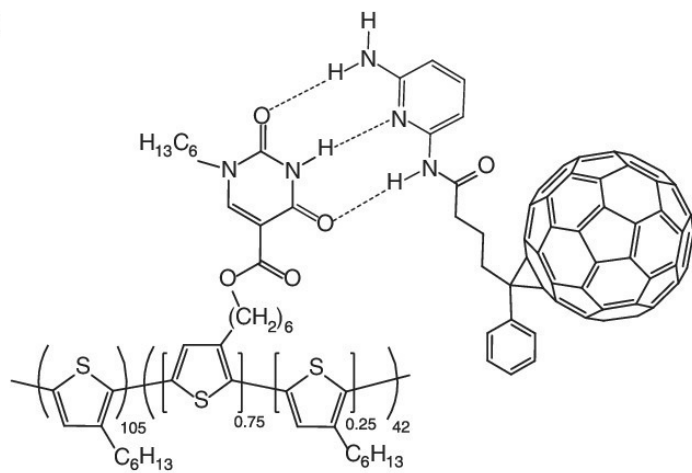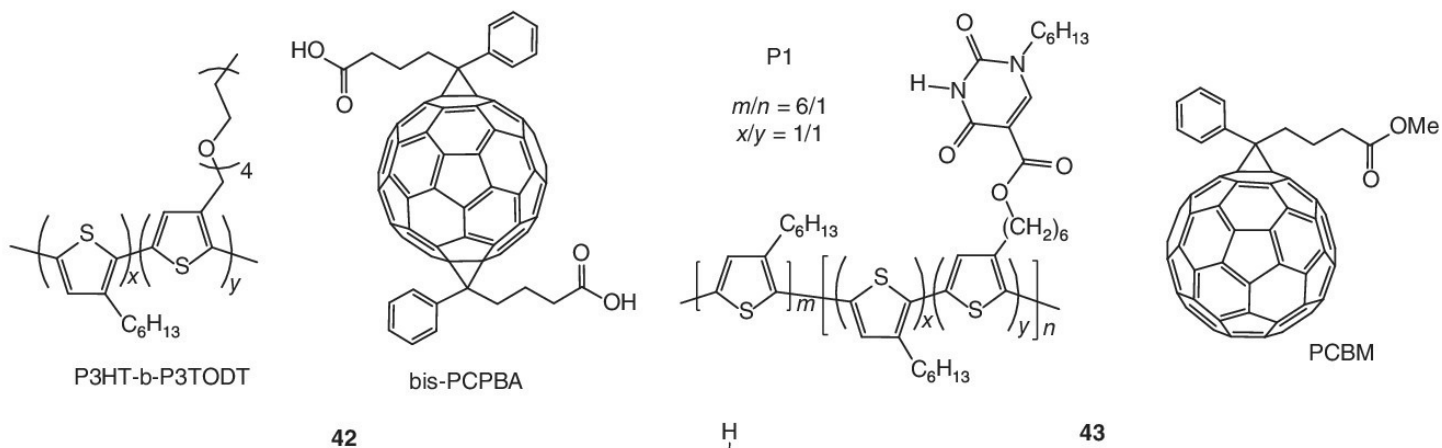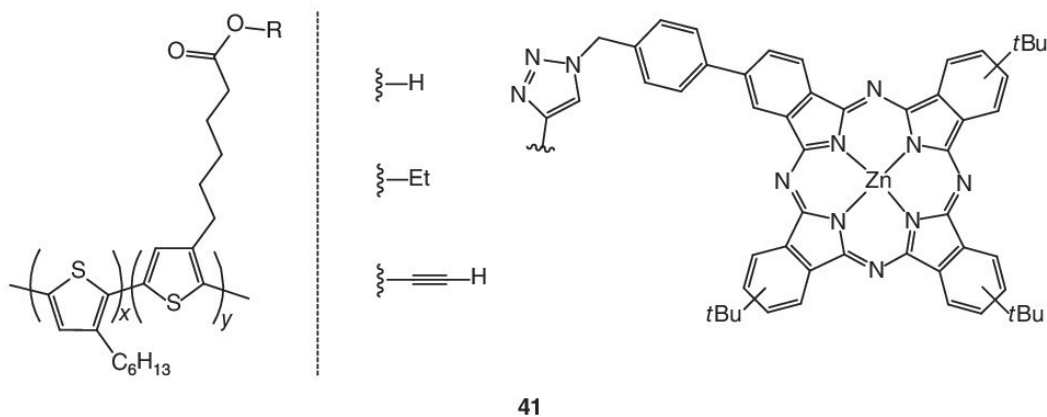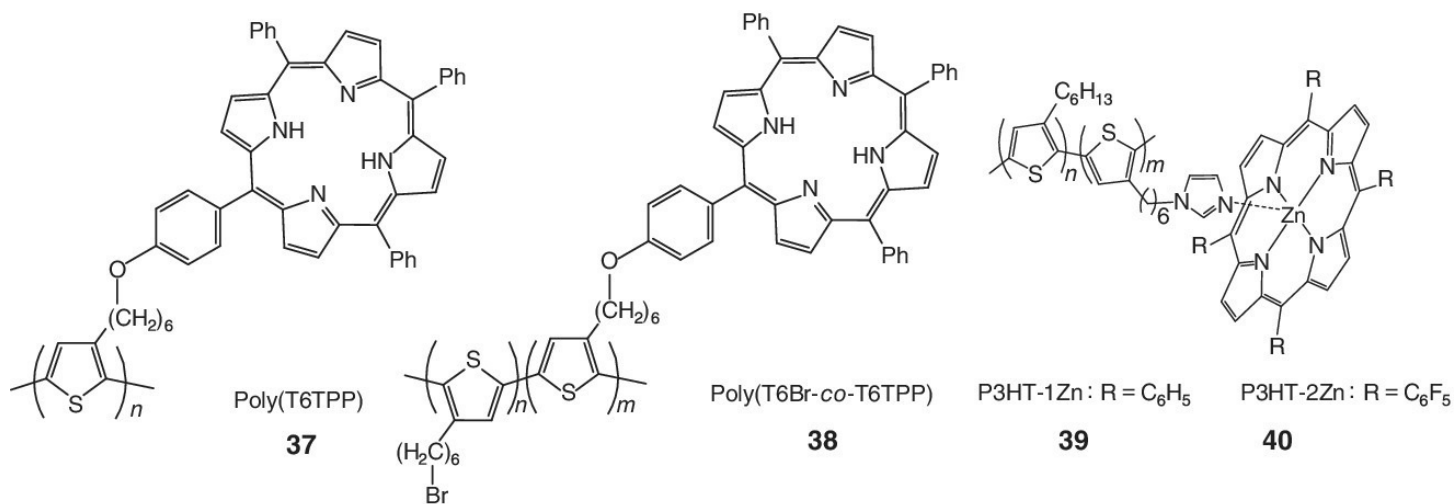
Coordination and hydrogen groups for side-functionalized P3HTs.

The functionalized random copolymers were completely soluble in common organic solvents, allowing to obtain very homogeneous thin films by drop-casting or spin-coating techniques. Although the presence of the porphyrin moieties in the PT copolymer side chains led to enhanced absorption in the visible spectrum, low PCEs (0.012–1.08%) were obtained probably due to the disturbed polymer organization by the presence of porphyrins in the side chains (Entry **10**, Table 4.2). In the same range, Clément *et al.* reported P3HT copolymer derivatives containing 10% appended porphyrin moieties using a supramolecular approach (**39–40**; Figure 4.21) [142]. By attaching 10 molar % of porphyrin by coordination with imidazole-side-functionalized P3HT, a strong contribution of the porphyrin moiety in absorption and photoinduced charge transfer was observed. Unfortunately, the self-assembly of the polymer was also disturbed, leading to poor PV performances (Entry **11**, Table 4.2).

Phthalocyanines (**Pc**) were also used as chromophores for functionalizing P3HT side chains (**41**; Figure 4.21). Phthalocyanines show intense absorptions in the red/near-infrared region with high extinction coefficients and fluorescence quantum yields, which make them ideal chromophore to enhance the spectral coverage [177]. Thus, phthalocyanines were attached to the side chains of P3HT with 10 molar % content. Despite the broadening absorption of the active layers due to the contribution of the **Pc** around 700 nm, solubility of this derivative was too low for the fabrication process. The nanoscale organization of the materials was not appropriate to achieve efficient devices (Entry **12**, Table 4.2).

4.3.3.3.3 Hydrogen Bonding

Hydrogen bonding represents one of the strongest non-covalent interactions and has been also widely applied to mediate the self-assembly of D–A blend and to stabilize photoactive layers in OPV [182]. Self-assembling of conjugated molecules and polymers into various nanostructures modulated by hydrogen bonding has been already well studied [183]. Watkins and coworkers reported the synthesis of a P3HT-*b*-poly[3-(2,5,8,11-tetraoxadodecane)thiophene] (**P3HT-*b*-P3TODT**) block copolymer of P3HT and blended it with bisphenyl C61-butyric acid (**bis-PCBA**) electron acceptor (**42**; Figure 4.21) [178]. The strong hydrogen bonding interactions operating between the carboxylic acid functionality of the fullerene derivative and oligo(ethyl oxide) side chains of the P3HT-based copolymers afforded well-defined nanostructured D–A interpenetrated networks with high fullerene loading (up to 40 wt%). **P3HT-*b*-P3TODT**/**bis-PCBA** device performances (2.04%) were found to be better than **P3HT-*b*-P3TODT**/$PC_{61}BM$ (0.95%) but unfortunately lower than the P3HT/$PC_{61}BM$ (3.01%) (Entry **13**, Table 4.2). Nevertheless, the hydrogen-bonded system showed significant improvements in terms of device stability by retaining 46% of its PCE after annealing at 150°C for 6 h against only 13% for P3HT/$PC_{61}BM$ reference. This better stability was assigned to the diffusion decrease of the fullerene due to the hydrogen bonding of PCBA with the donor copolymer. When PCBA was replaced by PCBM, fullerene aggregation was observed.

In a similar fashion, Qin *et al.* have prepared three different systems based on hydrogen bonding and found that block length ratios of the polymers and nature of fullerenes played crucial roles in morphology control and thus device performance. In order to increase the stability, a "three-point" complementary hydrogen bonding approach was employed for controlling donor and acceptor interactions (**43** and **44**; Figure 4.21) [184]. Blend with iso-orotic acid PT-based copolymer (**P3HT-*b*-P3IOA**) and diaminopyridine tethered fullerene derivative (**PCBP**) were found to be highly resistant to structural change. After 112 h at 110°C, P3HT/PCBM reference without hydrogen interaction retained less than 40% of its PCEs, whereas devices with **P3HT-*b*-P3IOA**/$PC_{61}BM$, having one hydrogen bond, and

P3HT-*b*-P3IOA/PCBP, having three hydrogen bonds, retained 65 and 75% of their PCEs, respectively.

Well-ordered block copolymers/PCBM blends were also reported by Hadziioannou and coworkers using a supramolecular strategy based on non-covalent hydrogen bonds between PCBM and poly(3-hexylthiophene)-*b*-poly(4-vinylpyridine) rod–coil block copolymer [185]. In this system, PTs acted as a hole carrier, while the **P4VP** block was used as a compatibilizer for PCBM. By exploiting the fact that poly(4-vinylpyridines) tend to coordinate electron-deficient species, a PCBM loading of 36 vol% was reached while maintaining P3HT-dominated structure. These systems also showed increased thermal stability over a long period of time (14 h) and high temperature (150°C).

Overall, the incorporation of hydrogen bonding units in the photoactive layer improved PV performance as a result of enhanced morphological stability.

4.4 Polymer–Metal Oxide Hybrid Solar Cells

Although PCEs now exceed 10% for BHJ polymer solar cell devices [4, 12], polymer–fullerene composites suffer from relatively low charge mobility, short diffusion lengths, and inherent long-term instability of the microphase segregation [186]. As indicated earlier, an alternative to fully organic BHJ consists of combining conjugated polymers with *n*-type inorganic semiconductors, taking benefit from their relatively high electron mobility and good physical and chemical stability [13, 187]. In this context, hybrid solar cells based on transition metal oxide compounds have attracted a great deal of interest. Among the metal oxides, titanium and zinc oxides (TiO_2 and ZnO) were probably the most widely studied [13b]. These metal oxides are promising acceptor candidates due to their low toxicity and low cost. They can be synthesized in various sizes and shapes, which offer the opportunity to optimize the charge transport in the PV devices [14–16].

Two different approaches exist for preparing polymer–metal oxide hybrid solar cells. One consists in mixing dispersed metal oxide NCs with the polymer (Figure 4.22) [188]. As the control of the morphology is a key point in BHJ solar cells for having the best PCEs, obtaining bicontinuous network with two intermixed components remains currently a challenge [188]. The other method is based on the polymer infiltration into nanostructured metal oxide directly grown on substrates (Figure 4.22) [187]. In this case, the morphology is ideal for forming distinct electron- and hole-transport paths, but the polymer infiltration into the free space is quite challenging [189].
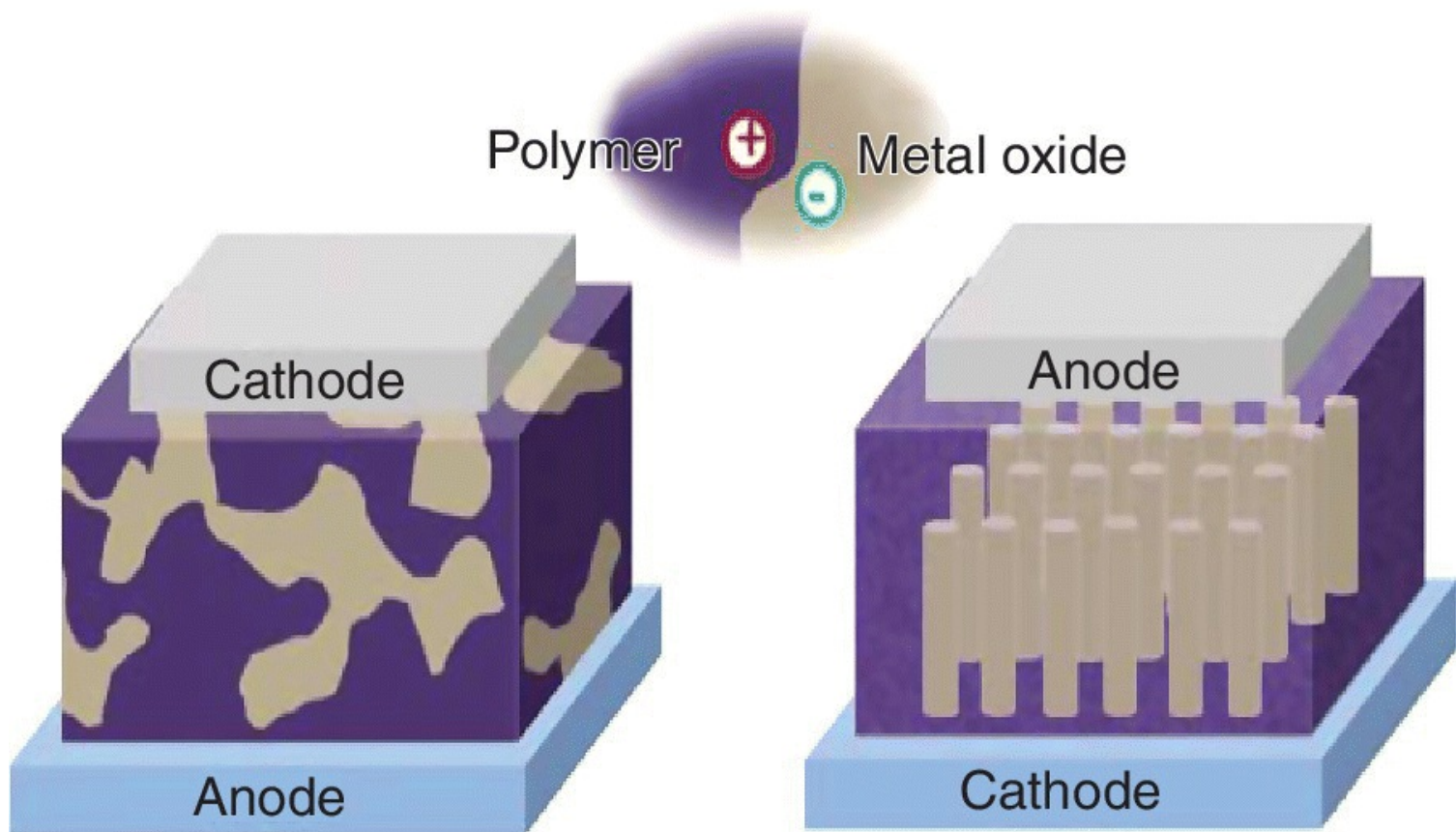
Figure 4.22 Different configurations of polymer–metal-oxide hybrid solar cells. The left panel shows the BHJ device architecture, and the right panel shows the nanostructured hybrid device architecture.

Besides, a critical point in these OIH materials lies on the inherent poor compatibility between the hydrophilic surface of the metal oxide and the hydrophobic nature of the conjugated polymers [187]. This incompatibility frequently implies phase segregation between the electron donor and acceptor components, leading to reduced carrier-dissociation efficiency [190]. Because both charge recombination and separation in blend are sensitive to the nature of the organic–inorganic interface, interfacial modification, separation, and transport of charge carriers are critical factors on the final performances of the devices [191]. To date, many methods have been employed to form a bicontinuous phase in order to facilitate charge separation and charge transport with the objective to improve device performances. While annealing treatments [192], additive additions [193], cosolvent mixtures [194], NC surface modifications [195], and *in situ* preparation methods [196] have been developed, the most elegant approach consists of chemically anchor conjugated polymers onto the inorganic NPs by the use of a covalent bond [121]. This approach results in a very favorable electron injection and benefits from a well photogenerated carrier separation [197].

Some significant examples illustrating the effect of end- and side-chain functionalization of P3HT-based polymers on hybrid material properties are provided in this section.

4.4.1 Anchoring Method

For the anchoring functional groups available, it has been demonstrated that the grafting method of the polymers influences the final hybrid material. Three different grafting approaches have been reported (Figure 4.23).
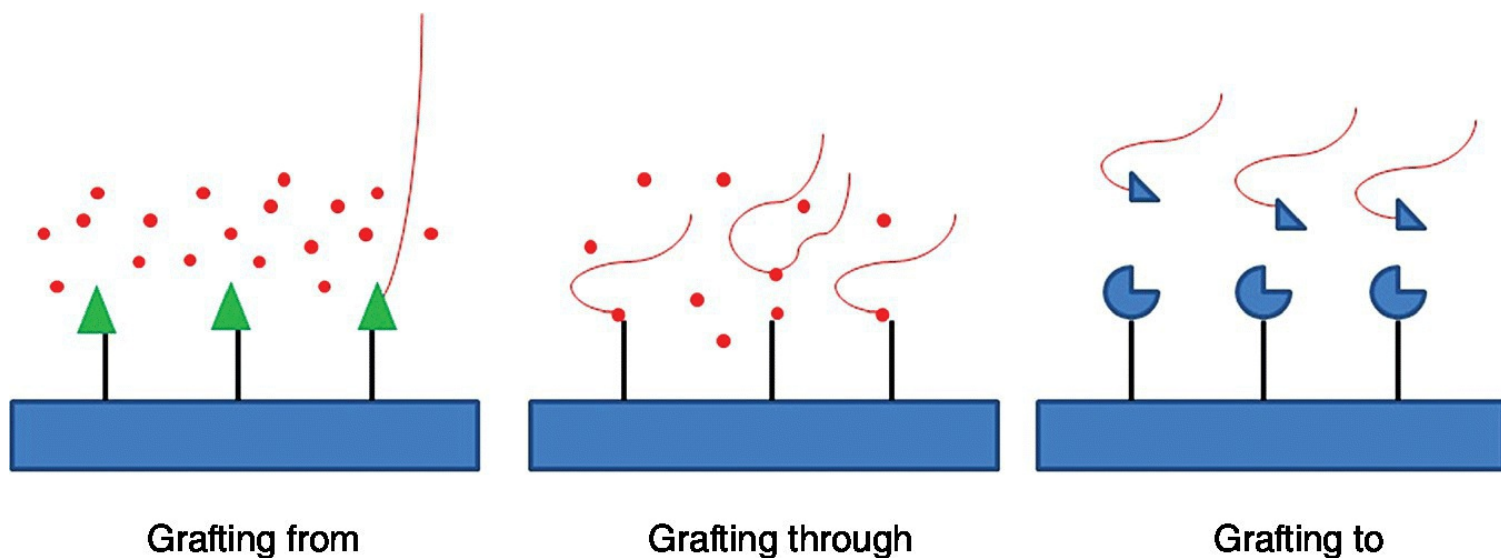
Figure 4.23 Representation of "grafting from," "grafting through," and "grafting to" anchoring methods.
Source: Bousquet *et al.* [13]. Reproduced with permission of John Wiley & Sons.

In "grafting to" approach, conjugated polymers containing a functionality at one chain end react with a complementary functional group on the surface [198]. Even if this approach was found to be efficient, this method suffers from the formation of low density polymer brushes due to the chemisorption of the first chain fraction impeding the diffusion of subsequent polymers to the surface [13a]. Higher grafting densities can however be obtained by applying the "grafting from" approach. In this method, a monolayer of initiator molecules is covalently bonded to a solid substrate, and, by initiation of the polymerization from the surface, chains can grow more easily [199]. Despite its higher efficiency, this process is tributary on the small organic compounds diffusion and/or the exhaustion of the starting monomer. Finally, a third process, called "grafting through" technique, can be also applied and is based on the anchoring of a polymerizable group during the macromolecule growing process [200]. During the propagation step, the growing chains react with the functional group bound on the substrate and allow the propagation of other monomers. In this case, the length and the surface density of the polymer chains are more difficult to control. In any case, for all the aforementioned methods, the nature of the anchoring group affording the attachment between the polymer and the substrate represents a crucial point for the elaboration of well-defined polymer monolayers.

In 2012, Clément *et al.* reported the preparation of hybrid NPs of TiO_2 using a carboxystyryl anchoring unit as an end group of a regioregular P3HT (**P3HT-COOH**) [126]. In 2014, the same group reported a "grafting from" approach for the synthesis of TiO_2 NPs supported with conjugated polymer brushes [73]. In this approach, the P3HT was selectively grown from TiO_2 NPs by surface-initiated KCTCP. Compared with the "grafting to" strategy, for which the weight percentage of P3HT achieved was 3 [126], a higher content of P3HT was grafted on the TiO_2 surface with the "grafting from" strategy (~13 wt%), demonstrating the clear advantage of this second method [73]. In contrast to the **P3HT−COOH**/TiO_2 hybrid material prepared by the "grafting to" approach, the "grafting from" procedure maintains the fibrillar structure of the P3HT as shown by AFM images and thus promotes the charge transport effect. Compared with the direct blend of P3HT and TiO_2, the photoinduced electron transfer in the **P3HT−COOH**/TiO_2 hybrid materials was improved due to the presence of carboxylic end group bound to the TiO_2 surface (Figure 4.24). Those examples clearly demonstrated that the grafting methods highly influenced the properties of the final hybrid materials.
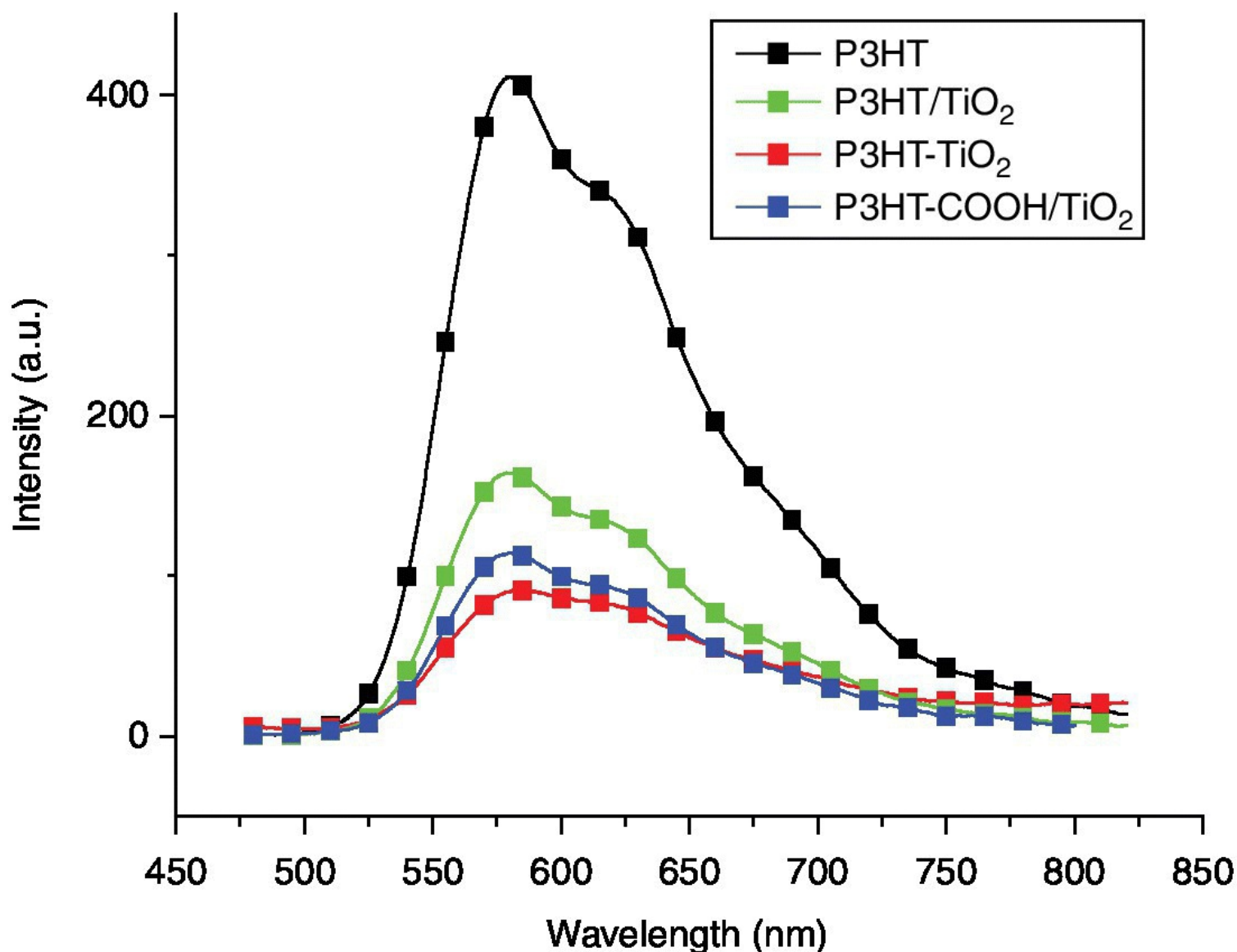
Figure 4.24 Emission spectra of P3HT, P3HT/TiO$_2$, and P3HT-COOH/TiO$_2$ prepared from "grafting to" and "grafting from" method in CHCl$_3$ (λ_{ex} = 440 nm).

4.4.2 Surface Modification Using End- and Side-Chain-Functionalized P3HT

4.4.2.1 End-Group Functionalization

During this past decade, P3HT end groups have been functionalized by multiple anchoring groups including carboxylic acid [126, 201–205], cyanoacrylic acid [125, 206], silane [18a], and phosphorus coupling agents [18b, 130d].

Among the anchoring groups, carboxylic acids are certainly the most studied due to its relative stability and easy synthesis [127]. Manthiram and coworkers reported that using mono-end-capped carboxylic P3HT (**45**; Figure 4.25) as an interfacial modifier in a P3HT/TiO$_2$ hybrid solar cell allowed improving device performances (Entry **1**, Table 4.3) [202]. Indeed, due to a better wetting of TiO$_2$ by the polymer, an improved fill factor (FF) was observed (45 vs. 22 for pristine P3HT). In addition, the reduced backward recombination or improved charge separation at the TiO$_2$–polymer interface led to an increase of V_{OC} and thus a better PCE. Significant PCE improvement was obtained by Thellakat *et al.* using 2,2′,7,7′-tetrakis-

(N,N-di-4-methoxyphenylamino)-9,9′-spirobifluorene (**spiro-OMeTAD**) as a solid hole conductor (Entry **2**, Table 4.3) [203]. In a similar fashion, bromine-terminated P3HT ($M_n = 5\,000$ g.mol^{-1}) enhanced hydrophobicity of TiO$_2$, enabling their better dispersion in the P3HT matrix and increased P3HT crystallinity (**47**; Figure 4.25) [204]. Due to efficient charge transport and reduced charge recombination in the hybrid system, PCE was increased (Entry **3**, Table 4.3).
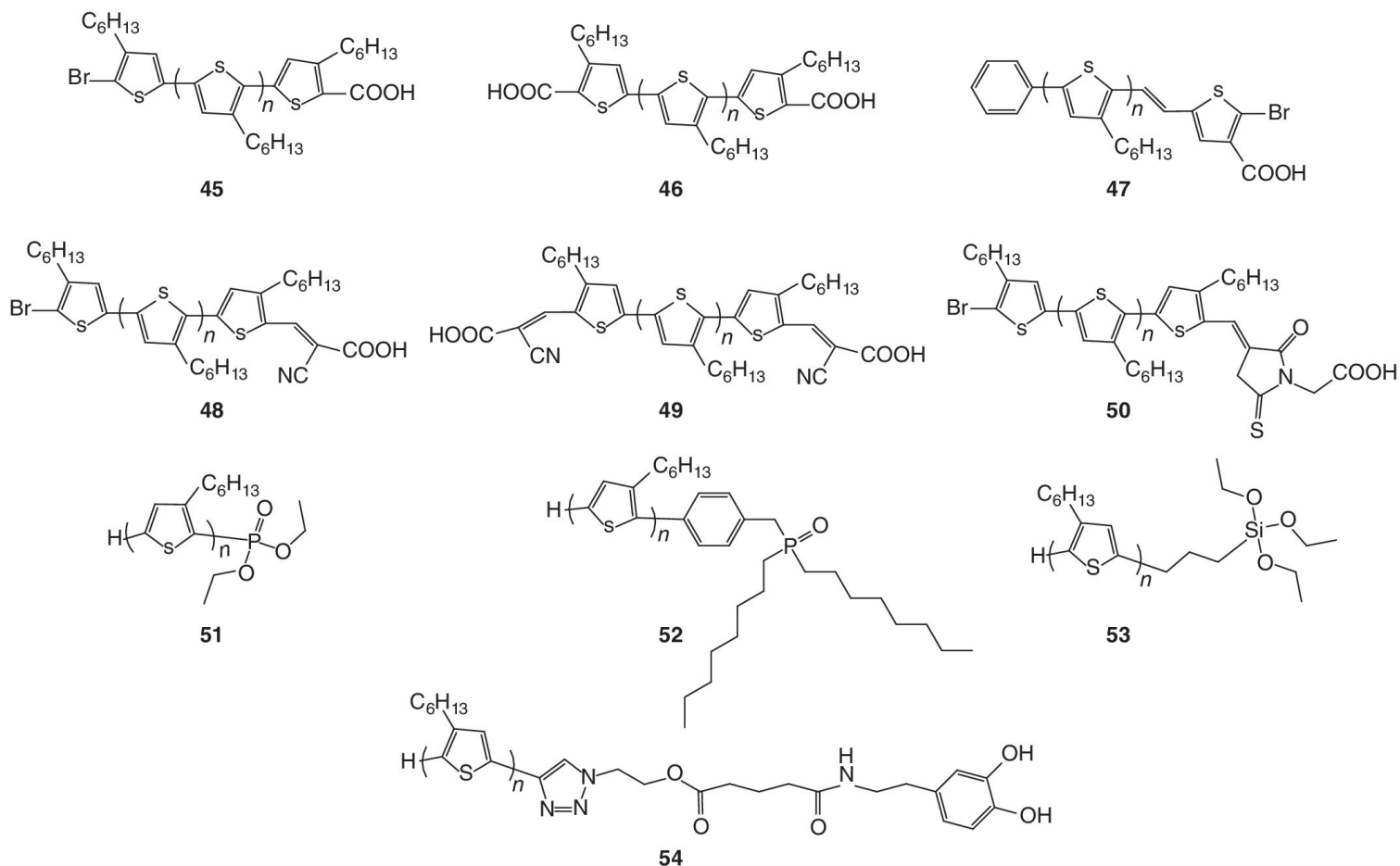
Figure 4.25 End-functionalized P3HTs for modifying ZnO and TiO$_2$ metal oxides.

Table 4.3 Bibliographic data of end- and side-chain-functionalized P3HTs extracted from the literature.

Entry	Device structure	PCE (%)	Reference
1	P3HT : TiO$_2$	0.01	[202]
	P3HT : **45** : TiO$_2$	0.05	
2	**46** : spiro-OMeTAD : TiO$_2$	0.90	[203]
3	P3HT : **47** : TiO$_2$	1.19	[204]
4	**45** : ZnO	0.42	[205]
5	P3HT : TiO$_2$	0.1	[125]
	48 : TiO$_2$	0.2	
	49 : TiO$_2$	2.2	
6	**48** : TiO$_2$	3.02	[206]

	50 : TiO$_2$	0.53	
7	51 : ZnO	0.036	[18b]
8	52 : ZnO	0.077	[130d]
9	55 : TiO$_2$	1.1	[207]
	56 : TiO$_2$	0.9	
10	57 : PPE-CO$_2$: TiO$_2$	0.89	[208]
11	57 : TiO$_2$ nanotube	2.1	[209]
12	57 : TiO$_2$	0.79	[210]
13	57 : TiO$_2$	0.70	[211]
14	58 : ZnO	0.83	[212]
	P3HT : ZnO	0.22	
15	P3HT : 59 : ZnO	0.68	[213]
16	P3HT : TiO$_2$	0.05	[214]
	P3HT : 60 : TiO$_2$	0.12	

Carboxylic end-functionalized P3HT was also exploited for the direct growth of ZnO (**45**; Figure 4.25) [205]. Its self-assembly into a periodic superstructure of amorphous and crystalline domains allowed the formation of nanostructured hybrid materials with length scale suitable for charge photogeneration, but low PCE (0.42%) was obtained (Entry **4**, Table 4.3).

Besides carboxylic anchoring groups, cyanoacrylic acid groups have emerged as a promising tool for grafting P3HT onto the metal oxide surface [125, 206]. Krüger *et al.* reported the synthesis of cyanoacrylic acid mono- and dicapped P3HT to sensitize TiO$_2$ (**48** and **49**; Figure 4.25) [125]. Device performances of these polymer materials were found to be highly dependent on the number of cyanoacetic binding groups. Thus, **49** exhibited a PCE of 2.2%, while pristine P3HT or **48** showed PCEs lower than 0.2% (Entry **5**, Table 4.3). The poor performance of **48** was attributed to polymer aggregation, which quenched the photoexcited states, whereas in the case of **49**, the close contact of the polymers chains with the TiO$_2$ surface led to efficient charge injection with low quenching opportunity (Figure 4.26). The withdrawing ability of cyanoacrylic acid anchoring groups was illustrated by Odobel *et al.* by comparing end-functionalized P3HTs **48** and **50** (Figure 4.25) [206]. Compared with P3HT dye bearing a rhodanine-3-acetic acid anchoring group, P3HT with cyanoacrylic acid exhibited much broader photoresponse range and greatly enhanced light harvesting efficiency (Entry **6**, Table 4.3).
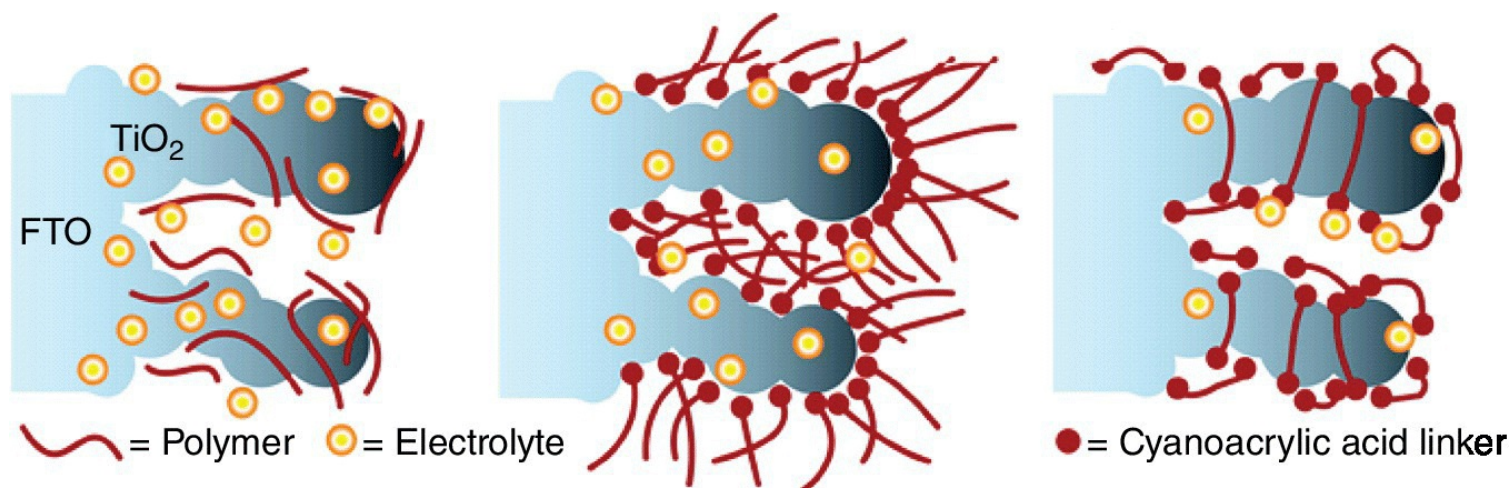
Figure 4.26 Model loading of pristine P3HT (left), **48** (middle), and **49** (right).

Phosphonic ester end-functionalized P3HTs were also developed by Fréchet *et al.* to graft polymer to an n-type ZnO nanowire to produce *p–n* heterojunction nanowires (**51**; Figure 4.25) [18b]. Although **51** was found to be able to self-assemble into lamellar structure as demonstrated by high-resolution TEM, PCE remained very low (Entry **7**, Table 4.3). More recently, Chen and coworkers reported the synthesis of benzyl-di-*n*-octyl-phosphine oxide end-functionalized P3HT for the preparation of ZnO-based nanocomposites used as active layer in BHJ solar cells (**52**; Figure 4.25) [130d]. Due to its well-defined interface, dispersion of ZnO NPs within the P3HT matrix and photoinduced charge transfer were improved in comparison with physical mixed P3HT–ZnO hybrid materials. The resulting hybrid PV devices exhibited improved PCE (0.077% vs. 0.036%) with respect to **51** (Entries **7** and **8**, Table 4.3). Similar findings were also observed when silane or catechol end-functionalized P3HT were combined with ZnO metal oxide (**53** and **54**; Figure 4.25) [18a, 215].

4.4.2.2 Side-Chain Functionalization

Although the attachment of end-functionalized P3HT onto 1D inorganic semiconductor was found to be efficient, this method presents several drawbacks such as the low degree of functionality and the hairpin folding of the backbone with hopping mechanism of charge transport [18b]. In this context, grafting of side-chain-functionalized P3HT has emerged as an alternative approach for grafting P3HT onto TiO_2 and ZnO metal oxides. Indeed, side-on attachment can promote coaxial arrangement of the polymer backbone and nanowires, favoring a high charge mobility [216].

Yanagida *et al.* first reported the use of poly(3-thiophene acetic acid) and its copolymer with P3HT (**55** and **56**; Figure 4.27) as polymer sensitizer in nanocrystalline TiO_2-based liquid junction DSSCs, leading to PCE around 1% without additives (Entry **9**, Table 4.3) [207]. Subsequently, Reynolds, Schanze, and coworkers prepared dual-polymer-sensitized TiO_2 solar cells to expand the light absorption of polymer dye and thus to enhance the device performances [208]. Indeed, by combining a carboxylated poly(*p*-phenylene ethynylene) (PPE-CO_2) and a carboxylated PT absorbing in the blue and red regions of the spectrum, respectively, the normalized incident photon-to-current conversion efficiency (ICPE) spectra was broadened, indicating a clear contribution of the combined polymers (**57**; Figure 4.27). Unfortunately, PCE remained quite low (Entry **10**, Table 4.3). Later on, Grimes *et al.* used **57** alone in TiO_2 nanotube-based liquid junction DSSCs, leading to an enhanced PCE of 2.1% (Entry **11**, Table 4.3). This higher PCE compared with **55** and **56** was in part explained by the presence of alkyl chains separating the π-

conjugated structure from the carboxylate moiety [209]. The performances of **57** in liquid and solid-state DSSCs were further investigated by other groups, leading to PCE around 0.7–0.8% (Entries **12** and **13**, Table 4.3) [210, 211].
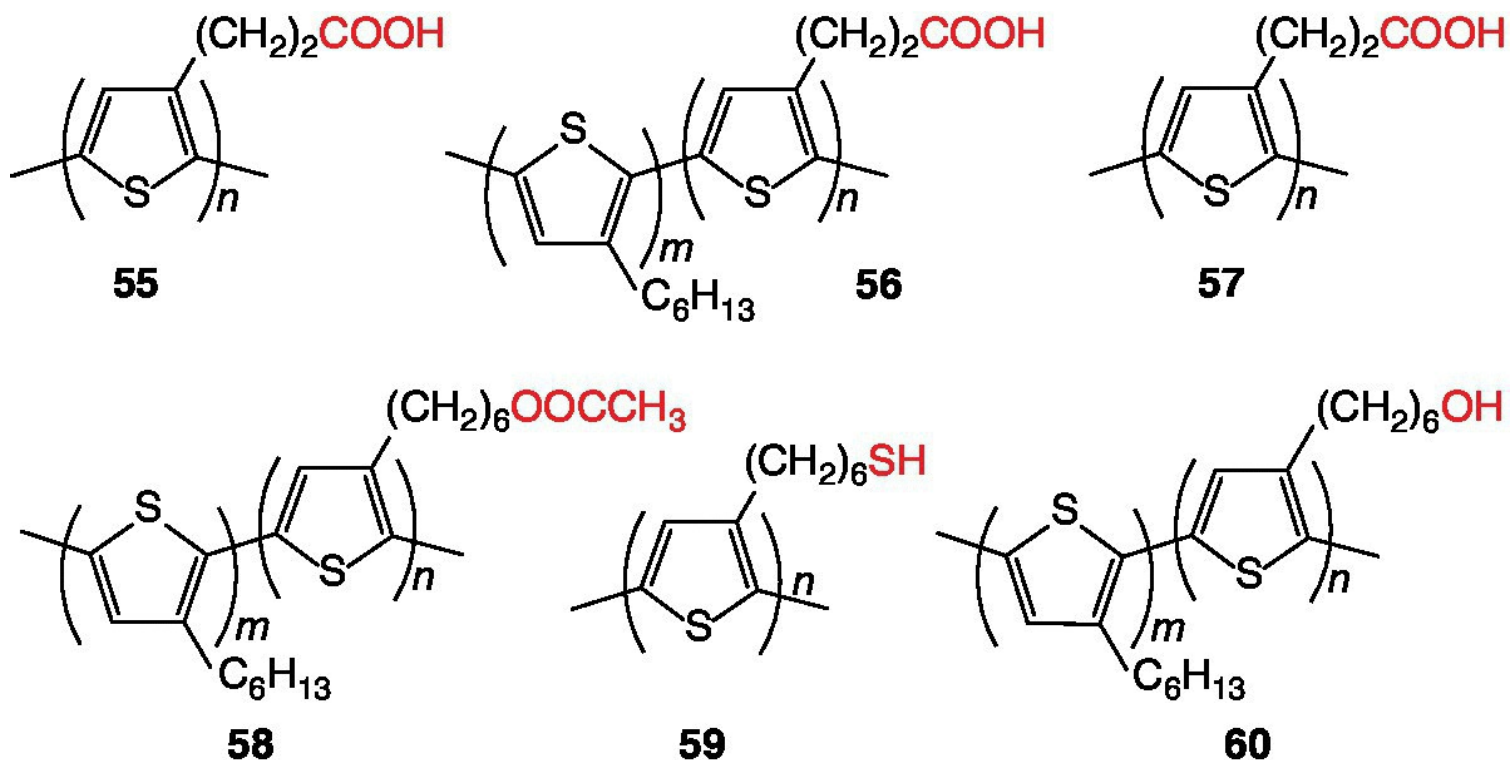
Figure 4.27 Side-chain-functionalized P3HTs for modifying ZnO and TiO$_2$ metal oxides.

More recently, Redeker and coworkers reported the direct covalent attachment of **57** onto ZnO nanowires [217]. The resulting hybrid material exhibited a fast charge transfer at the D–A interface. Compared with the pristine P3HT in bulk, the polymer confined on ZnO surface showed a better crystallinity preventing exciton recombination. The control of morphology and the improvement of efficiency of P3HT/ZnO solar cells were also achieved by using an ester-functionalized side-chain P3HT derivative (**58**; Figure 4.27) [212, 218]. Indeed, compared with pristine P3HT, a better compatibility toward the hydrophilic ZnO was observed, leading to a much finer phase separation. Thus, the obtained high surface area for exciton dissociation and charge generation between the two materials led to a significant PCE increase, as illustrated by Figure 4.28. Besides hybrid materials based on the carboxylic- and ester-functionalized side-chain P3HT derivatives, introducing thiol groups was also found to promote the dispersion of ZnO NPs and facilitate the electron injection process (**59**; Figure 4.27) [213]. This interfacial modification of ZnO surface allowed improving PV performance of P3HT/ZnO BHJ solar cells (Entry **15**, Table 4.3).
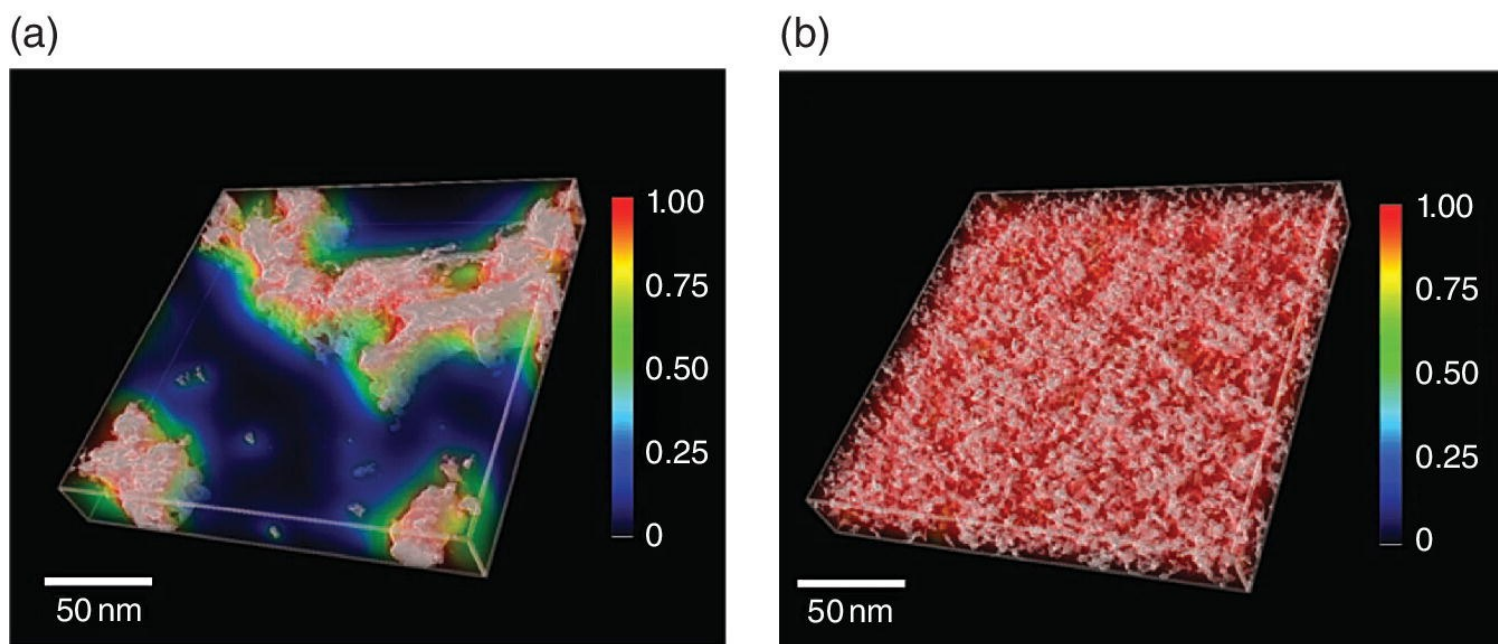
Figure 4.28 Calculated charge carrier generation efficiency in experimentally determined morphologies for ZnO/P3HT (a) and ZnO/P3HT-E (b). The ZnO appears white; the efficiency is indicated by the color.

Source: Oosterhout *et al.* [212]. Reproduced with permission of John Wiley & Sons.

Alcohol-functionalized side-chain P3HT derivatives were also used to increase the miscibility of P3HT into P3HT/TiO$_2$ hybrid materials (**60**; Figure 4.27) [214]. The polymer–titania interaction was promoted by the introduction of a hydroxyl moiety into the P3HT side chain, leading to the formation of homogeneous hybrid colloids. A dramatic decrease of the conjugation length was observed when increasing the TiO$_2$ content. However, introducing **60** as a compatibilizer in P3HT/TiO$_2$ BHJ solar cells resulted in a 2.4-fold increase of PCE (Entry **16**, Table 4.3).

4.5 Conclusion

Functionalizing regioregular P3HT, which is probably the most used hole conductors for organic electronics, especially photovoltaics, has proven to be a precious way for developing emerging materials. Combined with its environmental/thermal stability, its electrical conductivity, and its solution processability, progress in terms of P3HT synthesis allowed the preparation of multiple polymer topographies (homo-, random/block copolymers) with a high control of the regioregularity and molecular weight. These synthetic methods also offer the opportunity to functionalize P3HTs at both side and end chains and thus opened the door to the preparation new hybrid materials for photovoltaics, notably based on fullerene and metal oxides such as TiO$_2$ and ZnO. Developing efficient PV devices requires to well control the morphology for promoting the charge dissociation and transport toward the electrodes. Process optimizations including thermal and solvent annealing improved considerably this parameter, but the performances remain unstable upon extended use. Recently, it was shown that modifying the structure of P3HT by adding various functionalities could improve the morphology in OPV devices, whether BHJ or hybrid types. Whatever the type of functionality attached to the end or side chains in P3HT backbone, they were found to modify the phase separation between P3HT and fullerene/oxides in blends. Functionalized P3HTs used as donor materials or compatibilizers in BHJ/hybrid active layers allow to increase the miscibility between the two intermixed components, thus obtaining a well-defined bicontinuous phase morphology, a key point for the charge transport toward the electrodes. By judiciously

tuning the interaction nature between P3HT and fullerene/metal oxide or the loading content of the added functionality or by using different grafting strategies, the performances and the thermal stability of the BHJ/hybrid devices can be achieved. The functionalization of P3HT-based hybrid materials provides many opportunities to explore in various applications domains ranging from energy to biology.

Acknowledgments

References

1 (a) R. E. Blankenship, D. M. Tiede, J. Barber, G. W. Brudvig, G. Fleming, M. Ghirardi, M. R. Gunner, W. Junge, D. M. Kramer, A. Melis, T. A. Moore, C. C. Moser, D. G. Nocera, A. J. Nozik, D. R. Ort, W. W. Parson, R. C. Prince, T. R. Sayre, *Science* **2011**, *332*, 805; (b) D. Gust, T. A. Moore, A. L. Moore, *Acc. Chem. Res.* **2009**, *42*, 1890.

2 C. Philibert, "*Solar Energy Perspectives*", IEA, Paris, **2011**.

3 (a) M. A. Green, *Phil. Trans. R. Soc. A* **2013**, *371*, 20110413; (b) M. A. Green, K. Emery, Y. Hishikawa, W. Warta, E. D. Dunlop, *Prog. Photovolt.* **2013**, *21*, 827.

4 (a) H. Youn, H. J. Park, L. J. Guo, *Small* **2015**, *11*, 2228; (b) K. A Mazzio, C. K. Luscombe, *Chem. Soc. Rev.* **2015**, *44*, 78; (c) Current and Future Directions, G. Nisato, J. Hauch, in *Organic Photovoltaics: Materials, Device Physics, and Manufacturing Technologies* (Eds: C. J. Brabec, U. Scherf, V. Dyakonov), Wiley-VCH Verlag GmbH & Co. KGaA, Weinheim, Germany, **2014**, 587; (d) Y. Chen, X. Wan, G. Long, *Acc. Chem. Res.* **2013**, *46*, 2645; (e) Y.-W. Su, S.-C. Lan, K.-H. Wei, *Mater. Today* **2012**, *15*, 554; (f) G. Li, R. Zhu, Y. Yang, *Nat. Photonics* **2012**, *6*, 153; (g) A. Mishra, P. Bauerle, *Angew. Chem. Int. Ed. Engl.* **2012**, *51*, 2020.

5 (a) V. Sugathan, E. John, K. Sudhakar, *Renew. Sustain. Energy Rev.* **2015**, *52*, 54; (b) N. Sharifi, F. Tajabadi, N. Taghavinia, *ChemPhysChem* **2014**, *15*, 3902; (c) P. Docampo, S. Guldin, T. Leijtens, N. K. Noel, U. Steiner, H. J. Snaith, *Adv. Mater.* **2014**, *26*, 4013; (d) H. S. Jung, J.-K. Lee, *J. Phys. Chem. Lett.* **2013**, *4*, 1682; (e) B. E. Hardin, H. J. Snaith, M. D. McGehee, *Nat. Photonics* **2012**, *6*, 162; (f) A. Hagfeldt, G. Boschloo, L. Sun, L. Kloo, H. Pettersson, *Chem. Rev.* **2010**, *110*, 6595.

6 (a) S. Roland, S. Neubert, S. Albrecht, B. Stannowski, M. Seger, A. Facchetti, R. Schlatmann, B. Rech, D. Neher, *Adv. Mater.* **2015**, *27*, 1262; (b) J. Yan, B. R. Saunders, F. Gao, S. Ren, *RSC Adv.* **2014**, *4*, 43286; (c) J. Wang, *Energy Environ. Sci.* **2013**, *6*, 2020; (d) X. Fan, M. Zhang, X. Wang, F. Yang, X. Meng, *J. Mater. Chem. A*, **2013**, *1*, 8694.

7 (a) F. C. Krebs, S. A. Gevorgyan, J. Alstrup, *J. Mater. Chem.* **2009**, *19*, 5442; (b) J. Y. Kim, K. Lee, N. E. Coates, D. Moses, T.-Q. Nguyen, M. Dante, A. J. Heeger, *Science* **2007**, *317*, 222.

8 (a) F. C. Krebs, T. D. Nielsen, J. Fyenbo, M. Wadstrøm, M. S. Pedersen, *Energy Environ. Sci.* **2010**, *3*, 512; (b) S. B. Darling, *Energy Environ. Sci.* **2009**, *2*, 1266.

9 (a) J. J. M. Halls, C. A. Walsh, N. C. Greenham, E. A. Marseglia, R. H. Friend, S. C. Moratti, A. B. Holmes, *Nature* **1995**, *376*, 498; (b) G. Yu, J. Gao, J. C. Hummelen, F. Wudl, A. J. Heeger, *Science* **1995**, *270*, 1789.

10 P. E. Shaw, A. Ruseckas, I. D. Samuel, *Adv. Mater.* **2008**, *20*, 3516.

11 C. J. Brabec, N. S. Sariciftci, J. C. Hummelen, *Adv. Funct. Mater.* **2001**, *11*, 15.

12 M.-E. Ragoussia, T. Torres, *Chem. Commun.* **2015**, *51*, 3957.

13 (a) A. Bousquet, H. Awada, R. C. Hiorns, C. Dagron-Lartigau, L. Billon, *Prog. Polym. Sci.* **2014**, *39*, 1847; (b) J. Bouclé, J. Ackermann, *Polym. Int.* **2012**, *61*, 355.

14 (a) Y. Zhou, M. Eck, C. Veit, B. Zimmermann, F. Rauscher, P. Niyamakom, S. Yilmaz, I. Dumsch, S. Allard, U. Scherf, *Sol. Energy Mater. Sol. Cells* **2011**, *95*, 1232; (b) W. J. Beek, L. H. Slooff, M. M. Wienk, J. M. Kroon, R. A. Janssen, *Adv. Funct. Mater.* **2005**, *15*, 1703; (c) C. Y. Kwong, A. B. Djurisic, P. C. Chui, K. W. Cheng, W. K. Chan, *Chem. Phys. Lett.* **2004**, *384*, 372.

15 (a) Y. Wu, G. Zhang, *Nano Lett.* **2010**, *10*, 1628; (b) Y.-Y. Lin, T.-H. Chu, S.-S. Li, C.-H. Chuang, C.-H. Chang, W.-F. Su, C.-P. Chang, M.-W. Chu, C.-W. Chen, *J. Am. Chem. Soc.* **2009**, *131*, 3644.

16 (a) S. Dayal, N. Kopidakis, D. C. Olson, D. S. Ginley, G. Rumbles, *Nano Lett.* **2009**, *10*, 239; (b) B. Sun, H. J. Snaith, A. S. Dhoot, S. Westenhoff, N. C. Greenham, *J. Appl. Phys.* **2005**, *97*, 014914.

17 (a) W.-P. Liao, S.-C. Hsu, W.-H. Lin, J.-J. Wu, *J. Phys. Chem. C* **2012**, *116*, 15938; (b) G. K. V. V. Thalluri, J.-C. Bolsée, A. Gadisa, M. Parchine, T. Boonen, J. D'Haen, A. E. Boyukbayram, J. Vandenbergh, T. Cleij, L. Lutsen, D. Vanderzande, J. Manca, *Sol. Energy Mater. Sol. Cells* **2011**, *95*, 3262.

18 (a) H. Awada, H. Medlej, S. Blanc, M.-H. Deville, R.-C. Hiorns, A. Bousquet, C. Dagron-Lartigau, L. Billon, *J. Polym. Sci., Part A: Polym. Chem.* **2014**, *52*, 30; (b) A. L. Briseno, T. W. Holcombe, A. I. Boukai, E. C. Garnett, S. W. Shelton, J. J. M. Fréchet, P. Yang, *Nano Lett.* **2010**, *10*, 334.

19 J. Liu, T. Tanaka, K. Sivula, A. P. Alivisatos, J. M. J. Fréchet, *J. Am. Chem. Soc.* **2004**, *126*, 6550.

20 S. A. McDonald, G. Konstantatos, S. Zhang, P. W. Cyr, E. J. D. Klem, L. Levina, E. H. Sargent, *Nat. Mater.* **2005**, *4*, 138.

21 (a) Progress in the synthesis of poly(3-hexylthiophene), P. Sista, C. K. Luscombe in *P3HT Revisited – From molecular scale to solar cells devices* (Eds: S. Ludwigs), Springer-Verlag Berlin Heidelberg, **2014**, 1; (b) A. Marrocchi, D. Lanari, A. Facchetti, L. Vaccaro, *Energy Environ. Sci.* **2012**, *5*, 8457; (c) K. Vakhshouri, D. R. Kozub, C. Wang, A. Salleo, E. D. Gomez, *Phys. Rev. Lett.* **2012**, *108*, 026601; (d) M. T. Dang, L. Hirsch, G. Wantz, *Adv. Mater.* **2011**, *23*, 3597; (e) A. Salleo, R. J. Kline, D. M. DeLongchamp, M. L. Chabinyc, *Adv. Mater.* **2010**, *22*, 3812; (f) S. Gunes, H. S. Neugebauer, N. S. Sariciftci, *Chem. Rev.* **2007**, *107*, 1324.

22 (a) T. Yokozawa, Y. Ohta, *Chem. Commun.* **2013**, *49*, 8281; (b) Z. J. Bryan, A. J. McNeil, *Macromolecules* **2013**, *46*, 8395; (c) Advanced Functional Regioregular Polythiophenes, I. Osaka, R. D. McCullough in *Design and Synthesis of Conjugated Polymers* (Eds: M. Leclerc, J.-F. Morin), Wiley-VCH, Weinheim, **2010**, 91; (d) I. Osaka, R. D. McCullough, *Acc. Chem. Res.* **2008**, *41*, 1202.

23 T. Yamamoto, K. Sanechika, A. Yamamoto, *J. Polym. Sci., Polym. Lett. Ed.* **1980**, *18*, 9.

24 J. W. P. Lin, L. P. Dudek, *J. Polym. Sci., Polym. Chem. Ed.* **1980**, *18*, 2869.

25 M. Kobayashi, J. Chen, T. C. Chung, F. Moraes, A. J. Heeger, F. Wudl, *Synth. Met.* **1984**, *9*, 77.

26 A. Berlin, G. A. Pagani, F. Sannicolo, *J. Chem. Soc. Chem. Commun.* **1986**, 1663.

27 K. Yoshino, S. Hayashi, R.-I. Sugimoto, *Jpn. J. Appl. Phys.* **1984**, *23*, L899.

28 M. Ballauff, *Angew. Chem. Int. Ed. Engl.* **1989**, *28*, 253.

29 (a) R. L. Elsenbaumer, K. Y. Jen, R. Oboodi, *Synth. Met.* **1986**, *15*, 169; (b) K. Y. Jen, G. G. Miller, R. L. Elsenbaumer, *J. Chem. Soc. Chem. Commun.* **1986**, 1346.

30 (a) M. Pomerantz, J. J. Tseng, H. Zhu, S. J. Sproull, J. R. Reynolds, R. Uitz, H. J. Arnott, M. I. Haider, *Synth. Met.* **1991**, *41*, 825; (b) M.-A. Sato, S. Tanaka, K. Kaeriyama, *J. Chem. Soc. Chem. Commun.* **1986**, 873; (c) S. Ryu-ichi, S. Takeda, G. H. Bon, Y. Katsumi, *Chem. Express* **1986**, *1*, 635

31 T. Yamamoto, A. Morita, Y. Miyazaki, T. Maruyama, H. Wakayama, Z. H. Zhou, Y. Nakamura, T. Kanbara, S. Sasaki, K. Kubota, *Macromolecules* **1992**, *25*, 1214.

32 M. D. McClain, D. A. Whittington, D. J. Mitchell, M. D. Curtis, *J. Am. Chem. Soc.* **1995**, *117*, 3887.

33 M. Sato, H. Morii, *Macromolecules* **1991**, *24*, 1196.

34 (a) R. D. McCullough, S. Tristam-Nagle, S. P. Williams, R. D. Lowe, M. Jayaraman, *J. Am. Chem. Soc.* **1993**, *115*, 4910; (b) R. D. McCullough, R. D. Lowe, M. Jayaraman, D. L. Anderson, *J. Org. Chem.* **1993**, *58*, 904; (c) R. D. McCullough, R. D. Lowe, *J. Chem. Soc. Chem. Commun.* **1992**, 70.

35 T. A. Chen, R. D. Rieke, *J. Am. Chem. Soc.* **1992**, *114*, 10087.

36 H. Sirringhaus, P. J. Brown, R. H. Friend, M. M. Nielsen, K. Bechgaard, B. M. W. Langeveld-Voss, A. J. H. Spiering, R. A. J. Janssen, E. W. Meijer, P. Herwig, D. M. de Leeuw, *Nature* **1999**, *401*, 685.

37 T. J. Prosa, M. J. Winokur, J. Moulton, P. Smith, A. J. Heeger, *Macromolecules* **1992**, *25*, 4364.

38 A. Salleo, *Mater. Today* **2007**, *10*, 38.

39 (a) J.-S. Kim, J.-H. Kim, W. Lee, H. Yu, H. J. Kim, I. Song, M. Shin, J. Hak Oh, U. Jeong, T.-S. Kim, B. J. Kim, *Macromolecules* **2015**, *48*, 4339; (b) D. E. Johnston, K. G. Yager, H. Hlaing, X. H. Lu, B. M. Ocko, C. T. Black, *ACS Nano* **2014**, *8*, 243.

40 (a) P. Kohn, S. Huettner, H. Komber, V. Senkovskyy, R. Tkachov, A. Kiriy, R. H. Friend, U. Steiner, W. T. S. Huck, J. U. Sommer, M. Sommer, *J. Am. Chem. Soc.* **2012**, *134*, 4790; (b) C. H. Woo, B. C. Thompson, B. J. Kim, M. F. Toney, J. M. J. Frechet, *J. Am. Chem. Soc.* **2008**, *130*, 16324.

41 (a) R. C. G. Naber, M. Muldder, B. De Boer, P. W. M. Blom, D. M. De Leew, *Org. Electron.* **2006**, *7*, 132; (b) H. Yang, T. J. Shin, L. Yang, K. Cho, C. Y. Ryu, Z. Bao, *Adv. Funct. Mater.* **2005**, *15*, 671; (c) X. Jiang, R. Patil, Y. Harima, J. Ohshita, A. Kunai, *J. Phys. Chem. B* **2005**, *109*, 221; (d) Z. Bao, A. Dodabalapur, A. J. Lovinger, *Appl. Phys. Lett.* **1996**, *69*, 4108.

42 F. C. Spano, *J. Chem. Phys.* **2005**, *122*, 234701.

43 J.-F. Chang, J. Clark, N. Zhao, H. Sirringhaus, D. W. Breiby, J. W. Andreasen, M. M. Nielsen, M.

Giles, M. Heeney I. McCulloch, *Phys. Rev. B: Condens. Matter Mater. Phys.* **2006**, *74*, 115318/1.

44 M. Trznadel, A. Pron, M. Zagorska, R. Chrzaszcz, J. Pielichowski, *Macromolecules* **1998**, *31*, 5051.

45 (a) A. Zen, M. Saphiannikova, D. Neher, G. Wegner, *Macromolecules* **2006**, *39*, 2162; (b) A. Zen, J. Pflaum, S. Hirschmann, W. Zhuang, F. Jaiser, U. Asawapirom, J. P. Rabe, U. Scherf, D. Neher, *Adv. Funct. Mater.* **2004**, *14*, 757.

46 (a) R. Kline, M. McGehee, *J. Macromol. Sci., Polym. Rev.* **2006**, *46*, 27; (b) R. J. Kline, M. D. McGehee, E. N. Kadnikova, J. Liu, J. M. Frechet, M. F. Toney, *Macromolecules* **2005**, *38*, 3312; (c) R. J. Kline, M. D. McGehee, E. N. Kadnikova, J. Liu, J. M. J. Frechet, *Adv. Mater.* **2003**, *15*, 1519.

47 Z. Masri, A. Ruseckas, E. V. Emelianova, L. Wang, A. K. Bansal, A. Matheson, H. T. Lemke, M. M. Nielsen, H. Nguyen, O. Coulembier, P. Dubois, D. Beljonne, I. D. W. Samuel, *Adv. Mater.* **2013**, *3*, 1445.

48 F. Panzer, H. Bassler, R. Lohwasser, M. Thelakkat, A. Kohler, *J. Phys. Chem. Lett.* **2014**, *5*, 2742.

49 F. Liu, D. Chen, C. Wang, K. Luo, W. Gu, A. L. Briseno, J. W. P. Hsu, T. P. Russell, *ACS Appl. Mater. Interfaces* **2014**, *6*, 19876.

50 J. Gierschner, J. Cornil, H.-J. Egelhaaf, *Adv. Mater.* **2007**, 173.

51 T. C. Monson, M. T. Lloyd, D. Olson, Y.-J. Lee, J. W. Hsu, *Adv. Mater.* **2008**, *20*, 4755.

52 S. Himmelberger, K. Vandewal, Z. Fei, M. Heeney, A. Salleo, *Macromolecules* **2014**, *47*, 7151.

53 A. Zen, M. Saphiannikova, D. Neher, J. Grenzer, S. Grigorian, U. Pietsch, U. Asawapirom, S. Janietz, U. Scherf, I. Lieberwirth, G. Wegner, *Macromolecules* **2006**, *39*, 2162.

54 A. Kiriy, V. Senkovskyy, M. Sommer, *Macromol. Rapid Commun.* **2011**, *32*, 1503.

55 (a) K. Nakamura, S. Tamba, A. Sugie, A. Mori, *Chem. Lett.* **2013**, *42*, 1200; (b) S. Tamba, K. Fuji, H. Meguro, S. Okamoto, T. Tendo, R. Komobuchi, A. Sugie, T. Nishino, A. Mori, *Chem. Lett.* **2013**, *42*, 281; (c) S. Tamba, S. Mitsuda, F. Tanaka, A. Sugie, A. Mori, *Organometallics* **2012**, *31*, 2263; (d) S. Tamba, K. Shono, A. Sugie, A. Mori, *J. Am. Chem. Soc.* **2011**, *133*, 9700; (e) S. Tamba, S. Tanaka, Y. Okubo, S. Okamoto, H. Meguro, A. Mori, *Chem. Lett.* **2011**, *40*, 398.

56 (a) R. D. McCullough, S. P. Williams, S. Tristram-Nagle, M. Jayaraman, P. C. Ewbank, L. Miller, *Synth. Met.* **1995**, *279*, 69; (b) R. D. McCullough, R. D. Lowe, M. Jayaraman, P. C. Ewbank, D. L. Anderson, S. Tristam-Nagle, *Synth. Met.* **1993**, *55*, 1198.

57 S.-H. Kim, J.-G. Kim, *Bull. Kor. Chem. Soc.* **2010**, *31*, 193.

58 A. Krasovski, A. Malakhov, A. Gavryushin, P. Knochel, *Angew. Chem. Int. Ed.* **2006**, *45*, 6040.

59 J.-G. Kim, S.-H. Kim, R. D. Rieke, *Macromol. Res.* **2011**, *19*, 749.

60 (a) E. Goto, S. Nakamura, S. Kawauchi, H. Mori, M. Ueda, T. Higashihara, *J. Polym. Sci., Polym. Chem.* **2014**, *52*, 2287; (b) T. Higashihara, E. Goto, M. Ueda, *ACS Macro Lett.* **2012**, *1*, 167.

61 (a) R. Miyakoshi, A. Yokozawa, T. Yokozawa, *J. Am. Chem. Soc.* **2005**, *127*, 17542; (b) A. Yokoyama, R. Miyakoshi, T. Yokozawa, *Macromolecules* **2004**, *37*, 1169; (c) R. Miyakoshi, A. Yokozawa, T. Yokozawa, *Macromol. Rapid Commun.* **2004**, *25*, 1663; (d) R. S. Loewe, S. M.

Khersonsky, R. D. McCullough, *Adv. Mater.* **1999**, *11*, 250.

62 R. S. Loewe, P. C. Ewbank, J. Liu, L. Zhai, R. D. McCullough, *Macromolecules* **2001**, *34*, 4324.

63 (a) E. L. Lanni, A. J. McNeil, *Macromolecules* **2010**, *43*, 8039; (b) E. L. Lanni, A. J. McNeil, *J. Am. Chem. Soc.* **2009**, *131*, 16573.

64 T. Yokozawa, H. Shimura, *J. Polym. Sci., Part A: Polym. Chem.* **1999**, *37*, 2607.

65 (a) M. Jeffries-El, G. Sauvé, R. D. McCullough, *Macromolecules* **2005**, *38*, 10346; (b) M. Jeffries-El, G. Sauvé, R. D. McCullough, *Adv. Mater.* **2004**, 1017.

66 R. Tkachov, V. Senkovskyy, H. Komber, J.-U. Sommer, A. Kiriy, *J. Am. Chem. Soc.* **2010**, *132*, 7803.

67 (a) N. Khanduyeva, V. Senkovsky, T. Beryokzkina, M. Horecha, M. Stamm, C. Uhrich, M. Riede, K. Leo, A. Kiriy, *J. Am. Chem. Soc.* **2009**, *131*, 153; (b) V. Senkovsky, N. Khanduyeva, H. Komber, U. Oertel, M. Stamm, D. Kuckling, A. Kiriy, *J. Am. Chem. Soc.* **2007**, *129*, 6626.

68 N. Marshall, S. K. Sontag, J. Locklin, *Chem. Commun.* **2011**, *47*, 5681.

69 E. Negishi, *Acc. Chem. Res.* **1982**, *15*, 340.

70 H. A. Bronstein, C. K. Luscombe, *J. Am. Chem. Soc.* **2009**, *131*, 12894.

71 (a) R. Tkachov, V. Senkovskyy, M. Horecha, U. Oertel, M. Stamm, A. Kiriy, *Chem. Commun.* **2010**, *46*, 1425; (b) V. Senkovskyy, R. Tkachov, T. Beryozkina, H. Komber, U. Oertel, M. Horecha, V. Bocharova, M. Stamm, S. A. Gevorgyan, F. C. Krebs, A. Kiriy, *J. Am. Chem. Soc.* **2009**, *131*, 16445.

72 (a) S. K. Sontag, G. R. Sheppard, N. M. Usselman, N. Marshall, J. Locklin, *Langmuir* **2011**, *27*, 12033; (b) L. Yang, S. K. Sontag, T. W. LaJoie, W. Li, N. E. Huddleston, J. Locklin, W. You, *ACS Appl. Mater. Interfaces* **2012**, *4*, 5069.

73 F. Boon, D. Moerman, D. Laurencin, S. Richeter, Y. Guari, A. Mehdi, P. Dubois, R. Lazzaroni, S. Clément, *Langmuir* **2014**, *30*, 11340.

74 (a) Z. J. Brian, A. J. McNeil, *Chem. Sci.* **2013**, *4*, 1620; (b) S. R. Lee, Z. J. Bryan, A. M. Wagner, A. J. McNeil, *Chem. Sci.* **2012**, *3*, 1562; (c) E. L. Lanni, J. R. Locke, C. M. Gleave, A. J. McNeil, *Macromolecules* **2011**, *44*, 5136.

75 S. R. Lee, J. W. D. Bloom, S. E. Wheeler, A. J. McNeil, *Dalton Trans.* **2013**, *42*, 4218.

76 For examples see: (a) H. H. Zhang, C. H. Xing, Q. S. Hu, *J. Am. Chem. Soc.* **2012**, *134*, 13156; (b) N. E. Huddleston, S. K. Sontag, J. A. Bilbrey, G. R. Sheppard, J. Locklin, *Macromol. Rapid Commun.* **2012**, *33*, 2115; (c) T. Yokozawa, R. Suzuki, M. Nojima, Y. Ohta, A. Yokoyama, *Macromol. Rapid Commun.* **2011**, *32*, 801; (d) E. Elmalem, A. Kiriy, W. T. S. Huck, *Macromolecules* **2011**, *44*, 9057; (e) M. Verswyvel, P. Verstappen, L. De Cremer, T. Verbiest, G. Koeckelberghs, *J. Polym. Sci., Polym. Chem.* **2011**, *49*, 5339; (f) T. Beryozkina, K. Boyko, N. Khanduyeva, V. Senkovskyy, M. Orecha, U. Oertel, F. Simon, M. Stamm, A. Kiriy, *Angew. Chem. Int. Ed.* **2009**, *48*, 2695.

77 X. Shi, A. Sui, Y. Wang, Y. Li, Y. Geng, F. Wang, *Chem. Commun.* **2015**, *51*, 2138.

78 H. D. Magurudeniya, P. Sista, J. K. Westbrook, T. E. Ourso, K. Nguyen, M. C. Maher, M. G. Alemseghed, M. C. Biewer, M. C. Stefan, *Macromol. Rapid Commun.* **2011**, *32*, 1748.

79 S. Tanaka, S. Tamba, D. Tanaka, A. Sugie, A. Mori, *J. Am. Chem. Soc.* **2011**, *133*, 16734.

80 B. Carsten, F. He, H. J. Son, T. Xu, L. Yu, *Chem. Rev.* **2011**, *111*, 1493.

81 A. Iraqi, G. W. Barker, *J. Mater. Chem.* **1998**, *8*, 25.

82 S. Kang, R. J. Ono, C. W. Bielawski, *J. Am. Chem. Soc.* **2013**, *135*, 4984.

83 Y. Qiu, J. Mohin, C.-H. Tsai, S. Tristram-Nagle, R. R. Gil, T. Kowalewski, K. J. T. Noonan, *Macromol. Rapid Commun.* **2015**, *36*, 840.

84 (a) A. Suzuki, *Angew. Chem. Int. Ed.* **2011**, *50*, 6722; (b) N. Miyaura, A. Suzuki, *Chem. Rev.* **1995**, *95*, 2457.

85 I. A. Liversedge, S. J. Higgins, M. Giles, M. Heeney, I. McCulloch, *Tetrahedron Lett.* **2006**, *47*, 5143.

86 W. Li, Y. Han, B. Li, Z. Bo, *J. Polym. Sci., Polym. Chem.* **2008**, *46*, 4556.

87 T. Yokozawa, R. Suzuki, M. Nojima, Y. Ohta, A. Yojoyama, *Macromol. Rapid Commun.* **2011**, *32*, 801.

88 A. Sui, X. Shi, H. Tian, Y. Geng, F. Wang, *Polym. Chem.* **2014**, *5*, 7072.

89 (a) J. Wencel-Delord, F. Glorius, *Nat. Chem.* **2013**, *5*, 369; (b) R. Po, A. Bernardi, A. Calabrese, C. Carbonera, G. Corso, A. Pellegrino, *Energy Environ. Sci.* **2014**, *7*, 925.

90 (a) H. Jacobsen, A. Correa, A. Poater, C. Costabile, L. Cavallo, *Coord. Chem. Rev.* **2009**, *263*, 687; (b) S. Díez-González, N. Marion, S. P. Nolan, *Chem. Rev.* **2009**, *109*, 3612.

91 J. A. Carrillo, M. J. Ingleson, M. L. Turner, *Macromolecules* **2015**, *48*, 979.

92 K. Kosaka, Y. Ohta, T. Yokozawa, *Macromol. Rapid Commun.* **2015**, *36*, 373.

93 (a) P. Gandeepan, C.-H. Cheng, *Chem. Asian J.* **2015**, *10*, 824; (b) Y. Segawa, T. Maekawa, K. Itami, *Angew. Chem. Int. Ed.* **2015**, *54*, 66; (c) N. Dastbaravardeh, M. Christakakou, M. Haider, M. Schnuerch, *Synthesis* **2014**, *46*, 1421; (d) K. Okamoto, J. Zhang, J. B. Housekeeper, S. R. Marder, C. K. Luscombe, *Macromolecules* **2013**, *46*, 8059; (e) B. Li, P. H. Dixneuf, *Chem. Soc. Rev.* **2013**, *42*, 5744.

94 (a) O. Usluer, M. Abbas, G. Wantz, L. Vignau, L. Hirsch, E. Grana, C. Brochon, E. Cloutet, G. Hadziioannou, *ACS Macro Lett.* **2014**, *3*, 1134; (b) Z. B. Henson, K. Mullen, G. C. Bazan, *Nat. Chem.* **2012**, *4*, 699.

95 M. Sévignon, J. Papillon, E. Schulz, M. Lemaire, *Tetrahedron Lett.* **1999**, *40*, 5873.

96 A. E Rudenko, C. A. Wiley, J. F. Tannaci, B. C. Thompson, *J. Polym. Sci., Polym. Chem.* **2013**, *51*, 2660.

97 Q. Wang, R. Takita, Y. Kikuzaki, F. Ozawa, *J. Am. Chem. Soc.* **2010**, *132*, 11420.

98 Y.-Y. Lai, T.-C. Tung, W.-W. Liang, Y.-J. Cheng, *Macromolecules* **2015**, *48*, 2978.

99 M. N. Hopkinson, C. Richter, M. Schedler, F. Glorius, *Nature* **2014**, *510*, 485.

100 (a) G. L. Mercier, M. Leclerc, *Acc. Chem. Res.* **2013**, *46*, 1597; (b) K. Okamoto, J. Zhang, J. B.

Housekeeper, S. R. Marder, C. K. Luscombe, *Macromolecules* **2013**, *46*, 8059; (c) S. Kowalski, S. Allard, K. Zilberberg, T. Riedl, U. Scherf, *Prog. Polym. Sci.* **2013**, *38*, 1805.

101 S. Hayashi, Y. Kojima, T. Koizumi, *Polym. Chem.* **2015**, *6*, 881.

102 N. N. Li, Y.-L. Zhang, S. Mao, Y.-R. Gao, D.-D. Guo, Y.-Q. Wang, *Org. Lett.* **2014**, *16*, 2732.

103 N. V. Handa, A. V. Serrano, M. J. Robb, C. J. Hawker, *J. Polym. Sci., Polym. Chem.* **2015**, *53*, 831.

104 (a) A. Laiho, H. T. Nguyen, H. Sinno, I. Engquist, M. Berggren, P. Dubois, O. Coulembier, X. Crispin, *Macromolecules* **2013**, *46*, 4548; (b) H. Nguyen, O. Coulembier, J. Winter, P. Gerbaux, X. Crispin, P. Dubois, *Polym. Bull.* **2011**, *66*, 51; (c) C. R. Craley, R. Zhang, T. Kowalewski, R. D. McCullough, M. C. Stefan, *Macromol. Rapid Commun.* **2009**, *30*, 11; (d) G. Sauvé, R. D. McCullough, *Adv. Mater.* **2007**, *19*, 1822; (e) M. C. Iovu, R. Zhang, J. R. Cooper, D. M. Smilgies, A. E. Javier, E. E. Sheina, T. Kowalewski, R. D. McCullough, *Macromol. Rapid Commun.* **2007**, *28*, 1816; (f) M. C. Iovu, M. Jeffries-El, R. Zhang, T. Kowalewski, R. D. McCullough, *J. Macromol. Sci., Part A: Pure Appl. Chem.* **2006**, 1991; (g) M. C. Iovu, M. Jeffries-El, E. E. Sheina, J. R. Cooper, R. D. McCullough, *Polymer* **2005**, *46*, 8582; (h) J. Liu, E. Sheina, T. Kowalewski, R. D. McCullough, *Angew. Chem. Int. Ed.* **2002**, *41*, 329.

105 (a) M. Sommer, A. S. Lang, M. Thelakkat, *Angew. Chem. Int. Ed.* **2008**, *47*, 7901; (b) F. Richard, C. Brochon, N. Leclerc, D. Eckhardt, T. Heiser, G. Hadziioannou, *Macromol. Rapid Commun.* **2008**, *29*, 885; (c) M. C. Iovu, C. R. Craley, M. Jeffries-El, A. B. Krankowski, R. Zhang, T. Kowalewski, R. D. McCullough, *Macromolecules* **2007**, *40*, 4733.

106 C.-A. Dai, W.-C. Yen, Y.-H. Lee, C.-C. Ho, W.-F. Su, *J. Am. Chem. Soc.* **2007**, *129*, 11036.

107 (a) M. G. Alemseghed, J. Servello, N. Hundt, P. Sista, M. C. Biewer, M. C. Stefan, *Macromol. Chem. Phys.* **2010**, *211*, 1291; (b) M. G. Alemseghed, S. Gowrisanker, J. Servello, M. C. Stefan, *Macromol. Chem. Phys.* **2009**, *210*, 2007; (c) B. W. Boudouris, C. D. Frisbie, M. A. Hillmyer, *Macromolecules* **2007**, *41*, 67.

108 C. P. Radano, O. A. Scherman, N. Stingelin-Stutzmann, C. Müller, D. W. Breiby, P. Smith, R. A. J. Janssen, E. W. Meijer, *J. Am. Chem. Soc.* **2005**, *127*, 12502.

109 (a) C. N. Kempf, K. A. Smith, S. L. Pesek, X. Li, R. Verduzco, *Polym. Chem.* **2013**, *4*, 2158; (b) X. Pang, L. Zhao, C. Feng, R. Wu, H. Ma, Z. Lin, *Polym. Chem.* **2013**, *4*, 2025; (c) R. H. Lohwasser, M. Thelakkat, *Macromolecules* **2012**, *45*, 3070; (d) A. E. Javier, S. N. Patel, D. T. Hallinan, V. Srinivasan, N. P. Balsara, *Angew. Chem. Int. Ed.* **2011**, *50*, 9848; (e) M. Urien, H. Erothu, E. Cloutet, R. C. Hiorns, L. Vignau, H. Cramail, *Macromolecules* **2008**, *41*, 7033.

110 B. M. W. Langeveld-Voss, R. A. J. Janssen, R. A. J. Spiering, J. L. J. van Dongen, E. C. Vonk, H. A. Claessens, *Chem. Commun.* **2000**, 81.

111 W. M. Kochemba, S. M. Kilbey, D. L. Pickel, *J. Polym. Sci., Polym. Chem.* **2012**, *50*, 2762.

112 R. H. Lohwasser, M. Thelakkat, *Macromolecules* **2011**, *44*, 3388.

113 W. M. Kochemba, D. L. Pickel, B. G. Sumpter, J. Chen, S. M. Kilbey, *Chem. Mater.* **2012**, *24*, 4459.

114 C.-M. Chen, T.-H. Jen, S.-A. Chen, *ACS Appl. Mater. Interfaces* **2015**, *7*, 20548.

115 K. Okamoto, C. K. Luscombe, *Polym. Chem.* **2011**, *2*, 2424.

116 A. Smeets, K. Van den Bergh, J. De Winter, P. Gerbaux, T. Verbiest, G. Koeckelberghs, *Macromolecules* **2009**, *42*, 7638.

117 V. Senkovskyy, M. Sommer, R. Tkachov, H. Komber, W. T. S. Huck, A. Kiriy, *Macromolecules* **2010**, *43*, 10157.

118 V. Senkovskyy, R. Tkachov, T. Beryozkina, H. Komber, U. Oertel, M. Horecha, V. Bocharova, M. Stamm, S. A. Gevorgyan, F. C. Krebs, A. Kiriy, *J. Am. Chem. Soc.* **2009**, *131*, 16445.

119 N. Doubina, A. Ho, A. K. Y. Jen, C. K. Luscombe, *Macromolecules* **2009**, *42*, 7670.

120 (a) S. L. Fronk, C.-K. Mai, M. Ford, R. P. Noland, G. C. Bazan, *Macromolecules* **2015**, *48*, 6224; (b) P. A. Dalgarno, C.A. Traina, J. C. Penedo, G. C. Bazan, I. D. W. Samuel, *J. Am. Chem. Soc.* **2013**, *135*, 7187.

121 F. Monnaie, W. Brullot, T. Verbiest, J. De Winter, P. Gerbaux, A. Smeets, G. Koeckelberghs, *Macromolecules* **2013**, *46*, 8500.

122 A. Smeets, P. Willot, J. De Winter, P. Gerbaux, T. Verbiest, G. Koeckelberghs, *Macromolecules* **2011**, *44*, 6017.

123 J. Liu, R. D. McCullough, *Macromolecules* **2002**, *35*, 9882.

124 J. Liu, R. S. Loewe, R. D. McCullough, *Macromolecules* **1999**, *32*, 5777.

125 R. A. Krüger, T. J. Gordon, T. Baumgartner, T. C. Sutherland, *ACS Appl. Mater. Interfaces* **2011**, *3*, 2031.

126 F. Boon, A. Thomas, G. Clavel, D. Moerman, J. De Winter, D. Laurencin, O. Coulembier, P. Dubois, P. Gerbaux, R. Lazzaroni, S. Richeter, A. Mehdi, S. Clément, *Synth. Met.* **2012**, *162*, 1615.

127 R. H. Lohwasser, M. Thelakkat, *Macromolecules* **2010**, *43*, 7611.

128 A. L. Briseno, T. W. Holcombe, A. I. Boukai, E. C. Garnett, S. W. Shelton, J. J. M. Fréchet, P. Yang, *Nano Lett.* **2010**, *10*, 334.

129 (a) Z. Mao, K. Vakhshouri, C. Jaye, D. A. Fischer, R. Fernando, D. M. DeLongchamp, E. D. Gomez, G. Sauvé, *Macromolecules* **2013**, *46*, 103; (b) J. Liu, T. Tanaka, K. Sivula, A. P. Alivisatos, J. M. J. Fréchet, *J. Am. Chem. Soc.* **2004**, *126*, 6550.

130 (a) P. Giannopoulos, A. Nikolakopoulou, A. K. Andreopoulou, L. Sygellou, J. K. Kallitsisa, P. Lianos, *J. Mater. Chem. A* **2014**, *2*, 20748; (b) S.-K. Ahn, D. L. Pickel, W. M. Kochemba Jihua Chen, D. Uhrig, J. P. Hinestrosa, J.-M. Carrillo, M. Shao, C. Do, J. M. Messman, W. M. Brown, B. G. Sumpter, S. M. Kilbey, *ACS Macro Lett.* **2013**, *2*, 761; (c) P. Bauer, M. Sommer, J. Thurn, M. Pärs, J. Köhlerb, M. Thelakkat, *Chem. Commun.* **2013**, *49*, 4637; (d) F. Li, Y. Du, Y. Chen, L. Chen, J. Zhao, P. Wang, *Sol. Energy Mater. Sol. Cells* **2012**, *97*, 64.

131 K. Okamoto, C. K. Luscombe, *Chem. Commun.* **2014**, *50*, 5310.

132 (a) K. Muellen, W. Pisula, *J. Am. Chem. Soc.* **2015**, *137*, 9503; (b) Y. He, W. Hong, Y. Li, *J. Mater. Chem. C* **2014**, *2*, 8651; (c) X. Guo, M. Baumgarten, K. Muellen, *Prog. Polym. Sci.* **2013**, *38*, 1832; (d)

M. J. Robb, S.-Y. Ku, C. J. Hawker, *Adv. Mater.* **2013**, *25*, 5686; (e) X. He, T. Baumgartner, *RSC Adv.* **2013**, *3*, 11334; (f) P. M. Beaujuge, J. M. J. Fréchet, *J. Am. Chem. Soc.* **2011**, *133*, 20009; (g) C. Wang, H. Dong, W. Hu, Y. Liu, D. Zhu, *Chem. Rev.* **2011**, *112*, 2208; (h) Y.-J. Cheng, S.-H. Yang, C.-S. Hsu, *Chem. Rev.* **2009**, *109*, 5868.

133 J. Mei, Z. Bao, *Chem. Mater.* **2014**, *26*, 604.

134 (a) T. Lei, J.-Y. Wang, J. Pei, *Chem. Mater.* **2014**, *26*, 594; (b) S. A. Jenekhe, *Nat. Mater.* **2008**, *7*, 354; (c) A. Babel, S. A. Jenekhe, *Synth. Met.* **2005**, *148*, 169.

135 (a) J. Lee, M. Kim, B. Kang, S. B. Jo, H. G. Kim, J. Shin, K. Cho, *Adv. Energy Mater.* **2014**, *4*, 1400087; (b) W.-H. Chang, J. Gao, L. Dou, C.-C. Chen, Y. Liu, Y. Yang, *Adv. Energy Mater.* **2014**, *4*, 1300864; (c) L. Fang, Y. Zhou, Y.-X. Yao, Y. Ding, W.-Y. Lee, A. L. Appleton, R. Allen, J. Reinspach, S. C. B. Mannsfeld, Z. Bao, *Chem. Mater.* **2013**, *25*, 4874; (d) X. Guo, H. Xin, F. S. Kim, A. D. T. Liyanage, S. A. Jenekhe, M. D. Watson, *Macromolecules* **2011**, *44*, 269; (e) S. Subramaniyan, H. Xin, F. S. Kim, S. Shoaee, J. R. Durrant, S. A. Jenekhe, *Adv. Energy Mater.* **2011**, *1*, 854.

136 (a) F. Ouhib, M. Tomassetti, J. Manca, F. Piersimoni, D. Spoltore, S. Bertho, H. Moons, R. Lazzaroni, S. Desbief, C. Jerome, C. Detrembleur, *Macromolecules* **2013**, *46*, 785; (b) Y. Jianfei, S. Holdcroft, *Macromolecules* **2000**, *33*, 5073.

137 (a) F. Li, K. G. Yager, N. M. Dawson, Y.-B. Jiang, K. J. Malloy, Y. Qin, *Chem. Mater.* **2014**, *26*, 3747; (b) F. Li, J. Yang, Y. Qin, *J. Polym. Sci., Part A: Polym. Chem.* **2013**, *51*, 3339; (c) F. Li, K. G. Yager, N. M. Dawson, J. Yang, K. J. Malloy, Y. Qin, *Macromolecules* **2013**, *46*, 9021.

138 K. K. Stokes, K. Heuzé, R. D. McCullough, *Macromolecules* **2003**, *36*, 7114.

139 A. Iraqi, J. A. Crayston, J. C. Walton, *J. Mater. Chem.* **1998**, *8*, 31.

140 L. Zhai, R. L. Pilston, K. L. Zaiger, K. K. Stokes, R. D. McCullough, *Macromolecules* **2003**, *36*, 61.

141 S. Miyanishi, K. Tajima, K. Hashimoto, *Macromolecules* **2009**, *42*, 1610

142 M. Chevrier, J. Kesters, C. Blayo, S. Richeter, A. Van Der Lee, O. Coulembier, M. Surin, A. Mehdi, R. Lazzaroni, R. C. Evans, W. Maes, P. Dubois, S. Clément, *Macromol. Chem. Phys.* **2016**, *217*, 445.

143 J. M. Lobez, T. L. Andrew, V. Bulovi, T. M. Swager, *ACS Nano* **2012**, *6*, 3044.

144 M. Lanzi, E. Salatelli, T. Benelli, D. Caretti, L. Giorgini, F. Paolo Di-Nicola, *J. Appl. Polym. Sci.* **2015**, *132*, 42121.

145 H. J. Kim, A.-R. Han, C.-H. Cho, H. Kang, H.-H. Cho, M. Y. Lee, J. M. J. Fréchet, J. H. Oh, B. J. Kim, *Chem. Mater.* **2012**, *24*, 215.

146 S. Yamamoto, H. Yasuda, H. Ohkita, H. Benten, S. Ito, S. Miyanishi, K. Tajima, K. Hashimoto, *J. Phys. Chem. C* **2014**, *118*, 10584.

147 (a) H. J. Kim, M. Skinner, H. Yu, J. Hak Oh, A. L. Briseno, T. Emrick, B. J. Kim, R. C. Hayward, *Nano Lett.* **2015**, *15*, 5689; (b) M. G. Mohamed, C.-C. Cheng, Y.-C. Lin, C. W. Huang, F.-H. Lu, F.-C. Chang, S.-W. Kuo, *RSC Adv.* **2014**, *4*, 21830.

148 L. Hirsch, G. Wantz, J. D. Wuest, *Chem. Rev.* **2013**, *113*, 3734.

149 (a) L. Dong, W. S. Li, *Nanoscale* **2011**, *3*, 3447; (b) A. Cuendias, R. C. Hiorns, E. Cloutet, L. Vignau, H. Cramail, *Polym. Int.* **2010**, *59*, 1452; (c) M. Sommer, S. Huettner, M. Thelakkat, *J. Mater. Chem.* **2010**, *20*, 10788; (d) S. B. Darling, *Energy Environ. Sci.* **2009**, *2*, 1266.

150 P. D. Topham, A. J. Parnell, R. C. Hiorns, *J. Polym. Sci. B Polym. Phys.* **2011**, *49*, 1131.

151 Y. Kim, S. Cook, J. Kirkpatrick, J. Nelson, J. R. Durrant, D. D. C. Bradley, M. Giles, M. Heeney, R. Hamilton, I. McCulloch, *J. Phys. Chem. C* **2007**, *111*, 8137.

152 J. K. Park, J. Jo, J. H. Seo, J. S. Moon, Y. D. Park, K. Lee, A. J. Heeger, G. C. Bazan, *Adv. Mater.* **2011**, *23*, 2430.

153 J. S. Kim, Y. Lee, J. H. Lee, J. H. Park, J. K. Kim, K. Cho, *Adv. Mater.* **2010**, *22*, 1355.

154 (a) A. Thomas, J. E. Houston, N. Van den Brande, J. De Winter, M. Chevrier, R. K. Heenan, A. E. Terry, S. Richeter, A. Mehdi, B. Van Mele, P. Dubois, R. Lazzaroni, P. Gerbaux, R. C. Evans, S. Clément, *Polym. Chem.* **2014**, *5*, 3352; (b) Y. Chen, H. Cui, L. Li, Z. Tian, Z. Tang, *Polym. Chem.* **2014**, *5*, 4441; (c) I. Y. Song, J. Kim, M. Jeong Im, B. J. Moon, T. Park, *Macromolecules* **2012**, *45*, 5058; (d) M. C. Stefan, M. P. Bhatt, P. Sista, H. D. Magurudeniya, *Polym. Chem.* **2012**, *3*, 1693.

155 (a) J. Roncali, *Adv. Energy Mater.* **2011**, *1*, 147; (b) H. Jiang, *Macromol. Rapid Commun.* **2010**, *31*, 2007; (c) M. Sommer, S. Huettner, M. Thelakkat, *Adv. Polym. Sci.* **2010**, 123.

156 B. Lim, J. Jo, S.-I. Na, J. Kim, S.-S. Kim, D.-Y. Kim, *J. Mater. Chem.* **2010**, *20*, 10919.

157 (a) Y.-H. Chen, P.-T. Huang, K.-C. Lin, Y.-J. Huang, C.-T. Chen, *Org. Electron.* **2012**, *13*, 283; (b) P.-T. Huang, Y.-H. Chen, B.-Y. Lin, W.-P. Chuang, *Int. J. Photogr.*, **2015**, Article ID *982064*.

158 H. Chen, J. Chen, W. Yin, X. Yu, M. Shao, K. Xiao, K. Hong, D. L. Pickel, W. M. Kochemba, S. M. Kilbey, M. Dadmun, *J. Mater. Chem. A* **2013**, *1*, 5309.

159 J. U. Lee, Y. D. Kim, J. W. Jo, J. P. Kim, W. Ho Jo, *J. Mater. Chem.* **2011**, *21*, 17209.

160 (a) J. U. Lee, A. Cirpan, T. Emrick, T. P. Russell, W. H. Jo, *J. Mater. Chem.* **2009**, *19*, 1483; (b) J. U. Lee, A. Cirpan, T. Emrick, T. P. Russell, W. H. Jo, *Nanotechnology* **2010**, *21*, 105201.

161 C. Yang, J. K. Lee, A. J. Heeger, F. Wudl, *J. Mater. Chem.* **2009**, *19*, 5416.

162 J. U. Lee, J. W. Jung, T. Emrick, T. P. Russell, W. H. Jo, *J. Mater. Chem.* **2010**, *20*, 3287.

163 M. Chevrier, S. Richeter, O. Coulembier, M. Surin, A. Mehdi, R. Lazzaroni, R. C. Evans, P. Dubois, S. Clément, *Chem. Commun.* **2016**, *52*, 171.

164 (a) D. Deribew, E. Pavlopoulou, G. Fleury, C. Nicolet, C. Renaud, S. J. Mougnier, *Macromolecules* **2013**, *46*, 3015; (b) T. Antoun, A. Iraqi, L. Kergoat, L. Miozzo, A. Yassar, *Macromol. Chem. Phys.* **2011**, *212*, 1129; (c) S. Rajaram, P. B. Armstrong, B. J. Kim, J. M. J. Fréchet, *Chem. Mater.* **2009**, *21*, 1775.

165 K. Sivula, Z. T. Ball, N. Watanabe, J. M. J. Fréchet, *Adv. Mater.* **2006**, *18*, 206.

166 M. Dante, C. Yang, B. Walker, F. Wudl, T. Q. Nguyen, *Adv. Mater.* **2010**, *22*, 1835.

167 M. Hufnagel, M. Fischer, T. Thurn-Albrecht, M. Thelakka, *Polym. Chem.* **2015**, *6*, 813.

168 B. W. Boudouris, F. Molins, D. A. Blank, C. D. Frisbi, M. A. Hillmyer, *Macromolecules* **2009**, *42*, 4118.

169 B. J. Kim, Y. Miyamoto, B. Ma, J. M. J. Fréchet, *Adv. Funct. Mater.* **2009**, *19*, 2273.

170 C.-Y. Nam, Y. Qin, Y. S. Park, H. Hlaing, X. Lu, B. M. Ocko, C. T. Black, R. B. Grubbs, *Macromolecules* **2012**, *45*, 2338.

171 G. Brotas, J. Farinhas, Q. Ferreira, J. Morgado, A. Charas, *Synth. Met.* **2012**, *162*, 2052.

172 S. Miyanishi, Y. Zhang, K. Tajima, K. Hashimoto, *Chem. Commun.* **2010**, *46*, 6723.

173 S. Miyanishi, Y. Zhang, K. Hashimoto, K. Tajima, *Macromolecules* **2012**, *45*, 6424.

174 B. J. Campo, D. Bevk, J. Kesters, J. Gilot, H. J. Bolink, J. Zhao, J.-C. Bolsée, W. D. Oosterbaan, S. Bertho, J. D'Haen, J. Manca, L. Lutsen, G. Van Assche, W. Maes, R. A. J. Janssen, D. Vanderzande, *Org. Electron.* **2013**, *14*, 523.

175 L. Angiolini, T. Benelli, V. Cocchi, M. Lanzi, E. Salatelli, *React. Funct. Polym.* **2013**, *73*, 1198.

176 L. Angiolini, V. Cocchi, M. Lanzi, E. Salatelli, D. Tonelli, Y. Vlamidis, *Mater. Chem. Phys.* **2014**, *146*, 464.

177 B. J. Campo, J. Duchateau, C. R. Ganivet, B. Ballesteros, J. Gilot, M. M. Wienk, W. D. Oosterbaan, L. Lutsen, T. J. Cleij, G. de la Torre, R. A. J. Janssen, D. Vanderzande, T. Torres, *Dalton Trans.* **2011**, *40*, 3979.

178 Y. Lin, J. A. Lim, Q. Wei, S. C. B. Mannsfeld, A. L. Briseno, J. J. Watkins, *Chem. Mater.* **2012**, *24*, 622.

179 S.-H. Chan, C.-S. Lai, H.-L. Chen, C. Ting, C.-P. Chen, *Macromolecules* **2011**, *44*, 8886.

180 (a) L. Chen, S. Peng, Y. Chen, *ACS Appl. Mater. Interfaces* **2014**, *6*, 8115; (b) B. K. Kuila, C. Chakraborty, S. A. Malik, *Macromolecules* **2013**, *46*, 484.

181 (a) J. Kesters, P. Verstappen, M. Kelchtermans, L. Lutsen, D. Vanderzande, W. Maes, *Adv. Energy Mater.* **2015**, *5*, 1500218; (b) M. V. Martínez-Díaz, G. de la Torre, T. Torres, *Chem. Commun.* **2010**, *46*, 7090.

182 (a) S.K. Yang, A.V. Ambade, M. Weck, *Chem. Soc. Rev.* **2011**, *40*, 129; (b) Y. Matsushita, A. Noro, A. Takano, *Eur. Polym. J.* **2012**, *44*, 72.

183 F. Li, N. M. Dawson, Y.-B. Jiang, K. J. Malloy, Y. Qin, *Polymer* **2015**, *76*, 220.

184 (a) F. Li, K. G. Yager, N. M. Dawson, J. Yang, K. J. Malloy, Y. Qin, *Macromolecules*, **2013**, *46*, 9021; (b) F. Li, K. G. Yager, N. M. Dawson, J. Yang, K. J. Malloy, Y. Qin, *Chem. Mater.* **2014**, *26*, 3747; (c) F. Li, K. G. Yager, N. M. Dawson, J. Yang, K. J. Malloy, Y. Qin, *Polym. Chem.* **2015**, *6*, 721.

185 N. Sary, F. Richard, C. Brochon, N. Leclerc, P. Leveque, J. N. Audinot, S. Berson, T. Heiser, G. Hadziioannou, R. Mezzenga, *Adv. Mater.* **2010**, *22*, 763.

186 F. C. Krebs, *Sol. Energy Mater. Sol. Cells* **2008**, *92*, 715.

187 S.-S. Li, C.-W. Chen, *J. Mater. Chem. A* **2013**, *1*, 10574.

188 (a) J. Bouclé, S. Chyla, M. S. Shaffer, J. R. Durrant, D. D. Bradley, J. Nelson, *Adv. Funct. Mater.* **2008**, *18*, 622; (b) C. Kwong, W. Choy, A. Djurisic, P. Chui, K. Cheng, W. Chan, *Nanotechnology* **2004**, *15*, 1156.

189 Y.-Y. Lin, C.-W. Chen, T.-H. Chu, W.-F. Su, C.-C. Lin, C.-H. Ku, J.-J. Wu, C.-H. Chen, *J. Mater. Chem.* **2007**, *17*, 4571.

190 P. A. van Hal, M. M. Wienk, J. M. Kroon, W. J. Verhees, L. H. Slooff, W. J. van Gennip, P. Jonkheijm, R. A. Janssen, *Adv. Mater.* **2003**, *15*, 118.

191 Y.-C. Huang, G. C. Welch, G. C. Bazan, M. L. Chabinyc, W.-F. Su, *Chem. Commun.* **2012**, *48*, 7250.

192 Y.-C. Huang, Y.-C. Liao, S.-S. Li, M.-C. Wu, C.-W. Chen, W.-F. Su, *Sol. Energy Mater. Sol. Cells* **2009**, *93*, 888.

193 Y. Yao, J. Hou, Z. Xu, G. Li, Y. Yang, *Adv. Funct. Mater.* **2008**, *18*, 1783.

194 W. U. Huynh, J. J. Dittmer, A. P. Alivisatos, *Science* **2002**, *295*, 2425

195 W. J. Beek, M. M. Wienk, M. Kemerink, X. Yang, R. A. Janssen, *J. Phys. Chem. B* **2005**, *109*, 9505.

196 (a) E. Martínez-Ferrero, J. Albero, E. Palomares, *J. Phys. Chem. Lett.* **2010**, *1*, 3039; (b) S. Dayal, N. Kopidakis, D. C. Olson, D. S. Ginley, G. Rumbles, *J. Am. Chem. Soc.* **2009**, *131*, 17726.

197 L. Li, T. Zhai, Y. Bando, D. Golberg, *Nano Energy* **2012**, *1*, 91.

198 P. Mansky, Y. Liu, E. Huang, T. P. Russell, C. Hawker, *Science* **1997**, *275*, 1458.

199 A. Ulman, *Chem. Rev.* **1996**, *96*, 1533.

200 S. Kango, S. Kalia, A. Celli, J. Njuguna, Y. Habibi, R. Kumar, *Prog. Polym. Sci.*, **2013**, *38*, 1232.

201 J. Dervaux, P.-A. Cormier, S. Konstantinidis, R. Di Ciuccio, O. Coulembier, P. Dubois, R. Snyders, *Vacuum* **2015**, *114*, 213.

202 B. Reeja-Jayan, T. Adachi, R. J. Ono, D. A. V. Bout, C. W. Bielawski, A. Manthiram, *J. Mater. Chem. A* **2013**, *1*, 3258.

203 R. H. Lohwasser, J. Bandara, M. Thelakkat, *J. Mater. Chem.* **2009**, *19*, 4126.

204 R. S. Moghaddam, S. Huettner, Y. Vaynzof, C. Ducati, G. Divitini, R. H. Lohwasser, K. P. Musselman, A. Sepe, M. R. J. Scherer, M. Thelakkat, U. Steiner, R. H. Friend, *Nano Lett.* **2013**, *13*, 4499.

205 Y.-C. Huang, J.-H. Hsu, Y.-C. Liao, W.-C. Yen, S.-S. Li, S.-T. Lin, C.-W. Chen, W.-F. Su, *J. Mater. Chem.* **2011**, *21*, 4450.

206 J. Warnan, Y. Pellegrin, E. Blart, F. Odobel, W. Zhang, B. Liu, V. J. Babu, S. Ramakrishna, *Macromol. Rapid Commun.* **2011**, *32*, 1190.

207 S Yanagida, G. K. R Senadeera, K Nakamura, T. Kitamura, Y. Wada, *J. Photochem. Photobiol., A* **2004**, *166*, 75.

208 J. K. Mwaura, X. Y. Zhao, H. Jiang, K. S. Schanze, J. R. Reynolds, *Chem. Mater.* **2006**, *18*, 6109.

209 K. Shankar, G. K. Mor, H. E. Prakasam, O. K. Varghese, C. A. Grimes, *Langmuir* **2007**, *23*, 12445.

210 C. J. Bhongale, M. Thelakkat, *Sol. Energy Mater. Sol. Cells* **2010**, *94*, 817.

211 G. K. V. V. Thalluri, J.-C. Bolsée, A. Gadisa, M. Parchine, T. Boonen, J. D'Haen, A. E. Boyukbayram, J. Vandenbergh, T. J. Cleij, L. Lutsen, D. Vanderzande, J. Manca, *Sol. Energy Mater. Sol. Cells* **2011**, *95*, 3262.

212 S. D. Oosterhout, L. J. Anton Koster, S. S. van Bavel, J. Loos, O. Stenzel, R. Thiedmann, V. Schmidt, B. Campo, T. J. Cleij, L. Lutzen, D. Vanderzande, M. M. Wienk, R. A. J. Janssen, *Adv. Energy Mater.* **2011**, *1*, 90.

213 F. Li, Y. Du, Y. Chen, *Thin Solid Films* **2012**, *526*, 120.

214 Y.-M. Chang, W.-F. Su, L. Wang, *Macromol. Rapid Commun.* **2008**, *29*, 1303.

215 H. Awada, L. Mezzasalma, S. Blanc, D. Flahaut, C. Dagron-Lartigau, J. Lyskawa, P. Woisel, A. Bousquet, L. Billon, *Macromol. Rapid Commun.* **2015**, *36*, 1486.

216 K. Noori, F. Giustino, *Adv. Funct. Mater.* **2012**, *22*, 5089.

217 N. D. Redeker, C. D. Danesh, Y. Ding, S. Zhang, *Polymer* **2013**, *54*, 7004.

218 S. K. Das, K. Abe, K. Yoshino, Y. Ogomi, S. S. Pandey, S. Hayase, *Thin Solid Films* **2013**, *536*, 302.